# Aggregation-Diffusion Phenomena in Domains with Boundaries

by

**Daniel Ames Messenger**

B.Sc., University of Puget Sound, 2015

Thesis Submitted in Partial Fulfillment of the
Requirements for the Degree of
Master of Science

in the
Department of Mathematics
Faculty of Applied Science


**SIMON FRASER UNIVERSITY**
**Summer 2019**

# Approval

| | |
|---|---|
| **Name:** | **Daniel Ames Messenger** |
| **Degree:** | **Master of Science (Applied and Computational Mathematics)** |
| **Title:** | **Aggregation-Diffusion Phenomena in Domains with Boundaries** |
| **Examining Committee:** | **Chair:** JF Williams<br>Associate Professor |
| | **Razvan Fetecau**<br>Senior Supervisor<br>Professor |
| | **Ralf Wittenberg**<br>Supervisor<br>Associate Professor |
| | **Paul Tupper**<br>Examiner<br>Professor |
| **Date Defended:** | **July 18, 2019** |

# Abstract

This thesis is concerned with a class of mathematical models for the collective behaviour of autonomous agents, or particles, in general domains $D \subset \mathbb{R}^d$, where particles exhibit pairwise interactions and may be subject to environmental forces. Such models have been shown to exhibit non-trivial behaviour due to interactions with the boundary of the domain $\partial D$. More specifically, when there is a boundary, it has been observed that the swarm of particles readily evolves into unstable states. Given this behaviour, we investigate the regularizing effect of adding noise to the system in the form of Brownian motion at the particle level, which produces linear diffusion in the continuum limit. To investigate the effect of linear diffusion and interactions with the boundary $\partial D$ on swarm equilibria, we analyze critical points of the associated energy functional, establishing conditions under which global minimizers exist. Through this process we uncover a new metastability phenomenon which necessitates the use of external forces to confine the swarm. We then introduce numerical methods for computing critical points of the energy, along with examples to motivate further research. Finally, we consider the short-time dynamics of the stochastic particle system as the noise strength $\nu$ approaches zero. We verify that the analytical $\mathcal{O}(\nu)$ convergence rate is represented in numerics, which we believe validates and motivates the use of stochastic particle simulations for further exploration of the regularizing effect of Brownian motion on aggregation phenomena in domains with boundaries.

**Keywords:** nonlocal modeling, swarms, Brownian motion, domains with boundaries, energy minimizers, metastability, numerical methods

# Dedication

This thesis is dedicated to my loving partner Anna, my parents, my sisters Amanda and Nora, and my brother Peter.

# Acknowledgements

I would like to acknowledge my supervisors Razvan Fetecau and Ralf Wittenberg for their care, attention, guidance and untold hours spent helping me through my masters degree. Razvan and Ralf have always been accepting of my best efforts and willing to take the time to teach me fundamentals whenever gaps in my knowledge of applied mathematics appeared. It has been a pleasure working with them at SFU and because of their guidance I have been able to grow as a mathematician and gain the confidence to go further into applied mathematical research. As well, this thesis has greatly benefited from many conversations with fellow grad students and faculty at Simon Fraser and abroad. I would like to thank Mitchell Kovacic, Hui Huang, Anton Iatcenko, Ian May, Ray Walsh, Sebastián Dominguez and Mohsen Seifi for offering advice and encouragement as fellow grad students or post-docs. I would also not have been able to complete this thesis without the help from faculty members Weiran Sun (SFU), Paul Tupper (SFU), Theodore Kolokolnikov (Dalhousie) and Andrew Bernoff (Harvey Mudd).

# Table of Contents

# List of Figures

# Chapter 1

# Introduction

We study a well-known mathematical model for the collective behaviour of groups of autonomous agents, or particles, in the absence of a group leader. Such groups are referred to in general as *swarms*. In the mathematical community, the term *aggregation* is used to refer to the phenomenon of swarming. The mathematical model was originally developed to understand the behaviour of biological swarms, such as flocks of birds, schools of fish or bacterial colonies. In the $21^{st}$ century, it has the potential to advance the development of artificial life, for instance to control fleets of self-driving cars, and has even been used to model non-physical entities, such as opinion dynamics in social networks. In this way, the biological phenomenon of swarming has found a permanent place in human life and its study is now crucial for many emerging technologies. Two main topics we will try to address are the emergence of equilibria, or stationary patterns, within a swarm and short time evolution from a random state. Both topics deal with the level of noise within the swarm and the environment in which the swarm is placed, namely the physical boundaries of the spatial domain and any external forces.

In the models we consider, the main drivers of collective pattern formation are pairwise interactions between particles in the swarm as mediated by an interaction potential $K$ whose gradient gives the interaction force between two particles as a function of inter-particle distance. We model such systems in general domains $D \subset \mathbb{R}^d$ which may contain boundaries and assume that in addition to being subject to interaction and external forces, each particle exhibits random fluctuations given by Brownian motion. We will find that Brownian motion regularizes certain instabilities found in the swarming model posed in domains with boundaries, as well as induces metastable behaviour in the continuum limit. Before introducing the particle and continuum swarming models to be analyzed, the variational framework, and the specific problems to be addressed, we review the necessary tools and terminology from measure-theoretic probability theory.

## 1.1 Notation and Terminology

### 1.1.1 Definitions

- Let $\mathcal{L}^d$ be the $d$-dimensional Lebesgue measure, $\mathcal{B}^d$ be the Borel $\sigma$-algebra on $\mathbb{R}^d$ (generated by the open subsets of $\mathbb{R}^d$), and $B_R(x)$ denote the $d$-dimensional Euclidean ball of radius $R$ centred at $x \in \mathbb{R}^d$.
- For any $A \in \mathcal{B}^d$, let $|A| := \mathcal{L}^d(A)$ be the volume of $A$ and $\mathbb{1}_A$ be its indicator function.
- For $D \in \mathcal{B}^d$, let $\mathcal{P}(D)$ denote the set of Borel probability measures on $D$ and $\mathcal{P}^{ac}(D) \subset \mathcal{P}(D)$ be the set of absolutely continuous measures with respect to $\mathcal{L}^d$.
- Define the support of a measure $\mu \in \mathcal{P}(D)$ as the (closed) set

$$\operatorname{supp}(\mu) := \{x \in D \ : \ \text{for all } R > 0,\ \mu(B_R(x)) > 0\}.$$

- For a measure $\mu \in \mathcal{P}(D)$, a condition $\mathrm{Q}(x)$ is satisfied $\mu$-almost everywhere and we write $\mu$-a.e. if $\mu(\{x \in D : \mathrm{Q}(x) \text{ does not hold }\}) = 0$.
- For $\mu \in \mathcal{P}(D)$, $x \in \mathbb{R}^d$ and $\gamma \in \mathbb{R}$, define the $\gamma^{th}$ moment of $\mu$ centred at $x$ as

$$M_\gamma^x(\mu) := \int_D |y - x|^\gamma \, d\mu(y) \tag{1.1}$$

  with $M_\gamma(\mu) := M_\gamma^0(\mu)$.
- For $\mu \in \mathcal{P}(D)$ and measurable function $F : D \to D$ denote by $F_\#\mu \in \mathcal{P}(D)$ the push-forward of $\mu$ by $F$ defined by

$$F_\#\mu(B) = \mu\left(F^{-1}(B)\right)$$

  for all Borel sets $B \subset D$.

**Remark 1.1.** Recall that every measure $\mu \in \mathcal{P}^{ac}(D)$ can be written $d\mu(x) = \rho(x)\,dx$ for some $\rho \in L^1(D)$ with $\rho \geq 0$ and $\int_D \rho(x)\,dx = 1$. The function $\rho$ is referred to as the density of $\mu$. Throughout, we will often refer to an absolutely continuous measure directly by its density $\rho$, and by abuse of notation sometimes write $\rho \in \mathcal{P}^{ac}(D)$ to mean $d\rho(x) = \rho(x)\,dx$.

### 1.1.2 Weak-* Relative Compactness and Tightness of Measures

We say that a sequence $\{\mu_n\}_{n\geq 0} \subset \mathcal{P}(D)$ converges weakly-* to $\mu \in \mathcal{P}(D)$ and write $\mu_n \overset{*}{\rightharpoonup} \mu$ if for every bounded continuous function $f : D \to \mathbb{R}$ we have

$$\lim_{n\to\infty} \int_D f(x)\,d\mu_n(x) = \int_D f(x)\,d\mu(x).$$

A collection of measures $\mathcal{F} \subset \mathcal{P}(D)$ is said to be weakly-* relatively compact if for every sequence $\{\mu_n\}_{n\geq 0} \subset \mathcal{P}(D)$ there exists a subsequence $\{\mu_{n_k}\}_{k\geq 0}$ which converges weakly-* to some $\mu \in \mathcal{P}(D)$.

Another notion of compactness is *tightness*: a collection of measures $\mathcal{F} \subset \mathcal{P}(D)$ is said to be *tight* if for every $\epsilon > 0$ there exists a compact set $K_\epsilon \subset D$ such that

$$\mu(K_\epsilon^c) < \epsilon$$

for every $\mu \in \mathcal{F}$, where $K_\epsilon^c$ denotes the complement of $K_\epsilon$ within $D$ (i.e. $K_\epsilon^c = D \setminus K_\epsilon$). Weak-* relative compactness and tightness are related by the following lemma, which will be used extensively in Chapter 2 to prove existence of global minimizers:

**Lemma 1.2.** *(Prokhorov's theorem, [5, Chapter 1, Section 5]) A collection of measures $\mathcal{F} \subset \mathcal{P}(D)$ is weakly-* relatively compact if and only if it is tight.*

### 1.1.3 The $p$-Wasserstein Space

Solutions to the swarming models (1.14) and (1.20) below are measure-valued. As such, well-posedness is established with respect to convergence in a suitable $p$-Wasserstein distance $\mathcal{W}_p(\cdot,\cdot)$ for some $p \in [1,\infty]$ and can be found in [11, 33, 12] and [34]. Here we give a brief introduction to the topology of the $p$-Wasserstein spaces.

For $p \in [1,\infty)$, define the space

$$\mathcal{P}_p(D) := \{f \in \mathcal{P}(D) : \ M_p(f) < +\infty\} \tag{1.2}$$

where $M_p(f)$ is defined (1.1). The $p$-Wasserstein distance on $\mathcal{P}_p(D)$ is then

$$\mathcal{W}_p(f,g) = \left(\inf_{\pi\in\Lambda(f,\ g)} \left\{ \int_{D\times D} |x-y|^p \, d\pi(x,y)\right\}\right)^{\frac{1}{p}} = \left(\inf_{X\sim f, Y\sim g} \left\{\mathbb{E}[|X-Y|^p]\right\}\right)^{\frac{1}{p}} \tag{1.3}$$

where $\Lambda(f,\ g)$ is the set of joint probability measures on $D\times D$ with marginals $f$ and $g$, also known as *transport plans*, and $(X,Y)$ ranges over all possible couplings of random variables $X$ and $Y$ with laws $f$ and $g$, respectively. The expectation $\mathbb{E}$ in (1.3) is taken with respect to the product measure $\mathbb{P}_1 \times \mathbb{P}_2$ assuming $X$ is defined on some probability space $(\Omega_1, \mathcal{F}_1, \mathbb{P}_1)$ and $Y$ is defined on $(\Omega_2, \mathcal{F}_2, \mathbb{P}_2)$ (see [27] for an introduction to the theory of random variables).

We will also use the space $\mathcal{P}_\infty(D)$ of probability measures on $D$ with compact support together with the $\infty$-Wasserstein distance

$$\mathcal{W}_\infty(f,g) = \inf_{X\sim f, Y\sim g} \mathbb{P}\text{-ess sup } |X-Y| = \inf_{\pi\in\Lambda(f,\ g)} \pi\text{ -ess sup}_{(x,y)\in D\times D} |x-y| \tag{1.4}$$

where

$$\mathbb{P}\text{-ess sup } |X-Y| := \inf\{\lambda \geq 0 : \mathbb{P}(|X-Y|>\lambda) = 0\} \tag{1.5}$$

and

$$\pi\text{ -ess sup}_{(x,y)\in D\times D} |x-y| := \inf\{\lambda \geq 0 : \pi(\{(x,y)\in D\times D : |x-y|>\lambda\}) = 0\}. \tag{1.6}$$

Some essential facts about $\mathcal{W}_p$ are:

1. For $p\in[1,\infty]$, the metric space $(\mathcal{P}_p(D),\mathcal{W}_p)$ is complete.
2. Convergence in $(\mathcal{P}_p(D),\mathcal{W}_p)$ for $p\in[1,\infty)$ is equivalent to weak-* convergence of measures, while convergence in $(\mathcal{P}_\infty(D),\mathcal{W}_\infty)$ implies weak-* convergence but the converse is not true.
3. For all $1\leq p\leq q\leq\infty$,
$$\mathcal{W}_p(f,g)\leq\mathcal{W}_q(f,g). \tag{1.7}$$

We refer readers to the books [1, 32] for further background on $p$-Wasserstein spaces.

## 1.2 Modeling Aggregation

In this section we introduce the mathematical models for aggregation. We direct readers to [8] for a review of deterministic mathematical models for collective behaviour and [21] for a review of mean-field limit theory for both deterministic and stochastic particle systems.

### 1.2.1 Plain Aggregation in Free Space

The first model we consider is the *plain aggregation* model, where "plain" here refers to swarming in the absence of Brownian motion. We start by describing the evolution of an $N$-particle system $X_t = \{X_t^i\}_{i=1}^N$ as the solution to the initial value problem

$$\begin{cases} \dfrac{d}{dt}X_t^i = -\dfrac{1}{N}\displaystyle\sum_{j\neq i}^{N} \nabla_{X_t^i} K\left(X_t^i - X_t^j\right) - \nabla V\left(X_t^i\right) \\ X_0^i = x_0^i \in \mathbb{R}^d. \end{cases} \tag{1.8}$$

The motion of particles is determined by an external potential $V : \mathbb{R}^d \to \mathbb{R}$ which encodes environmental forces such as gravity and an interaction potential $K : \mathbb{R}^d \to \mathbb{R}$ through which particles sense each other and feel pairwise interaction forces. We denote by $\nabla_x$ the gradient with respect to $x$ and for radial $K$, with some abuse of notation, we write $K(x) = K(|x|)$ such that

$$\nabla_x K(x-y) = K'(|x-y|) \cdot \frac{x-y}{|x-y|}.$$

See Figure 1.1 for examples of pairwise forces between particles imparted from an interaction potential $K$.

The first-order system (1.8) was introduced as a model for biological swarms by Mogilner, Edelstein-Keshet, Bent and Spiros in [26], and arrives as an approximation of the following second-order system in which particle trajectories are governed by Newton's Second Law $F = m\ddot{x}$:

$$m_i \frac{d^2}{dt^2} X_t^i = -m_i \frac{d}{dt} X_t^i - m_i \sum_{j \neq i}^{N} m_j \nabla_{X_t^i} K\left(X_t^i - X_t^j\right) - m_i \nabla V\left(X_t^i\right), \tag{1.9}$$

where a linear drag force $F^i_{drag} := -m_i \frac{d}{dt} X_t^i$ has been assumed. Assuming in addition that transient inertial forces are negligible (i.e. that changes in velocity are felt instantaneously) one arrive at the right-hand side of (1.9) being $\mathcal{O}(1)$ while the inertial term on the left $m_i \frac{d^2 X_t^i}{dt^2}$ is $o(1)$ and can be neglected. Rearranging terms and dividing by $m_i$ then gives the first-order dynamics (1.8), under the assumption that all particles have equal mass $\frac{1}{N}$. In [26] the authors argue that these approximations are valid for modeling biological aggregations, as individuals in a large system of organisms and which respond quickly to social cues, such as with flocks of birds or schools of fish, can be interpreted as having negligible inertia.

To obtain a continuum description of the swarm in the limit of large $N$, we consider the initial positions $X_0$ to (1.8) being drawn independently from some probability measure $\mu_0 \in \mathcal{P}(\mathbb{R}^d)$. With $X_t$ in hand, we can define the empirical measure

$$\mu_t^X := \frac{1}{N} \sum_{i=1}^{N} \delta_{X_t^i} \tag{1.10}$$

where $\delta_x$ is the Dirac mass centred at $x$. Under suitable conditions on $K$, $V$ and $\mu_0$, it is possible to justify the mean-field limit [21]

$$\mu_t^X \xrightarrow[N\to\infty]{*} \mu_t$$

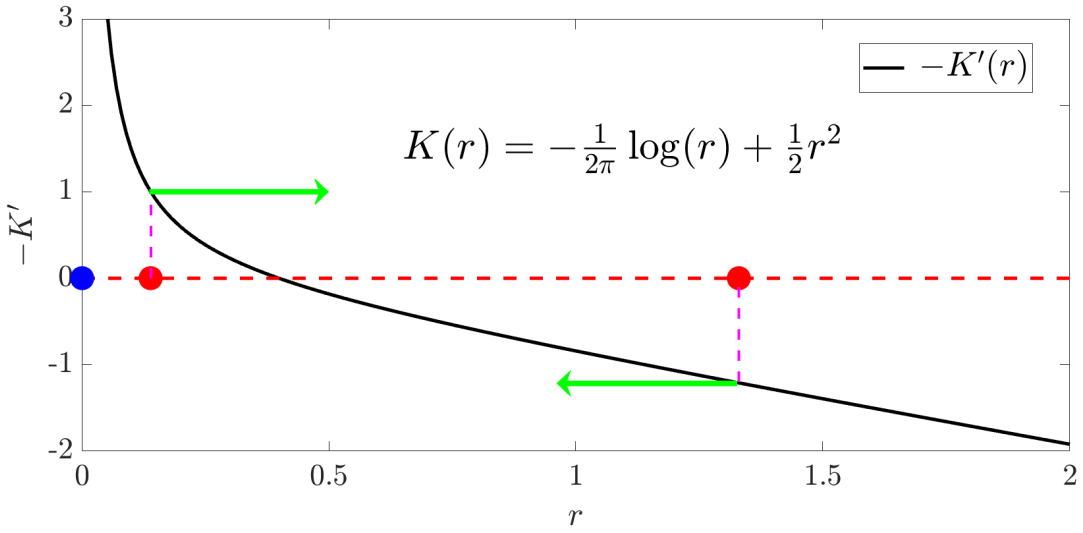


Figure 1.1: Interaction force imparted by the attractive-repulsive $K_{QANR}$ potential used in Chapter 4. The leftmost red particle feels a repulsive (positive) force from the blue particle since it lies in the region where $-K'(r) > 0$. The rightmost red particle feels an attractive (negative) force from the blue particle since it lies in the region where $-K'(r) < 0$.

---

for almost every $t > 0$, where $\overset{*}{\rightharpoonup}$ again denotes the weak-* convergence of measures. The limiting measure $\mu_t$ then solves the transport problem

$$\begin{cases} \dfrac{\partial}{\partial t}\mu_t + \nabla \cdot (\mu_t\, v) = 0, \quad t \in (0, T] \\ \mu_t\big|_{t=0} = \mu_0 \in \mathcal{P}_2(\mathbb{R}^d) \end{cases} \tag{1.11}$$

for some $T > 0$ and velocity $v(x)$ given nonlocally by

$$v(x) := -\nabla K * \mu_t - \nabla V = -\int_{\mathbb{R}^d} \nabla K(x - y)\, d\mu_t(y) - \nabla V(x). \tag{1.12}$$

Strictly speaking, the velocity $v(x)$ should be written $v[\mu_t](x)$ as it depends on $\mu_t$; however, for notational convenience we simply write $v(x)$. The integro-differential continuity equation (1.11) is called the *plain aggregation equation* and conveys the conservation of mass: no mass enters or leaves the swarm. At each time $t \in [0, T]$, the measure $\mu_t$ is the probability distribution for the location of particles and can be interpreted as a continuum of mass with total mass normalized to 1. In this way, an infinitesimal parcel of mass $d\mu_t(x)$ centred at $x$ at time $t$ travels through space with velocity $v(x)$. Although it is not a partial differential equation (PDE) in the traditional sense, we will often refer to (1.11) in shorthand as a PDE, and use the same convention for the continuum models below.

### 1.2.2 Plain Aggregation with Boundaries

The model we use for plain aggregation in general domains $D \subset \mathbb{R}^d$ for which the boundary $\partial D$ is nonempty was introduced by Wu and Slepčev in [33] for convex domains with $C^1$ boundary and extended to non-convex domains with non-differentiable boundaries by Carrillo, Slepčev and Wu in [12]. The model employs a velocity projection operator $P_x : \mathbb{R}^d \to \mathbb{R}^d$ to ensure that particles remain within $D$:

$$P_x(v) = \begin{cases} v\,, & \text{if } x \in \operatorname{int}(D) \quad \text{or if} \quad x \in \partial D \ \text{ and } \ v \cdot n \leq 0\,, \\ \Pi_{\partial D} v\,, & \text{otherwise.} \end{cases} \tag{1.13}$$

Here $\operatorname{int}(D)$ denotes the interior of the domain $D$ and $\Pi_{\partial D} v$ represents the projection of $v$ onto the tangent plane of $\partial D$ at $x \in \partial D$. In words, $P_x(v(x))$ is the identity map unless $x$ lies on the boundary of $D$ and $v(x)$ points outside $D$. With this we arrive at the plain aggregation model in domains with boundaries,

$$\begin{cases} \dfrac{\partial}{\partial t}\mu_t + \nabla \cdot (\mu_t P_x(v)) = 0, \quad t \in (0, T] \\ \mu_t\big|_{t=0} = \mu_0 \in \mathcal{P}_2(D), \end{cases} \tag{1.14}$$

where $v$ is defined above by (1.12). The associated particle system then satisfies

$$\begin{cases} \dfrac{d}{dt} X_t^i = P_x \left( -\dfrac{1}{N} \displaystyle\sum_{j \neq i}^{N} \nabla_{X_t^i} K\left(X_t^i - X_t^j\right) - \nabla V\left(X_t^i\right) \right) \\ X_0^i = x_0^i \in \mathbb{R}^d, \end{cases} \tag{1.15}$$

where $P_x$ enforces so-called "slip/no-flux" boundary conditions.

Solutions to (1.11) and (1.14) are to be interpreted in the weak-measure sense: a curve $\mu_t : [0, T] \to \mathcal{P}(D)$ is said to be a weak-measure solution of (1.14) if for all $\phi \in C_c^\infty(D \times (0, T))$ we have

$$\int_0^T \int_D \left( \frac{\partial}{\partial t}\phi(x,t) + \nabla \phi(x,t) \cdot P_x(v(x)) \right) d\mu_t(x)\, dt = 0. \tag{1.16}$$

Returning to the finite particle system $X_t$, by simply substituting a solution of the form (1.10) into the definition of a weak-measure solution (1.16), we see that empirical measures are indeed weak-measure solutions to (1.14) if we assume that $\nabla K(0)$ is finite. In this way, we recover the particle dynamics (1.8) from the continuum model (1.11).

### 1.2.3 Aggregation-Diffusion in Free Space

Now, consider again a swarm of $N$ particles $X_t^\nu = \left\{X_t^{\nu,i}\right\}_{i=1}^N$, this time prescribed with $N$ independent Brownian motions $\{B_t^i\}_{i=1}^N$ and obeying the system of stochastic differential equations (SDEs)

$$\begin{cases} dX_t^{\nu,i} = \left( -\dfrac{1}{N}\displaystyle\sum_{j\neq i}^{N} \nabla_{X_t^{\nu,i}} K\left(X_t^{\nu,i} - X_t^{\nu,j}\right) - \nabla V\left(X_t^{\nu,i}\right)\right) dt + \sqrt{2\nu}\, dB_t^i, \\ \text{Law}\left(X_0^{i,\nu}\right) = \mu_0^\nu \in \mathbb{R}^d. \end{cases} \tag{1.17}$$

This is the stochastic analogue of the free-space system (1.8), in which randomness occurs in the form of Brownian motion as well as in the initial conditions, which are independently drawn and identically distributed (i.i.d.) with law $\mu_0^\nu$. As before, we arrive at a continuum description by defining the empirical measure

$$\mu_t^{\nu,X} := \frac{1}{N}\sum_{i=1}^{N} \delta_{X_t^{\nu,i}}$$

and taking the limit as $N \to \infty$. This produces the mean-field dynamics

$$\begin{cases} \dfrac{\partial}{\partial t}\mu_t^\nu + \nabla\cdot(\mu_t^\nu\, v^\nu) = \nu\Delta\mu_t^\nu \\ \mu_t^\nu\big|_{t=0} = \mu_0^\nu \in \mathcal{P}_2(\mathbb{R}^d), \end{cases} \tag{1.18}$$

with nonlocal velocity $v^\nu(x)$ defined as in (1.12) by

$$v^\nu(x) := -\int_D \nabla K(x-y)\, d\mu_t^\nu(y) - \nabla V(x). \tag{1.19}$$

The integro-differential equation now contains the diffusion term $\nu\Delta\mu_t^\nu$ which gives the model the name aggregation-diffusion and distinguishes it from the plain aggregation model.

### 1.2.4 Aggregation-Diffusion with Boundaries

We now wish to extend the free-space aggregation-diffusion model to more general domains $D \subset \mathbb{R}^d$ with boundaries. Since (1.18) is second-order in space, it is natural to impose homogeneous Neumann boundary conditions for mass conservation and containment within

$D$, which gives us the system

$$\begin{cases} \dfrac{\partial}{\partial t}\mu_t^\nu + \nabla \cdot (\mu_t^\nu \, v^\nu) = \nu \Delta \mu_t^\nu, & x \in D \\ \Big\langle n(x),\, \mu_t^\nu(x)\, v^\nu(x) + \nu \nabla \mu_t^\nu(x) \Big\rangle = 0, & x \in \partial D \\ \mu_t^\nu\big|_{t=0} = \mu_0^\nu \in \mathcal{P}_2(D) \end{cases} \tag{1.20}$$

where $n(x)$ denotes the unit outward normal to $\partial D$ at $x$ and $\langle \cdot, \cdot \rangle$ is the Euclidean inner product. At each time $t \in (0, T]$ we require $\mu_t^\nu$ to be absolutely continuous with respect to $\mathcal{L}^d$ with density $\rho_t^\nu$, and again we look for a weak-measure solution to (1.20), which is defined as a curve $\mu_t^\nu : [0, T] \to \mathcal{P}^{ac}(D)$ such that for all $\phi \in C_c^\infty(D \times (0, T))$ with $\langle n, \nabla \phi \rangle = 0$ along $\partial D$ it holds that

$$\int_0^T \int_D \left( \frac{\partial}{\partial t}\phi(x,t) + \nabla \phi(x,t) \cdot v(x) + \nu \Delta \phi(x,t) \right) d\mu_t^\nu(x)\, dt = 0. \tag{1.21}$$

The stochastic particle system underlying (1.20) obeys the system of *reflected* SDEs,

$$\begin{cases} dX_t^{\nu,i} = \left( -\dfrac{1}{N} \displaystyle\sum_{j \neq i}^{N} \nabla_{X_t^{\nu,i}} K\left( X_t^{\nu,i} - X_t^{\nu,j} \right) - V\left( X_t^{\nu,i} \right) \right) dt + \sqrt{2\nu}\, dB_t^i + dR_t^i \\ \text{Law}\left( X_0^{i,\nu} \right) = \mu_0^\nu \in \mathcal{P}_2(D). \end{cases} \tag{1.22}$$

A solution to (1.22) is a pair of random processes $(X_t^\nu, R_t)$. The reflection processes $R_t^i$ have bounded variation and satisfy

$$R_t^i = \int_0^t n(X_s^{\nu,i})\, d|R^i|_s, \quad |R^i|_t = \int_0^t \mathbf{1}_{\partial D}(X_s^{\nu,i})\, d|R^i|_s \,,$$

where $|R^i|_t$ is the total variation of $R_t^i$ on $[0, t]$:

$$|R^i|_t = \sup \sum_k |R_{t_k}^i - R_{t_{k-1}}^i| \,, \tag{1.23}$$

where the supremum is taken over all partitions $0 = t_0 < t_1 < \cdots < t_n = t$ of $[0, t]$. In the event that $X_t^{\nu,i} \in \partial D$ at time $t$, the process $R_t^i$ imparts sufficient force in the direction $n(X_t^{\nu,i})$ to guarantee that $X_t^{\nu,i}$ remain in $D$, while for all other times $t$, $R_t^i$ does nothing. Solutions to reflected SDEs as joint processes $(X_t^\nu, R_t)$, first considered by Skorokhod in 1961 in [28, 29] and extended to interacting particle systems by Sznitman in 1991 in [31], have become the preferred way of describing stochastic particle systems which underlie solutions to PDEs with no-flux boundary conditions.

This defines the aggregation-diffusion model in general domains $D$.

Having introduced the underlying models for swarms in domains with boundaries, let us emphasize the differences between plain aggregation and aggregation-diffusion.

- For plain aggregation, boundary conditions are imposed on the velocity $v(x)$ through the projection operator $P_x$, while for aggregation-diffusion, confinement of particles to $D$ is facilitated by the stochastic reflection processes $R_t^i$ and by Neumann (no-flux) boundary conditions at the continuum level.
- Once the initial positions are drawn (which may occur randomly), the motion of particles in the plain aggregation is deterministic, while the motion of particles in the aggregation-diffusion is stochastic.
- The plain aggregation equation is first-order in space, while aggregation-diffusion is second-order.

In essence, while aggregation-diffusion can be seen as an immediate generalization of plain aggregation in free space (simply setting $\nu = 0$ recovers the latter), when boundaries are present, the limit $\nu \to 0$ is highly singular, causing not only a reduction from second-order to first-order in space, but a complete alteration in boundary conditions. This is what makes the zero diffusion limit challenging, providing part of the motivation for Chapter 4.

## 1.3 Energy Framework

An indispensable part of the analysis of the swarming models above is the variational framework given by the associated energy functionals. Given a measure $\mu \in \mathcal{P}(D)$ we define the energy $\mathcal{E}^\nu : \mathcal{P}(D) \to (-\infty, +\infty]$ by

$$\mathcal{E}^\nu[\mu] := \mathcal{K}[\mu] + \nu\mathcal{S}[\mu] + \mathcal{V}[\mu] \tag{1.24}$$

where

$$\mathcal{K}[\mu] := \frac{1}{2}\int_D \int_D K(x-y)\, d\mu(y)\, d\mu(x) \tag{1.25}$$

is the interaction energy,

$$\mathcal{S}[\mu] := \begin{cases} \displaystyle\int_D \rho(x)\log(\rho(x))\, dx, & \mu \in \mathcal{P}^{ac}(D) \text{ with } d\mu(x) = \rho(x)\, dx \\ +\infty, & \text{otherwise,} \end{cases} \tag{1.26}$$

is the negative of the Gibbs-Boltzmann entropy, and

$$\mathcal{V}[\mu] := \int_D V(x)\, d\mu(x) \tag{1.27}$$

is the external energy.

The energies associated to the swarming models (1.14) and (1.20) are $\mathcal{E} = \mathcal{E}^0$ and $\mathcal{E}^\nu$, respectively. It is known that under suitable conditions on $K$ and $V$, weak-measure solutions to (1.14) and (1.20) are gradient flows of $\mathcal{E}$ and $\mathcal{E}^\nu$, respectively, on the Wasserstein space $(\mathcal{P}_2(D), \mathcal{W}_2)$ [11, 12, 1]. This identifies equilibria of (1.14) and (1.20) as critical points of the associated energies $\mathcal{E}$ and $\mathcal{E}^\nu$. We now make precise the notions of equilibria of the aggregation models, stability of equilibria, and critical points of the energies. Many of the following conventions can be found in [10].

### 1.3.1 Model Equilibria

Denote an open ball of radius $r$ centred at $\mu \in \mathcal{P}_p(D)$ by

$$B_p(\mu, r) := \{\eta \in \mathcal{P}_p(D) \,:\, \mathcal{W}_p(\mu, \eta) < r\}.$$

*Equilibria*, or steady states, of the aggregation models (1.14) and (1.20) are defined as probability measures for which swarm velocities are zero:

$$\mu_\infty \text{ is an equilibrium of (1.14)} \quad \Longleftrightarrow \quad P_x(v(x)) = 0 \qquad \mu_\infty\text{-a.e.} \tag{1.28}$$

$$\mu^\nu_\infty \text{ is an equilibrium of (1.20)} \quad \Longleftrightarrow \quad v^\nu(x) + \nu \frac{\nabla \rho^\nu_\infty(x)}{\rho^\nu_\infty(x)} = 0 \qquad \mu^\nu_\infty\text{-a.e.} \tag{1.29}$$

where $d\mu^\nu_\infty(x) = \rho^\nu_\infty(x)\, dx$.

The *stability* of equilibria refers to the time dynamics of the model. An equilibrium $\mu_\infty$ is *locally asymptotically stable* if it is attracting in the ball $B_p(\mu_\infty, r)$ for some $r > 0$. In other words, for all initial data $\mu_0 \in B_p(\mu_\infty, r)$, solutions to the corresponding PDE satisfy $\lim_{t\to\infty} \mu_t = \mu_\infty$. Otherwise the equilibrium $\mu_\infty$ is said to be unstable.

### 1.3.2 Critical Points of the Associated Energies

*Critical points* of the energy $\mathcal{E}^\nu$ have no direct reference to time dynamics of the aggregation models. Before giving a complete definition of a critical point, we first give a more natural definition in the case of maxima or minima of $\mathcal{E}^\nu$. For $r > 0$ we define a $\mathcal{W}_p$-$r$ local minimizer of $\mathcal{E}^\nu$ to be a measure $\overline{\mu}$ such that

$$\mathcal{E}^\nu[\overline{\mu}] \le \mathcal{E}^\nu[\eta] \quad \text{ for all } \quad \eta \in B_p(\overline{\mu}, r) \tag{1.30}$$

and a $\mathcal{W}_p$-$r$ local maximizer analogously by reversing the inequality. In what follows, we will simply use the terms *minimizer*, *maximizer* or *extremizer* in reference to condition (1.30)

if the choice of $\mathcal{W}_p$ metric has been established.

In Theorem 2.3 we show that condition (1.30) implies that $\overline{\mu}$ satisfies the Euler-Lagrange equation

$$K * \overline{\mu}(x) + \nu \log(\overline{\rho}(x)) + V(x) = \lambda \quad \text{for} \quad \overline{\mu}\text{-a.e. } x \in D \tag{1.31}$$

for some unknown constant $\lambda \in \mathbb{R}$, where $d\overline{\mu}(x) = \overline{\rho}(x)\,dx$. As such, we extend the definition of a critical point of the energy $\mathcal{E}^\nu$ to be any measure $\overline{\mu} \in \mathcal{P}^{ac}(D)$ which satisfies the Euler-Lagrange equation (1.31). This definition allows for much more general critical points to enter the analysis, including saddle points, as will appear in the next section.

**Remark 1.3.** Taking the gradient of the Euler-Lagrange equation (1.31), we see that a critical point $\overline{\mu}$ also satisfies the conditions for equilibria of the PDE model. For the case of the aggregation-diffusion model, we can also integrate the equilibrium condition (1.29) to recover (1.31), and so model equilibria and critical points of $\mathcal{E}^\nu$ are equivalent. For the plain aggregation model, however, this is not exactly the case because of the projection operator $P_x$ in (1.28). Since the main focus of this thesis is on the aggregation-diffusion model, we will conduct analysis of critical points under the assumption that they correspond exactly to model equilibria.

Deriving the Euler-Lagrange equation requires showing that the first variation of $\mathcal{E}^\nu$ is zero with respect to all admissible perturbations of $\overline{\mu}$, which must at least preserve the properties

$$\overline{\mu}(D) = 1 \quad \text{and} \quad \overline{\mu} \geq 0$$

in order to remain in $\mathcal{P}(D)$. Such perturbations will be described by convex combinations of the form

$$\eta = (1-\alpha)\overline{\mu} + \alpha\mu \tag{1.32}$$

for some $\alpha \in (0,1]$ and $\mu \in \mathcal{P}(D)$. We will sometimes instead use $\eta = \overline{\mu} + \xi$ where $\xi \in L^1(D)$ satisfies

$$\int_D \xi(x)\,dx = 0 \quad \text{and} \quad \xi(x) \geq -\overline{\rho}(x),$$

but the formulation (1.32) is more general since it does not require $\overline{\mu}$ to be absolutely continuous. It is also more useful from the $\mathcal{W}_p$ perspective, as the following lemma shows.

**Lemma 1.4.** *For $p \in [1,\infty)$ and $\overline{\mu}, \mu \in \mathcal{P}_p(D)$, define $\eta$ as in* (1.32)*. Then*

*(i) If $\mu \in B_p(\overline{\mu}, r)$, then $\eta \in B_p(\overline{\mu}, r)$, and*

*(ii) If $\mu \notin B_p(\overline{\mu}, r)$, then there exists $\alpha_c \in (0,1)$ such that $\eta \in B_p(\overline{\mu}, r)$ for all $\alpha \in [0, \alpha_c)$.*

*Proof.* Let $\pi_\mu$ be an optimal transport plan between $\overline{\mu}$ and $\mu$ under $\mathcal{W}_p$ and define $\pi_\eta \in \mathcal{P}(D \times D)$ by

$$\pi_\eta := (1-\alpha) I_{D\#}\overline{\mu} + \alpha\pi_\mu$$

where $I_D : D \to D \times D$ is the diagonal map $I_D(x) = (x, x)$. Then $\pi_\eta$ defines a transport plan between $\overline{\mu}$ and $\eta$, as for any Borel set $B \subset D$ we have

$$\pi_\eta(B \times D) = (1-\alpha)\overline{\mu}(B) + \alpha\overline{\mu}(B) = \overline{\mu}(B)$$

and

$$\pi_\eta(D \times B) = (1-\alpha)\overline{\mu}(B) + \alpha\mu(B) = \eta(B).$$

Thus,

$$\mathcal{W}_p^p(\overline{\mu}, \eta) \leq \int_{D\times D} |x-y|^p \, d\pi_\eta(x,y) = \alpha \int_{D\times D} |x-y|^p \, d\pi_\mu(x,y) = \alpha \, \mathcal{W}_p^p(\overline{\mu}, \mu).$$

From this we immediately deduce (i) and (ii). □

Lemma 1.4 is not directly used to prove any theorems in this thesis, but it should emphasize how general the set of measures $\eta \in B_p(\overline{\mu}, r)$ can be, particularly through implication (ii). Addressing this generality is central to the problem of establishing existence of minimizers.

## 1.4 Unstable Equilibria and Diffusive Regularizations

It was observed by Razvan Fetecau and Mitchell Kovacic in [18] that in domains with boundaries, the plain aggregation model (1.14) routinely evolves into equilibria $\overline{\mu}_{ds}$ that consist of two components with disjoint supports: an aggregation on the boundary and an aggregation in free space. On the half line, these equilibria can be written

$$\overline{\mu}_{ds} = (1-S)\delta_0 + S\mu$$

for some $S \in (0,1)$ and $\mu \in \mathcal{P}([0,\infty))$ with $\text{supp}(\mu) \subset (0,\infty)$. It was found in [18] that these states are unstable to the class of perturbations that displace mass from the boundary, and so from the energy perspective, they are saddle points of $\mathcal{E}$.

Given the gradient flow structure of the plain aggregation model, it seems unlikely that such saddle points would arise so routinely, and predicting this behaviour seems out of reach of the current abstract gradient flow theory. By including diffusion in the model, hence arriving at the aggregation-diffusion model in domains with boundaries (1.20), the hope is to *regularize* the plain aggregation model in domains with boundaries, in the sense of achieving stable equilibria $\mu_\infty^\nu$ as $t \to \infty$. The motivation behind taking $\nu \to 0$ in (1.20) is then to arrive at the physically-relevant weak solution to the plain aggregation model (1.14), employing the notion of viscosity or entropy solutions commonly used to select the physically-relevant weak solution to hyperbolic PDEs.

Work has already been done by Fetecau, Kovacic and Topaloglu in [19] to examine the regularizing effect of adding nonlinear diffusion to (1.14), which results in a PDE with associated energy

$$\mathcal{E}^{\nu,m}[\mu] = \mathcal{K}[\mu] + \nu\mathcal{S}_m[\mu] + \mathcal{V}[\mu] \tag{1.33}$$

where the Gibbs-Boltzmann entropy $\mathcal{S}[\mu]$ has been replaced with

$$\mathcal{S}_m[\mu] := \begin{cases} \displaystyle\int_D \frac{\rho^m(x)}{m-1}\,dx, & \mu \in \mathcal{P}^{ac}(D) \text{ with } d\mu(x) = \rho(x)\,dx \\ +\infty, & \text{otherwise} \end{cases} \tag{1.34}$$

for $m > 1$. Some results from [19] include

(i) Existence of global minimizers of $\mathcal{E}^{\nu,m}$.

(ii) Zero-diffusion limit for finite times: $\mu_t^\nu \xrightarrow[\nu\to 0]{*} \mu_t$ for a.e. $t \in [0,T]$ along with explicit convergence rate.

(iii) Zero-diffusion limit for energy minimizers: let $\{\mu_\infty^\nu\}_{\nu>0}$ denote minimizers of the energies $\{\mathcal{E}^{\nu,m}\}_{\nu>0}$. Then $\mu_\infty^\nu \xrightarrow[\nu\to 0]{*} \mu_\infty \in \mathcal{P}(D)$ where $\mu_\infty$ is a minimizer of $\mathcal{E}^0$.

These and many other insightful results concerning swarm equilibria in domains with boundaries and subsequent regularization by *nonlinear* diffusion can be found in Mitchell Kovacic's doctoral dissertation [24], which has inspired us to consider more closely the model with linear diffusion.

There are advantages and disadvantages of regularizing the plain aggregation model with nonlinear versus linear diffusion. For nonlinear diffusion, solutions have compact support and the energy $\mathcal{E}^{\nu,m}$ is more amenable to analysis, as $\mathcal{S}_m$ is bounded below, which is not the case for $\mathcal{S}$. The primary benefit of modeling with linear diffusion, on the other hand, is the stochastic particle interpretation (1.22), which allows for numerical simulation in higher dimensions and general geometries via particle methods. Stochastic particle systems also directly relate back to physical swarms, where randomness is often inherent: a good example of this is the run-and-tumble motion of bacteria. For this reason, we focus on regularization by linear diffusion in this thesis, and specifically extend results (i) and (ii) above to this case.

As we will see below, the regularizing effect of linear diffusion is quite volatile. Specifically, due to the fact that $\mathcal{S}$ is not bounded below on $\mathcal{P}(D)$, it is always energetically favourable for mass to spread and fill the entire domain under the gradient flow of $\mathcal{S}$. As such, a delicate balance must be struck between the aggregation energy $\mathcal{K}$ and Gibbs-Boltzmann entropy $\mathcal{S}$ to guarantee existence of global minimizers, and often a confining external potential $V$ is necessary to prevent metastable translation of the swarm. In Chap-

ter 2 we address these problems and arrive at conditions for existence versus non-existence of minimizers.

## 1.5 Thesis Contributions

Having introduced the models, energy framework and motivation, we now state the contributions of this thesis. The following chapters are devoted to:

(Ch. 2) Establishing existence and non-existence criteria for global minimizers of the energy $\mathcal{E}^\nu$ in general domains $D \subset \mathbb{R}^d$.

(Ch. 3) Introducing numerical methods for computing critical points of $\mathcal{E}^\nu$ and motivating future work through numerical examples.

(Ch. 4) Numerically verifying the rate of convergence in the $\mathcal{W}_\infty$ metric as the empirical measure $\mu_t^{\nu,X}$ approaches $\mu_t^X$ in the $\nu \to 0$ limit, work which was recently submitted for publication in [17] in collaboration with Razvan Fetecau, Hui Huang and Weiran Sun.

In the final chapter we discuss open problems and future directions.

# Chapter 2

# Critical Points of the Energy

In this chapter we establish conditions for the existence and nonexistence of global minimizers of $\mathcal{E}^\nu$ for $\nu > 0$, extending results from free space recently proven by Carrillo, Delgadino and Patacchini in [10] to general domains $D$. Throughout this chapter we consider only absolutely continuous measures and so the energy $\mathcal{E}^\nu$ is defined

$$\mathcal{E}^\nu[\mu] = \frac{1}{2}\int_D \int_D K(x-y)\, d\mu(x)\, d\mu(y) + \nu \int_D \log(\rho(x))\, d\mu(x) + \int_D V(x)\, d\mu(x) \tag{2.1}$$

where $d\mu(x) = \rho(x)\, dx$. First we derive the Euler-Lagrange equation satisfied by critical points of the energy $\mathcal{E}^\nu$ along with some interesting properties of minimizers. We then compare and contrast the existence conditions in $\mathbb{R}^d$ and more general domains, presenting examples domains for which the results in free space do not generalize and providing new conditions for existence. Because measures are assumed to be absolutely continuous, we will often refer only to their densities.

Throughout this chapter we will assume the following about potentials $K$ and $V$ and the domain $D$.

**Assumption 1** (Potentials)**.**

(i) (Local integrability) $K, V \in L^1_{loc}(\mathbb{R}^d)$.

(ii) (Lower semicontinuity) $K$ and $V$ are lower semicontinuous.

(iii) (Symmetry of $K$) $K(x) = K(-x)$ for all $x \in \mathbb{R}^d$.

(iv) (Boundedness of $K$ away from origin) For all $0 < r < R < +\infty$, $K$ is bounded on $B_R(0) \setminus B_r(0)$.

(v) (Power-law growth of $K$) There exist constants $p_K \geq 0$, $R_K > 0$ and $C_K > 0$ such that

$$0 \leq K(x) \leq C_K |x|^{p_K} \qquad \text{for all} \qquad |x| > R_K.$$

**Assumption 2** (Domain)**.**

(i) (Domain topology) $D \subset \mathbb{R}^d$ is closed, connected, and $d$-dimensional (i.e. $|D| > 0$).

(ii) (Boundary regularity) There exists a unique outward normal vector $n(x)$ associated to each $x \in \partial D$ .

(iii) (Interior ball condition, see Figure 2.1) There exists a constant $\alpha_D > 0$ such that for all $x \in \partial D$

$$B_{\alpha_D}(x - \alpha_D n(x)) \subset D.$$

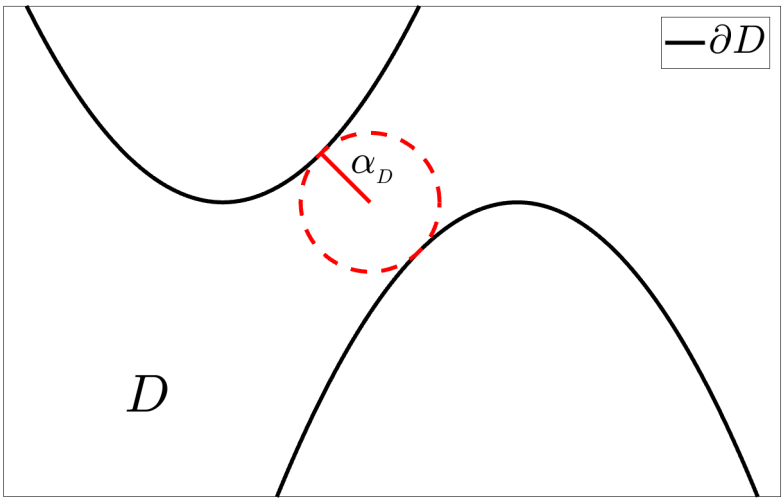


Figure 2.1: Illustration of the interior ball condition. In words, at every point $x \in \partial D$, a ball of radius $\alpha_D$ touching the boundary at $x$ can fit inside the domain.

---

## 2.1 Euler-Lagrange Equation

The Euler-Lagrange equation is a classical tool in the calculus of variations to characterize, and in our case define, critical points of energy functionals. In the aggregation-diffusion community, it is well known that critical points of the energy $\mathcal{E}^\nu$ in free space satisfy the Euler-Lagrange equation (2.3) below. This is derived by Balagué, Carrillo, Laurent and Raoul in [2] under the $\mathcal{W}_2$ metric for $\mathcal{E}^\nu$ without diffusion, and by Carrillo, Delgadino and Patacchini in [10] under the $\mathcal{W}_\infty$ metric for $\mathcal{E}^\nu$ with general diffusion. For lack of a reference for its derivation in the present context, we include a derivation of (2.3) here under general $\mathcal{W}_p$ metrics for $\mathcal{E}^\nu$ with linear diffusion and over general domains $D$, using the techniques in [2] and [10]. Equation (2.3) is then used throughout this chapter to prove existence results and in Chapter 3 to numerically calculate critical points.

First, we wish to highlight the crucial property that minimizers of $\mathcal{E}^\nu$ for every $\nu > 0$ are supported on the whole domain $D$. This is briefly mentioned in [10] for free space and is justified by the authors using the Euler-Lagrange equation. We wish to prove this property before deriving (2.3) because there is no reason *a priori* why in general domains $D$ a minimizer $\overline{\rho}$ should simultaneously satisfy equation (2.3) and $\operatorname{supp}(\overline{\rho}) = D$.

We use the following lemma to prove Theorems 2.2 and 2.3.

**Lemma 2.1.** *[32, Ch. 6] For all $p \in [1, \infty]$, $x_0 \in D$ and $\mu, \eta \in \mathcal{P}_p(D)$,*

$$\mathcal{W}_p^p(\mu, \eta) \leq 2^{(p-1)} \int_D |x - x_0|^p d|\mu - \eta|(x).$$

**Theorem 2.2.** *Assume that $\overline{\rho} \in \mathcal{P}_p^{ac}(D)$ is a $\mathcal{W}_p$-r local minimizer of $\mathcal{E}^\nu$ where $p \in [\max\{1, p_K\}, \infty]$. Then supp $(\overline{\rho}) = D$.*

*Proof.* We proceed by contradiction. Let $\overline{\rho}$ be a $\mathcal{W}_p$-$r$ local minimizer and assume to the contrary that $\operatorname{supp}(\overline{\rho}) \subsetneq D$. By definition, $\operatorname{supp}(\overline{\rho})$ is a closed subset of $D$, hence $D \setminus \operatorname{supp}(\overline{\rho})$ must have positive Lebesgue measure. This implies that there exists a point $x_0 \in \partial \operatorname{supp}(\overline{\rho})$ and $\delta > 0$ such that the set $A = B_\delta(x_0) \cap \left(D \setminus \operatorname{supp}(\overline{\rho})\right)$ has positive Lebesgue measure $|A|$. We now construct a measure $\eta$ with $\mathcal{W}_p(\overline{\rho}, \eta) < r$ such that $\mathcal{E}^\nu[\eta] < \mathcal{E}^\nu[\overline{\rho}]$, contradicting the assumption that $\overline{\rho}$ is a $\mathcal{W}_p$-$r$ local minimizer of $\mathcal{E}^\nu$. Define

$$\eta = (1 - \alpha)\overline{\rho} + \alpha \frac{1}{|A|} \mathbb{1}_A$$

where $\alpha \in (0, 1)$ will be picked in two stages.

First, using Lemma 2.1 we have

$$\begin{aligned}
\mathcal{W}_p^p(\overline{\rho}, \eta) &\leq 2^{(p-1)} \int_D |x - x_0|^p \, d|\overline{\rho} - \eta|(x) \\
&= \alpha \, 2^{(p-1)} \left( \int_D |x - x_0|^p \, d\overline{\rho}(x) + \frac{1}{|A|} \int_A |x - x_0|^p \, dx \right) \\
&\leq \alpha \, 2^{(p-1)} \left( M_p^{x_0}(\overline{\rho}) + \delta^p \right),
\end{aligned}$$

and so we choose

$$\alpha < \min\left\{1, \ \frac{r^p}{2^{(p-1)} \left(M_p^{x_0}(\overline{\rho}) + \delta^p\right)}\right\} \tag{2.2}$$

to ensure that $\mathcal{W}_p(\overline{\rho}, \eta) < r$.

Next, we find an additional constraint on $\alpha$ to ensure that $\mathcal{E}^\nu[\eta] < \mathcal{E}^\nu[\overline{\rho}]$ by bounding terms in the energy. For any $x \in \mathbb{R}$ we have $(1 - \alpha)^2 x < x + 2\alpha|x|$, and so a direct calculation of

the interaction energy yields the bound

$$\mathcal{K}[\eta] = (1-\alpha)^2\mathcal{K}[\overline{\rho}] + \frac{\alpha(1-\alpha)}{|A|}\int_D\left(\int_A K(x-y)dy\right)\overline{\rho}(x)\,dx + \frac{\alpha^2}{2|A|^2}\int_A\int_A K(x-y)\,dxdy$$
$$< \mathcal{K}[\overline{\rho}] + \alpha\left(2\,|\mathcal{K}[\overline{\rho}]| + \frac{1}{|A|}\underbrace{\int_D\left(\int_A |K(x-y)|\;dy\right)\overline{\rho}(x)\,dx}_{=:\,I} + \frac{1}{2|A|}\,\|K\|_{L^1(B_{2\delta}(0))}\right).$$

The integral $I$ is finite independently of $\alpha$, and hence so is the entire expression in parentheses, due to the power-law growth and local integrability of $K$ (Assumptions 1.i and 1.v above) together with the fact that $\overline{\rho}$ has finite $p_{_K}$-th moment. Indeed, fixing $R > R_{_K} + 2\delta$, we partition the integral to get

$$\begin{aligned} I &= \int_{B_R(x_0)\cap D}\left(\int_A |K(x-y)|\,dy\right)\overline{\rho}(x)\,dx + \int_{B_R^c(x_0)\cap D}\left(\int_A |K(x-y)|\,dy\right)\overline{\rho}(x)\,dx \\ &\le \left(\|K\|_{L^1(B_{R+\delta}(0))}\right)\int_{B_R(x_0)\cap D}\overline{\rho}(x)\,dx + C_K|A|\int_{B_R^c(x_0)\cap D}(|x-x_0|+\delta)^{p_K}\,\overline{\rho}(x)\,dx \\ &\le \|K\|_{L^1(B_{R+\delta}(0))} + C_K|A|\left(1+\frac{\delta}{R}\right)^{p_K} M_{p_K}^{x_0}(\overline{\rho}) \end{aligned}$$

which is finite. From this bound we have that for some $C > 0$ independent of $\alpha$,

$$\mathcal{K}[\eta] < \mathcal{K}[\overline{\rho}] + \alpha C.$$

For the entropy, since $A \cap \mathrm{supp}(\overline{\rho}) = \emptyset$ we have

$$\begin{aligned} \mathcal{S}[\eta] &= (1-\alpha)\int_D \overline{\rho}(x)\log((1-\alpha)\overline{\rho}(x))\,dx + \frac{\alpha}{|A|}\int_A \log\left(\frac{\alpha}{|A|}\right)\,dx \\ &= (1-\alpha)\mathcal{S}[\overline{\rho}] + (1-\alpha)\log(1-\alpha) + \alpha\log\left(\frac{\alpha}{|A|}\right) \\ &< (1-\alpha)\mathcal{S}[\overline{\rho}] + \alpha\log\left(\frac{\alpha}{|A|}\right) \\ &= \mathcal{S}[\overline{\rho}] + \alpha\left(-\mathcal{S}[\overline{\rho}] + \log\left(\frac{\alpha}{|A|}\right)\right). \end{aligned}$$

Together this allows us to bound the difference in energy as follows:

$$\mathcal{E}^\nu[\eta] - \mathcal{E}^\nu[\overline{\rho}] < \alpha\left(C - \nu\mathcal{S}[\overline{\rho}] + \nu\log\left(\frac{\alpha}{|A|}\right) - \mathcal{V}[\overline{\rho}] + \frac{1}{|A|}\int_A V(x)\,dx\right),$$

Now, choosing $\alpha$ such that

$$\alpha < |A|\,\exp\left(-\frac{C}{\nu} + \mathcal{S}[\overline{\rho}] + \frac{1}{\nu}\mathcal{V}[\overline{\rho}] - \frac{1}{\nu|A|}\int_A V(x)\,dx\right)$$

along with the constraint (2.2), we see by the monotonicity of the logarithm that

$$\mathcal{E}^\nu[\eta] < \mathcal{E}^\nu[\overline{\rho}].$$

Since $\eta$ has lower energy than $\overline{\rho}$ and lives in the ball $B_p(\overline{\rho}, r)$, $\overline{\rho}$ cannot be a $\mathcal{W}_p$-$r$ local minimizer, giving us the desired contradiction. Thus, the support of $\overline{\rho}$ must be the entire domain $D$.

□

We now derive the Euler-Lagrange equation.

**Theorem 2.3.** *Assume that $\overline{\rho} \in \mathcal{P}_p^{ac}(D)$ is a $\mathcal{W}_p$-$r$ local extremizer of $\mathcal{E}^\nu$ where $p \in [\max\{1, p_K\}, \infty]$. Then there exists a constant $\lambda \in \mathbb{R}$ such that*

$$K * \overline{\rho}(x) + \nu \log(\overline{\rho}(x)) + V(x) = \lambda \quad \text{for} \quad \overline{\rho}\text{-a.e. } x \in D. \tag{2.3}$$

*Proof.* Without loss of generality, assume $\overline{\rho}$ is a $\mathcal{W}_p$-$r$ local *minimizer* (the case where $\overline{\rho}$ is a maximizer follows similarly by reversing the following inequality). As in [10], it follows that

$$\frac{d}{dt}\mathcal{E}_\nu[\overline{\rho} + t(\eta - \overline{\rho})]\bigg|_{t=0} \geq 0$$

for all $\eta \in B_p(\overline{\rho}, r)$. From this a direct calculation then yields

$$\int_D (K * \overline{\rho} + \nu \log(\overline{\rho}) + V)\, d\eta \geq \int_D (K * \overline{\rho} + \nu \log(\overline{\rho}) + V)\, d\overline{\rho}. \tag{2.4}$$

We now construct a suitably general $\eta$ to deduce (2.3). Choose $\phi$ in $L^\infty(D; \overline{\rho}) \cap L^1(D; \overline{\rho})$ and define

$$\eta = \overline{\rho} + \epsilon \left(\phi - \int_D \phi\, d\overline{\rho}\right) \overline{\rho}$$

where $\epsilon$ will be chosen such that $\eta \in B_p(\overline{\rho}, r)$. It is clear that $\eta(D) = 1$. To ensure that $\eta \geq 0$ and hence $\eta \in \mathcal{P}_p(D)$, it suffices to pick $\epsilon \leq \frac{1}{2\|\phi\|_\infty}$. Another application of Lemma 2.1 gives

$$\begin{aligned}
\mathcal{W}_p^p(\overline{\rho}, \eta) &\leq 2^{p-1} \int_D |x|^p\, d|\overline{\rho} - \eta| \\
&= \epsilon\, 2^{p-1} \int_D |x|^p \left|\phi - \int_D \phi\, d\overline{\rho}\right| d\overline{\rho} \\
&\leq \epsilon\, 2^p \|\phi\|_\infty M_p(\overline{\rho})
\end{aligned}$$

and so $\mathcal{W}_p(\overline{\rho}, \eta) < r$ provided

$$\epsilon < \min\left\{\frac{r^p}{2^p \|\phi\|_\infty M_p(\overline{\rho})}, \frac{1}{2\|\phi\|_\infty}\right\},$$

which guarantees that $\eta \in B_p(\overline{\rho}, r)$. Substituting $\eta$ into (2.4) then gives us

$$\int_D \left(\phi - \int_D \phi \, d\overline{\rho}\right) (K * \overline{\rho} + \nu \log(\overline{\rho}) + V) \, d\overline{\rho} \geq 0.$$

The above calculations work for both $\phi$ and $-\phi$, hence upon multiplying by $-1$ we see that

$$\int_D \left(\phi - \int_D \phi \, d\overline{\rho}\right) (K * \overline{\rho} + \nu \log(\overline{\rho}) + V) \, d\overline{\rho} = 0.$$

Now, by setting $\phi = \mathbb{1}_B$ for any Borel set $B \subset \operatorname{supp}(\overline{\rho})$ with $\overline{\rho}(B) > 0$, we further have

$$\frac{1}{\overline{\rho}(B)} \int_B (K * \overline{\rho} + \nu \log(\overline{\rho}) + V) \, d\overline{\rho} = \int_D (K * \overline{\rho} + \nu \log(\overline{\rho}) + V) \, d\overline{\rho}. \tag{2.5}$$

From this we deduce (2.3) by contradiction. Define

$$\Lambda(x) := K * \overline{\rho}(x) + \nu \log(\overline{\rho}(x)) + V(x) \tag{2.6}$$

and assume that $\Lambda$ is not constant $\overline{\rho}$-a.e. Then there exists $\lambda^* \in \mathbb{R}$ such that the sets $B_1 = \{\Lambda < \lambda^*\}$ and $B_2 = \{\Lambda > \lambda^*\}$ satisfy $\overline{\rho}(B_1) > 0$ and $\overline{\rho}(B_2) > 0$. Using $B = B_1$ and $B = B_2$ in (2.5) then gives us

$$\lambda^* > \int_D \Lambda(x) \, d\overline{\rho} \quad \text{and} \quad \lambda^* < \int_D \Lambda(x) \, d\overline{\rho},$$

respectively, which is a contradiction, thus $\Lambda$ must be constant $\overline{\rho}$–a.e. This completes the proof. □

### 2.1.1 Fixed-Point Characterization

The Euler-Lagrange equation (2.3) can be recast in the following way if the critical point $\overline{\rho}$ satisfies $\operatorname{supp}(\overline{\rho}) = D$. Solving for $\overline{\rho}$ using the logarithm we have

$$\overline{\rho}(x) = \frac{1}{Z(\overline{\rho})} \exp\left(-\frac{K * \overline{\rho}(x) + V(x)}{\nu}\right)$$

where

$$Z(\overline{\rho}) := \int_D \exp\left(-\frac{K * \overline{\rho}(x) + V(x)}{\nu}\right) dx. \tag{2.7}$$

By integrating (2.3) against $d\overline{\rho}(x)$, we can also identify the constant $\lambda$ as

$$\lambda = \mathcal{E}^\nu[\overline{\rho}] + \mathcal{K}[\overline{\rho}] = -\nu \log(Z(\overline{\rho})).$$

This motivates the following corollary which will be used below.

**Corollary 2.4.** *Let $\overline{\rho} \in \mathcal{P}^{ac}(D)$ have supp $(\overline{\rho}) = D$. Then $\overline{\rho}$ satisfies* (2.3) *if and only if $\overline{\rho}$ is a fixed point of the map $T : \mathcal{P}(D) \to \mathcal{P}^{ac}(D)$ defined by*

$$T(\mu) = \frac{1}{Z(\mu)} \exp\left(-\frac{K * \mu(x) + V(x)}{\nu}\right) \tag{2.8}$$

*for $Z$ defined in* (2.7).

**Remark 2.5.** With no interaction forces (i.e. $K = 0$), (2.8) is the well-known Gibbs density

$$\rho_{_G}(x) = Z^{-1} \exp\left(-\frac{V(x)}{\nu}\right)$$

which arises in statistical mechanics as the stationary state of the linear, *local* Fokker-Planck equation

$$\frac{\partial}{\partial t}\rho = \nabla \cdot (\rho \nabla V) + \nu \Delta \rho.$$

Equations of this type were the first to be analyzed using Wasserstein gradient flow theory, for instance in the seminal work by Jordan, Kinderlehrer and Otto in [22] which proved, among other things, that weak solutions to the heat equation $\rho_t = \Delta\rho$ are gradient flows of the entropy $\mathcal{S}$ on the Wasserstein space $\Big(\mathcal{P}_2(\mathbb{R}^d), \mathcal{W}_2\Big)$. This providing novel justification for the notion that diffusion maximizes entropy. In our nonlocal scenario, we recover a similar stationary state as the Gibbs density, but in the form of a nonlinear integral equation (2.8) which has a possibly infinite number of solutions. It is this equation that we discretize in Chapter 3 for numerical computation of critical points.

## 2.2 Non-Existence of Global Minimizers

Here we establish conditions for non-existence of global minimizers of $\mathcal{E}^\nu$ in general domains $D$. This is broken into the two cases: (1) non-existence as a result of $\mathcal{E}^\nu$ being unbounded from below and (2) non-existence despite $\mathcal{E}^\nu$ having a finite lower bound. In the former case, non-existence follows immediately from the lower semicontinuity of the energy, and results from an imbalance between aggregative and diffusive forces. In the latter case, non-existence is more subtle and results entirely from domain asymmetries.

### 2.2.1 Imbalance of Forces

Physically, $\mathcal{E}^\nu$ is not bounded below if there is an imbalance between diffusive and aggregative forces. If the attraction imparted by $K$ is too weak, diffusion dominates and the swarm may spread infinitely throughout the domain, eventually reaching zero everywhere. If attraction is too strong, the swarm may contract onto a discrete set of points. Theorem 2.6 below covers both infinite spreading and infinite contraction and is a direct extension to general domains $D$ of the non-existence results in free space recently proven by Carrillo,

Delgadino and Patacchini in [10]. For the infinite spreading case, we use a similar technique as in [10] and explicitly construct a sequence of probability measures on $D$ which vanishes and lowers the energy to $-\infty$. For the case of infinite contraction, results are the same as in free space, and we refer readers to [10] for details.

**Theorem 2.6.** *Let Assumptions 1 and 2 hold with $V = 0$. Then the energy $\mathcal{E}^\nu$ is not bounded below on $\mathcal{P}(D)$ provided either*

$$\limsup_{r\to\infty}\left(\frac{1}{2}\sup_{x\in B_{2r}}\nabla K(x)\cdot x-\nu\right)<0 \quad \text{if} \quad |D|=+\infty \tag{2.9}$$

*or*

$$\liminf_{r\to 0}\left(\frac{1}{2}\inf_{x\in B_{2r}}\nabla K(x)\cdot x-\nu d\right)>0. \tag{2.10}$$

Conditions (2.9) and (2.10) above are given in the same form as they appear in [10] for direct comparison to the results in free space. The following lemma provides more intuitive conditions which are used in the proof.

**Lemma 2.7.** *Condition* (2.9) *implies that there exists $\delta_0$ with $-\nu<\delta_0<0$, $C_0\in\mathbb{R}$ and $R_0>0$ such that*

$$K(x)\le 2(\delta_0+\nu)\log|x|+C_0, \qquad |x|\ge R_0, \tag{2.11}$$

*while condition* (2.10) *implies that there exists $\delta_1>0$, $C_1\in\mathbb{R}$ and $R_1>0$ such that*

$$K(x)\le 2(\delta_1+\nu d)\log|x|+C_1, \qquad |x|\le R_1, \tag{2.12}$$

*Proof.* Both expressions in parenthesis of (2.9) and (2.10) are monotonically increasing in their respective limits in $r$. From this we are able to relax the lim sup and lim inf to regular limits. In the case of (2.9), this guarantees the existence of $\delta_0$ with $-\nu<\delta_0<0$ and $R'>0$ such that for all $r>R'$,

$$\frac{1}{2}\sup_{x\in B_{2r}}\nabla K(x)\cdot x-\nu\le\delta_0,$$

or

$$\nabla K(x)\cdot x\le 2(\nu+\delta_0) \qquad \text{for all} \quad |x|>2R'. \tag{2.13}$$

Now take arbitrary $x\in\mathbb{R}^d$ with $|x|>2R'$ and let $\widetilde{x}=su$ for $u=\frac{x}{|x|}$ where $2R'<s\le|x|$. From (2.13) we then have

$$\frac{d}{ds}K(su)=\frac{1}{s}\nabla K(su)\cdot su=\frac{1}{s}\nabla K(\widetilde{x})\cdot\widetilde{x}\le\frac{2(\nu+\delta_0)}{s}.$$

Integrating in $s$ from $2R'$ to $|x|$ and letting $R_0 = 2R'$, we get the desired estimate (2.11) with

$$C_0 = \max_{|y|=R_0} K(y) - 2(\delta_0 + \nu)\log(R_0).$$

Using similar logic, we show (2.12). Since the $\liminf_{r\to 0}$ reduces to a $\lim_{r\to 0}$, there exists $\delta_1 > 0$ and $R'' > 0$ such that for all $r < R''$ we have

$$\frac{1}{2}\inf_{x\in B_{2r}} \nabla K(x)\cdot x - \nu \geq \delta_1$$

or

$$\nabla K(x)\cdot x \geq 2(\nu + \delta_1) \qquad \text{for all} \quad x \in B_{2R''}. \tag{2.14}$$

Using the same line-integral argument, we deduce (2.12) where $R_1 = 2R''$ and

$$C_1 = \max_{|y|=R_1} K(y) - 2(\delta_1 + \nu d)\log(R_1).$$

□

We now prove the non-existence result.

*Proof of Theorem 2.6.* We will focus on the spreading case (2.9). Let $\{B_{\alpha_D}(x_i)\}_{i=1}^{\infty}$ be a sequence of disjoint balls contained in $D$ such that the finite union $B^n := \cup_{i=1}^n B_{\alpha_D}(x_i)$ satisfies

$$\sup_{x,y\in B^n} |x - y| \leq 2n\alpha_D \tag{2.15}$$

for each $n$. This construction is always possible if $D$ is an unbounded domain satisfying the interior sphere condition in Assumption 2. For instance, (2.15) turns into an equality if the collection of balls lie adjacent on a ray with $x_i = (2i-1)\alpha_D y$ for some fixed $y$ with $|y| = 1$.

Define $B_i := B_{\alpha_D}(x_i)$ for convenience. Without loss of generality we may assume that $B_{\alpha_D}(0) \subset D$, and so we let $x_1 = 0$ such that $B_1 := B_{\alpha_D}(0)$. Since $B_i \cap B_j = \emptyset$ we have $|\cup_{i=1}^n B_i| = n\alpha_D^d\omega_d$, where $\omega_d$ is the volume of the $d$-dimensional unit ball, hence we may define the sequence of probability measures $\{\mu_n\}_{n=1}^{\infty}$ by

$$\mu_n = \frac{1}{n\alpha_D^d\omega_d}\sum_{i=1}^n \mathbb{1}_{B_i}.$$

The energy of each $\mu_n$ is then

$$\mathcal{E}^\nu[\mu_n] = \frac{1}{2(n\alpha_D^d\omega_d)^2}\sum_{i,j=1}^n \int_{B_i}\int_{B_j} K(x-y)\,dx\,dy - \nu\log\left(n\alpha_D^d\omega_d\right).$$

By defining $u = x_i - x_j$, the pairwise interactions between balls in the finite set $\{B_i\}_{i=1}^n$ can be rewritten using

$$\int_{B_i}\int_{B_j} K(x-y)\,dx\,dy = \int_{B_1}\int_{B_1} K(x-(y-u))\,dx\,dy.$$

Taking $R_0$ as in Lemma 2.7, we now split the sum of pairwise interactions into so-called "near-field" and "far-field" interactions, where near-field interactions are those between $B_i$ and $B_j$ such that $\operatorname{dist}(B_i, B_j) < R_0$, where

$$\operatorname{dist}(A,B) := \inf_{x\in A, y\in B} |x-y|,$$

and the remaining interactions are far-field. From this partitioning we can use Lemma 2.7 to provide an upper bound on the interaction portion of $\mathcal{E}^\nu[\mu_n]$ which is uniform in $n$ and then show that the diffusion portion ultimately dominates, sending the energy to $-\infty$.

To achieve such an upper bound, we bound above the number of possible near-field and far-field interactions simultaneously for each $B_i$. All near-field interactions for a fixed $B_i$ take place within the ball $B_{R_0+\alpha_D}(x_i)$, hence the maximum number of near-field interactions is bounded above by the volume ratio

$$\frac{|B_{R_0+\alpha_D}(0)|}{|B_{\alpha_D}(0)|} = \frac{(R_0+\alpha_D)^d\omega_d}{\alpha_D^d\omega_d} = \left(\frac{R_0}{\alpha_D}+1\right)^d.$$

For the far-field, we simply bound the number of far-field interactions for each $B_i$ above by $n$. Using these bounds, we have

$$\begin{aligned}\sum_{i,j=1}^n \int_{B_i}\int_{B_j} K(x-y)\,dx\,dy &\le n\left(\frac{R_0}{\alpha_D}+1\right)^d\left(\sup_{|u|\le R_0+2\alpha_D}\int_{B_1}\int_{B_1} K(x-(y-u))\,dx\,dy\right)\\ &\quad + \quad n^2\left(\sup_{R_0+2\alpha_D\le|u|\le 2(n-1)\alpha_D}\int_{B_1}\int_{B_1} K(x-(y-u))\,dx\,dy\right)\\ &\le \widetilde{C}n + (\alpha_D^d\omega_d)^2\left(\sup_{R_0<|x|\le 2n\alpha_D} K(x)\right)n^2\end{aligned}$$

where $\widetilde{C}$ is finite due to the local integrability of $K$ and independent of $n$. Substituting this into the energy and using Lemma 2.7 gives us

$$\begin{aligned}
\mathcal{E}^\nu[\mu_n] &\leq \frac{\widetilde{C}}{2n\left(\alpha_D^d\omega_d\right)^2} + \frac{1}{2}\left(\sup_{R_0<|x|\leq 2n\alpha_D} K(x)\right) - \nu\log\left(n\alpha_D^d\omega_d\right) \\
&\leq \frac{\widetilde{C}}{2n\left(\alpha_D^d\omega_d\right)^2} + (\delta_0+\nu)\log(2n\alpha_D) + \frac{1}{2}C_0 - \nu\log\left(n\alpha_D^d\omega_d\right) \\
&\leq (\delta_0+\nu)\log(n\alpha_D) - \nu\log\left(n\alpha_D\right) + A \\
&= \delta_0\log(n\alpha_D) + A
\end{aligned}$$

where $A$ is a constant independent of $n$. Since $\delta_0 < 0$, we have

$$\lim_{n\to\infty}\mathcal{E}^\nu[\mu_n] = -\infty$$

which shows that the energy is not bounded below in the spreading case of (2.9).

As mentioned above, the proof of the case (2.10) of infinite contraction is shown in [10] and needs no modification for general domains. This is because the limiting sequence constructed in [10] to send $\mathcal{E}^\nu \to -\infty$ involves the contraction of a ball to a single point, which can be done in any $d$-dimensional domain $D$. □

**Remark 2.8.** There is a subtle difference in the spreading case between general domains and free space. In free space, spreading occurs if $K$ grows more slowly than $2\nu d\log|x|$ as $|x| \to \infty$, while in general domains we have shown that spreading occurs only if $K$ grows more slowly than $2\nu\log|x|$ (see (2.9) and (2.11)), which is clearly more restrictive in higher dimensions than the free-space bound. This reflects the fact that when the domain $D$ confines the swarm in such a way that spreading can only "effectively" occur in fewer dimension (e.g. when $D$ is an infinite tube spreading effectively occurs in one dimension), diffusion must work harder to overcome the attraction forces, and so weaker attraction results in infinite spreading. We are currently attempting to utilize this property to achieve a tight bound of the form $K \lesssim 2\nu\widetilde{d}\log|x|$ for characterizing infinite spreading in general domains, where $\widetilde{d}$ characterizes the "effective" number of dimensions in which the domain extends to infinity.

### 2.2.2 Domain Asymmetries

To exhibit the role played by domain geometry in determining existence of global minimizers, we briefly review existence results in free space when $V = 0$. When $D = \mathbb{R}^d$ and $V = 0$, existence of a global minimizer is guaranteed as soon as the energy is bounded below,

which is conveyed in the following theorem, reproduced here for the sake of discussion. As we will show, this is not the case in domains with boundaries.

**Theorem 2.9.** *[10, Thm 6.1] Suppose $K \in L^1_{loc}(\mathbb{R}^d)$ is positive, lower semicontinuous and symmetric, and $V = 0$. Then there exists $\mu_\infty \in \mathcal{P}(\mathbb{R}^d)$ such that*

$$\mathcal{E}^\nu(\mu_\infty) = \inf \mathcal{E}^\nu > -\infty$$

*provided*

$$\liminf_{|x|\to\infty} \nabla K(x) \cdot x > 2d\nu. \tag{2.16}$$

The hypotheses in Theorem 2.9 have natural physical interpretations. Enforcing that $K$ is positive excludes potentials such as $K(x) = -\frac{1}{|x|}$ which produce an infinite well of (pairwise) attraction at the origin. This is needed to prevent infinite contraction of the swarm onto $\delta$-aggregations. We then have the constraint (2.16), which is shown in [10] to imply

$$K(x) \geq \frac{2\nu d}{1-\delta} \log|x| + C \tag{2.17}$$

for some $\delta \in (0, 1/2)$ and $C \in \mathbb{R}$, similar to Lemma 2.7. (Note that (2.17) holds for every $x \in \mathbb{R}^d$ by the positivity of $K$). By requiring that $K$ grow at least logarithmically as $|x| \to \infty$, the case of infinite spreading is prevented. In words, Theorem 2.9 says that in free space, if the two force-imbalance pathologies from the previous subsection are prevented, then existence of a global minimizer is guaranteed.

We sketch the proof of Theorem 2.9 here, as the following crucial lemmas will be used in the existence proofs in the next section.

**Lemma 2.10.** *[10, Section 2.2] Assume that $K$ and $V$ are both lower semicontinuous, that is for all $x_0 \in \mathbb{R}^d$,*

$$\liminf_{x\to x_0} K(x) \geq K(x_0) \quad \text{and} \quad \liminf_{x\to x_0} V(x) \geq V(x_0).$$

*Then $\mathcal{E}^\nu$ is weakly-* lower semicontinuous, that is for any sequence $\{\mu_n\}_{n\geq 0} \subset \mathcal{P}(D)$ such that $\mu_n \overset{*}{\rightharpoonup} \mu \in \mathcal{P}(D)$, it holds that*

$$\liminf_{n\to\infty} \mathcal{E}^\nu[\mu_n] \geq \mathcal{E}^\nu[\mu].$$

**Lemma 2.11.** *(Logarithmic Hardy-Littlewood-Sobolev (HLS) inequality [10, Lemma 2.6]) Let $\rho \in \mathcal{P}^{ac}(\mathbb{R}^d)$ satisfy $\log(1 + |\cdot|^2)\rho \in L^1(\mathbb{R}^d)$. Then there exists $C_0 \in \mathbb{R}$ depending only on $d$ such that*

$$-\int_{\mathbb{R}^d}\int_{\mathbb{R}^d} \log(|x-y|)\rho(x)\rho(y)\,dx\,dy \leq \frac{1}{d}\int_{\mathbb{R}^d} \rho(x)\log(\rho(x))\,dx + C_0. \tag{2.18}$$

**Lemma 2.12.** *[10, Lemma 2.9] Let $K(x) \in L^1_{loc}(\mathbb{R}^d)$ be positive, symmetric and satisfying*

$$\lim_{|x|\to\infty} K(x) = +\infty.$$

*Given a sequence $\{\mu_n\}_{n\in\mathbb{N}} \subset \mathcal{P}(\mathbb{R}^d)$, if*

$$\liminf_{n\to\infty} \int_{\mathbb{R}^d}\int_{\mathbb{R}^d} K(x-y)\, d\mu_n(x)\, d\mu_n(y) < \infty,$$

*then $\{\mu_n\}_{n\in\mathbb{N}}$ is weakly-* relatively compact up to translations.*

To prove Theorem 2.9 the authors of [10] first use the logarithmic HLS inequality (2.18) together with the estimate (2.17) to show that $\mathcal{E}^\nu$ is bounded below on $\mathcal{P}(\mathbb{R}^d)$. It is then deduced from Lemma 2.12 that any minimizing sequence of $\mathcal{E}^\nu$ is weakly-* relatively compact up to translation and so admits a subsequence which converges to some $\overline{\rho} \in \mathcal{P}(D)$. Finally, since $K$ is assumed to be lower semicontinuous, by Lemma 2.10 the energy $\mathcal{E}^\nu$ is also lower semicontinuous, and so $\overline{\rho}$ must realize the infimum of $\mathcal{E}^\nu$.

In general domains $D$, boundedness from below of the energy and subsequent tightness-up-to-translation arguments are not enough to guarantee existence of a minimizer. This is shown in the following theorem, where (2.16) is clearly satisfied, hence $\inf \mathcal{E}^\nu > -\infty$, yet no energy minimizer exists for $V = 0$. It is then shown that, for any $g > 0$, adding a confining external potential of the form $V = gx$ enforces the existence of a *unique* critical point.

**Theorem 2.13.** *Let $D = [0, +\infty)$, $K(x) = \frac{1}{2}x^2$ and $V(x) = gx$ for $g \geq 0$. We then have the following for any $\nu > 0$:*

*(i) If $g = 0$, then the energy $\mathcal{E}^\nu$ has no minimizers.*

*(ii) For any $g > 0$, there exists a unique critical point $\overline{\rho}$ for $\mathcal{E}^\nu$ in the space of measures $\mathcal{P}_2^{ac}(D)$ having support equal to $D$.*

*Proof.* The energy is given by

$$\mathcal{E}^\nu[\rho] = \frac{1}{4}\int_0^\infty\int_0^\infty (x-y)^2\, \rho(x)\rho(y)\, dx\, dy + \nu\int_0^\infty \rho(x)\log(\rho(x))\, dx + g\int_0^\infty x\rho(x)\, dx. \quad (2.19)$$

(i) Let $g = 0$. We proceed by contradiction. Assume that a minimizer $\overline{\rho} \in \mathcal{P}_2^{ac}(D)$ of (2.19) exists. Then $\overline{\rho}$ has $\operatorname{supp}(\overline{\rho}) = D$ by Theorem 2.2 and satisfies the Euler-Lagrange equation (2.3), and so by Corollary 2.4,

$$\overline{\rho}(x) = Z^{-1}\exp\left(-\frac{K * \overline{\rho}(x)}{\nu}\right)$$

where

$$Z = \int_0^\infty \exp\left(-\frac{K * \overline{\rho}(x)}{\nu}\right) dx.$$

From an elementary calculation,

$$\begin{aligned} K * \overline{\rho}(x) &= \frac{1}{2}\int_0^\infty (x-y)^2 \overline{\rho}(y)\, dy \\ &= \frac{1}{2}(x - M_1(\overline{\rho}))^2 - \frac{1}{2}\left(M_1(\overline{\rho})^2 - M_2(\overline{\rho})\right), \end{aligned}$$

hence $\overline{\rho} = \rho_c$ for some $c \in \mathbb{R}$, where

$$\rho_c(x) = A(c)\, \exp\left(-\frac{1}{2\nu}\,(x-c)^2\right)$$

is a shifted and truncated Gaussian. Here $c = M_1(\overline{\rho})$ and $A(c)$ is the normalization constant[1]

$$A(c) = \frac{2/\sqrt{2\pi\nu}}{1 + \operatorname{erf}(c/\sqrt{2\nu})}.$$

Let $\Gamma_c = \{\rho_c\}_{c\geq 0}$ be the family of shifted and truncated Gaussians on $[0, +\infty)$. Then since $\overline{\rho} \in \Gamma_c$ and $\overline{\rho}$ is a critical point of $\mathcal{E}^\nu$ over $\mathcal{P}(D)$, $\overline{\rho}$ is a critical point of $\mathcal{E}^\nu$ over $\Gamma_c$ as well, and so the function $c \to \mathcal{E}^\nu[\rho_c]$ has a critical point at some $c \in \mathbb{R}$. By direct calculation of $\mathcal{E}^\nu[\rho_c]$, we now show that no such critical point exists.

For the entropy, we have

$$\begin{aligned} \mathcal{S}[\rho_c] &= A(c)\int_0^\infty \exp\left(-\frac{1}{2\nu}\,(x-c)^2\right)\left(-\frac{1}{2\nu}\,(x-c)^2 + \log(A(c))\right) dx \\ &= \log(A(c)) - \frac{1}{2\nu}\underbrace{A(c)\int_0^\infty (x-c)^2 \exp\left(-\frac{1}{2\nu}(x-c)^2\right) dx}_{I}. \end{aligned}$$

[1]For reference,

$$\operatorname{erf}(a) = \frac{2}{\sqrt{\pi}}\int_0^a e^{-y^2}\, dy.$$

For the interaction energy, we get

$$\begin{aligned}\mathcal{K}[\rho_c] &= \frac{1}{4}A(c)^2\int_0^\infty\int_0^\infty (x-y)^2\exp\left\{-\frac{1}{2\nu}(x-c)^2-\frac{1}{2\nu}(y-c)^2\right\}\,dx\,dy\\ &= \frac{1}{2}\underbrace{A(c)\int_0^\infty (x-c)^2\exp\left(-\frac{1}{2\nu}(x-c)^2\right)\,dx}_{I}\\ &\qquad -\frac{1}{2}\left[A(c)\int_0^\infty (x-c)\exp\left(-\frac{1}{2\nu}(x-c)^2\right)\,dx\right]^2\\ &= \frac{1}{2}I-\frac{\nu^2}{2}\left(A(c)\exp\left(-\frac{c^2}{2\nu}\right)\right)^2.\end{aligned}$$

The total energy $\mathcal{E}^\nu[\rho_c]$ then reduces to

$$\begin{aligned}\mathcal{E}^\nu[\rho_c] &= \mathcal{K}[\rho_c]+\nu\mathcal{S}[\rho_c]\\ &= \nu\log(A(c))-\frac{\nu^2}{2}\left(A(c)\exp\left(-\frac{c^2}{2\nu}\right)\right)^2\\ &= \nu\log\left(\frac{2}{\sqrt{2\pi\nu}}\right)-\nu\log\left(1+\operatorname{erf}\left(\frac{c}{\sqrt{2\nu}}\right)\right)-\frac{\nu}{4}\left(\frac{\frac{2}{\sqrt{\pi}}\exp\left(-\frac{c^2}{2\nu}\right)}{1+\operatorname{erf}\left(\frac{c}{\sqrt{2\nu}}\right)}\right)^2,\end{aligned}$$

or letting $\widetilde{c}=c/\sqrt{2\nu}$,

$$\mathcal{E}^\nu[\rho_c]=\nu\log\left(\frac{2}{\sqrt{2\pi\nu}}\right)-\nu\left(f(\widetilde{c})+\frac{1}{4}f'(\widetilde{c})^2\right) \tag{2.20}$$

where

$$f(\widetilde{c})=\log\left(1+\operatorname{erf}(\widetilde{c})\right).$$

Then, since $c\to\mathcal{E}^\nu[\rho_c]$ has a critical point and is a smooth function, we have

$$\frac{d}{dc}\mathcal{E}^\nu[\rho_c]=-\sqrt{\frac{\nu}{2}}f'(\widetilde{c})\left(1+\frac{1}{2}f''(\widetilde{c})\right)=0 \tag{2.21}$$

for some $\widetilde{c}\in\mathbb{R}$. Since $f'>0$ and $\min f''=-\frac{4}{\pi}>-2$, however, (2.21) has no solutions. This contradicts the assumption that $\mathcal{E}^\nu$ has a critical point.

(ii) Now choose $g>0$. We proceed as before, only in terms of fixed points of the map $T(\rho)$ defined in (2.8). Borrowing from the calculations above, for any $\rho\in\mathcal{P}_2^{ac}(D)$ we have

$$T(\rho)=Z^{-1}\exp\left(-\frac{K*\rho(x)+V(x)}{\nu}\right)=A(c)\,\exp\left(-\frac{1}{2\nu}\,(x-c)^2\right)$$

where now $c = M_1(\rho) - g$. Since $T$ maps $\mathcal{P}_2^{ac}(D)$ into $\Gamma_c$, by Corollary 2.4 it suffices to look for critical points in $\Gamma_c$. We then proceed as above and first attempt to satisfy the necessary condition $\frac{d}{dc}\mathcal{E}^\nu[\rho_c] = 0$. With $g > 0$ the energy (2.20) becomes

$$\mathcal{E}^\nu[\rho_c] = \nu \log\left(\frac{2}{\sqrt{2\pi\nu}}\right) - \nu\left(f(\widetilde{c}) + \frac{1}{4}f'(\widetilde{c})^2\right) + g\left(\sqrt{\frac{\nu}{2}}f'(\widetilde{c}) + \sqrt{2\nu}\,\widetilde{c}\right)$$

whereby solving $\frac{d}{dc}\mathcal{E}^\nu[\rho_c] = 0$ reduces to finding a root $\widetilde{c}$ to

$$\left(\sqrt{\frac{2}{\nu}}g - f'(\widetilde{c})\right)\left(1 + \frac{1}{2}f''(\widetilde{c})\right) = 0.$$

From (2.21), we know that the second term is strictly positive, so we may divide by it and further reduce the problem to solving

$$f'(\widetilde{c}) = \sqrt{\frac{2}{\nu}}\,g. \tag{2.22}$$

For any $g, \nu > 0$, (2.22) has a unique solution since $f' : \mathbb{R} \to [0, \infty)$ is smooth and monotonically decreasing, so we have that there exists a unique *candidate* critical point $\rho_{c^*} \in \Gamma_c$ where $\frac{c^*}{\sqrt{2\nu}}$ solves (2.22). The measure $\rho_{c^*}$ is then a critical point of $\mathcal{E}^\nu$ over the space $\Gamma_c$. All that remains is to show that $T(\rho_{c^*}) = \rho_{c^*}$ to conclude that $\rho_{c^*}$ is in fact a critical point of $\mathcal{E}^\nu$ over all of $\mathcal{P}_2^{ac}(D)$. Indeed, since $T$ maps into $\Gamma_c$, we have $T(\rho_{c^*}) = \rho_{c'} \in \Gamma_c$ for some $c' \in \mathbb{R}$, and by direct calculation,

$$c' = M_1(\rho_{c^*}) - g = \sqrt{\frac{\nu}{2}}f'\left(\frac{c^*}{\sqrt{2\nu}}\right) + c^* - g = c^*,$$

since $\frac{c^*}{\sqrt{2\nu}}$ solves (2.22). This shows that $\rho_{c'} = \rho_{c^*}$ since every member in $\Gamma_c$ is uniquely determined by its shift $c$. This completes the proof.

□

**Remark 2.14.** For $g = g_c := \sqrt{\frac{2\nu}{\pi}}$, the solution $c$ to (2.22) is exactly $c = 0$, which says that the critical point $\overline{\rho}$ is exactly a half-Gaussian, and for $g \geq g_c$, the peak of $\overline{\rho}$ lies at $x = 0$. We verify this numerically in Chapter 3, Figure 3.1.

The non-existence result (i) in Theorem 2.13 is an example of a more general phenomenon which we refer to as the *escaping mass phenomenon*. The name is in contrast to Lions' concentration compactness lemma [25], which states that any sequence $\{\mu_n\}_{n\in\mathbb{N}}$ of probability measures on $\mathbb{R}^d$ contains a subsequence which is either (i) tight up to translations, (ii) vanishing or (iii) splitting. We will not go into the details of these cases here, but only say that in general domains $D$, it happens that minimizing sequences $\{\mu_n\}_{n\in\mathbb{N}}$ of $\mathcal{E}^\nu$ can be of an entirely different breed: they can be *escaping* in the sense that the centre of

mass $\mathcal{C}(\mu_n)$, defined for $\mu \in \mathcal{P}_1(D)$ by

$$\mathcal{C}(\mu) = \int_D x \, d\mu(x),$$

reaches infinity without the measures actually vanishing. The sequence $\Gamma_c$ of shifted and truncated Gaussians in Theorem 2.13 is one such escaping sequence. Dynamically, the escaping mass phenomenon manifests as a persistent, metastable translation of the centre of mass of the swarm (see Remark 2.17).

Analytically, asymmetries in $D$ cause the energy $\mathcal{E}^\nu$ to lose translation invariance, and so the same tight-up-to-translations arguments from free space do not apply. To enforce the existence of a global minimizer, we can add a confining potential $V$ and exploit any symmetries within $D$. This process is described in Theorems 2.18 and 2.19. To complete the discussion on escaping mass, Theorem 2.15 below provides a necessary condition for the existence of a minimizer in the case of radial $K$ which comes as a direct corollary of the Euler-Lagrange equation.

**Theorem 2.15.** *Let Assumptions 1 and 2 be satisfied and let $K, V \in W^{1,1}_{loc}(D)$ with $K$ radial. Then if $\overline{\rho}$ is a critical point of the energy $\mathcal{E}^\nu$ with $\mathrm{supp}(\overline{\rho}) = D$, then $\overline{\rho}$ satisfies*

$$\nu \int_{\partial D} n(x)\overline{\rho}(x) \, dS(x) = -\int_D \overline{\rho}(x)\nabla V(x) \, dx, \tag{2.23}$$

*where $n(x)$ is the unit normal to the boundary at $x \in \partial D$.*

*Proof.* Assume that $\overline{\rho}$ is such a critical point. Then from Corollary 2.4 we have that

$$\overline{\rho} = Z^{-1} \exp\left(-\frac{K * \overline{\rho} + V}{\nu}\right).$$

Since $K$ is radial and in $W^{1,1}(D)$, we have $K(x) = f(|x|)$ for some $f \in W^{1,1}([0,\infty))$ which implies that $f$ is absolutely continuous, and hence differentiable almost everywhere. Using this regularity, we have that $\overline{\rho}$ is differentiable almost everywhere. Taking the gradient of both sides of the Euler-Lagrange equation (2.3) and integrating against $\overline{\rho}(x) \, dx$ then gives us

$$\nu \int_D \nabla\overline{\rho}(x) \, dx = -\int_D \overline{\rho}(x)\nabla K * \overline{\rho}(x) \, dx - \int_D \overline{\rho}(x)\nabla V(x) \, dx,$$

where the first term on the right-hand side integrates to zero, since

$$\int_D \overline{\rho}(x)\nabla K * \overline{\rho}(x) \, dx = \int_D \int_D f'(|x-y|) \cdot \frac{x-y}{|x-y|}\overline{\rho}(x)\overline{\rho}(y) \, dx \, dy = 0.$$

To integrate the left-hand side we use the divergence theorem. Consider a sequence of bounded sets $A_n \subset D$ with smooth boundary such that $\lim_{n\to\infty} A_n = D$ and $\lim_{n\to\infty} \partial A_n =$

$\partial D$. Then for any fixed $\vec{a} \in \mathbb{R}^d$,

$$\vec{a} \cdot \int_{A_n} \nabla \overline{\rho}(x)\, dx = \int_{A_n} \nabla \cdot (\overline{\rho}(x)\vec{a})\ dx = \int_{\partial A_n} n(x) \cdot (\overline{\rho}(x)\vec{a})\ dS(x) = \vec{a} \cdot \int_{\partial A_n} n(x)\overline{\rho}(x)\, dS(x).$$

Since this holds for any $\vec{a} \in \mathbb{R}^d$, we have $\displaystyle\int_{A_n} \nabla \overline{\rho}(x)\, dx = \int_{\partial A_n} n(x)\overline{\rho}(x)\, dS(x)$, and so

$$\int_D \nabla \overline{\rho}(x)\, dx = \lim_{n\to\infty} \int_{A_n} \nabla \overline{\rho}(x)\, dx = \lim_{n\to\infty} \int_{\partial A_n} n(x)\overline{\rho}(x)\, dS(x) = \int_{\partial D} n(x)\overline{\rho}(x)\, dS(x).$$

By Assumption 2.2 on the smoothness of $D$, we can apply classical trace theorems from [14, Ch. 5] to conclude that the right-most integral is finite. This yields the result. □

**Remark 2.16.** Theorem 2.15 indicates that minimizers of $\mathcal{E}^\nu$ cannot exist for $V = 0$ in a large class of domains (see the Examples section below). This is because when $V = 0$, the right-hand side of (2.23) is zero yet the formula

$$\overline{\rho}(x) = Z^{-1} \exp\left(-\frac{K * \overline{\rho}(x)}{\nu}\right)$$

implies that $\overline{\rho}(x) > 0$ for all $x \in \partial D$, which in turn implies that the left-hand side of (2.23) is nonzero, and so (2.23) cannot hold.

**Remark 2.17.** Condition (2.23) relates to the dynamics of the aggregation-diffusion model (1.20) in the following way. Consider the evolution in time of the centre of mass:

$$\begin{aligned}
\frac{d}{dt}\mathcal{C}(\mu_t^\nu) &= \int_D x \left(\frac{\partial}{\partial t}\rho_t^\nu(x)\right) dx \\
&= \int_D x\nabla \cdot \Big(\rho_t^\nu(x)\Big(\nabla K * \rho_t^\nu(x) + \nabla V(x)\Big) + \nu\nabla\rho_t^\nu(x)\Big)\, dx \\
&= -\int_D \nabla K * \rho_t^\nu(x)\rho_t^\nu(x)\, dx - \int_D \nabla V(x)\rho_t^\nu(x)\, dx - \nu\int_D \nabla\rho_t^\nu(x)\, dx
\end{aligned}$$

(integrating by parts and utilizing the boundary conditions)

$$= -\int_D \nabla V(x)\rho_t^\nu(x)\, dx - \nu\int_{\partial D} n(x)\rho_t^\nu(x)\, dS(x).$$

For $V = 0$, this is exactly

$$\frac{d}{dt}\mathcal{C}\left(\mu_t^\nu\right) = -\nu\int_{\partial D} n(x)\rho_t^\nu(x)\, dS(x), \tag{2.24}$$

which says that the swarm translates in the direction opposite the average outward normal vector with speed proportional to the mass along the boundary, weighted by $\nu$. Unless the

domain is bounded or symmetric enough that mass may be distributed along the boundary in such a way that the right-hand side of (2.24) is zero, translation will occur indefinitely, further justifying the terminology "escaping-mass phenomenon". Clearly this takes effect as soon as $\nu > 0$.

**Examples**

The following are a few example domains where a minimizer $\overline{\rho}$ cannot exist by the argument in Remark 2.16.

1. Half-space: Here $D = \mathbb{R}^d_+ := \mathbb{R}^{d-1} \times [0, \infty)$ where $n(x) = -\hat{e}_d$ is constant for all $x \in \partial D$. This gives

$$\int_{\partial D} n(x)\overline{\rho}(x) dS(x) \;=\; -\hat{e}_d \int_{\mathbb{R}^{d-1}} \overline{\rho}(x)\, dx_1 \dots\, dx_{d-1} \;<\; 0.$$

   Note that Theorem 2.13 demonstrates this case for $d = 1$.

2. Wedge domain: $D = \{x \in \mathbb{R}^2 \;:\; 0 \le x_2 \le \tan(\phi) x_1\}$ for $\phi \in (0, \pi/2)$. Then

$$\int_{\partial D} n(x)\overline{\rho}(x)\, dS(x) \;=\; (N_1, N_2)$$

   where

$$N_1 = -\sin(\phi) \int_0^\infty \overline{\rho}(z, \tan(\phi) z)\, dz < 0.$$

3. Paraboloid: Let $x = (x_1, \dots, x_{d-1}, x_d) = (x', x_d) \in \mathbb{R}^d$ and define

$$D = \left\{ x \in \mathbb{R}^d \;:\; x_d \ge |x'|^2 \right\}.$$

   Then $n(x) = \dfrac{1}{\sqrt{|x'|^2 + \frac{1}{4}}} \left( x', -\frac{1}{2} \right)$ and so

$$\int_{\partial D} n(x)\overline{\rho}(x)\, dS(x) = (N', N_d)$$

   where again $N_d$ cannot be zero.

In the next section we establish a relation between the domain geometry and the external potential $V$, motivated by Theorem 2.15, that ensures existence of a minimizer.

## 2.3 Existence of Global Minimizers

Given the considerations above, in the absence of an external potential $V$ there does not exist a global minimizer for $\mathcal{E}^\nu$ in many canonical domains, despite $\mathcal{E}^\nu$ being bounded below. With insight from Theorem 2.15, we present here a recipe for guaranteeing existence

of a global minimizer through the addition of a suitable external potential $V$. Recall that this was done above in the case of $K(x) = \frac{1}{2}x^2$ and $D = [0, \infty)$ for $V(x) = gx$. Theorem 2.18 establishes a condition on $V$ (2.26) that is in some sense minimal and that guarantees existence of a global minimizer of $\mathcal{E}^\nu$ for general domains $D$ satisfying Assumption 2. Theorem 2.19 then provides a weaker set of requirements on $V$ which takes advantage of symmetries within the domain.

**Theorem 2.18.** *Suppose $K$ and $V$ are positive and satisfy Assumption 1, and that $D \subset \mathbb{R}^d$ satisfies Assumption 2. Then there exists a global minimizer $\overline{\rho} \in \mathcal{P}^{ac}(D)$ of $\mathcal{E}^\nu$, that is,*

$$\mathcal{E}^\nu[\overline{\rho}] = \inf_{\rho \in \mathcal{P}(D)} \mathcal{E}^\nu[\rho] > -\infty,$$

*if for some $\delta \in (0, 1/2)$ and $C_K \in \mathbb{R}$*

$$K(x) \geq \frac{2d\nu}{1-\delta} \log|x| + C_K, \tag{2.25}$$

*and $V$ satisfies, for some $x_0 \in D$,*

$$\liminf_{R \to \infty} \left( \inf_{x \in B_R^c(x_0)} V(x) \right) = +\infty. \tag{2.26}$$

*Proof.* We will first show that the energy $\mathcal{E}^\nu$ is bounded below and then prove that minimizing sequences are tight. Indeed, the boundedness from below of $\mathcal{E}^\nu$ follows from results in free space. By Theorem 2.9 above, relation (2.25) between $K$ and $\nu$ is sufficient to guarantee that $\mathcal{E}^\nu$ is bounded below over $\mathcal{P}(\mathbb{R}^d)$ by a constant $C \in \mathbb{R}$ when $V = 0$.

Since $|D| > 0$ and we are not requiring any regularity of measures other than absolute continuity with respect to Lebesgue measure, from any $\mu \in \mathcal{P}^{ac}(D)$ with density $\rho$ we can define a measure $\mu_0 \in \mathcal{P}^{ac}(\mathbb{R}^d)$ with density $\rho_0(x)$ by extending $\rho$ by zero:

$$\rho_0(x) = \begin{cases} \rho(x), & x \in D \\ 0, & x \in D^c. \end{cases}$$

For each $\mu \in \mathcal{P}^{ac}(D)$ we then have the lower bound

$$\begin{aligned} \mathcal{E}^\nu[\mu] &= \frac{1}{2} \int_D \int_D K(x-y)\, d\mu(x)\, d\mu(y) + \nu \int_D \rho(x) \log(\rho(x))\, dx + \int_D V(x)\, d\mu(x) \\ &= \frac{1}{2} \int_{\mathbb{R}^d} \int_{\mathbb{R}^d} K(x-y)\, d\mu_0(x)\, d\mu_0(y) + \nu \int_{\mathbb{R}^d} \rho_0(x) \log(\rho_0(x))\, dx + \int_D V(x)\, d\mu(x) \\ &> C + \int_D V(x)\, d\mu(x), \end{aligned}$$

which implies

$$\int_D V(x)\, d\mu(x) < \mathcal{E}^\nu[\mu] - C. \tag{2.27}$$

Now consider a minimizing sequence $\{\mu_n\}_{n\geq 0} \subset \mathcal{P}^{ac}(D)$ of $\mathcal{E}^\nu$. The following argument shows that $\{\mu_n\}_{n\geq 0}$ is tight. Since $\{\mu_n\}_{n\geq 0}$ is minimizing, we can assume $\{\mathcal{E}^\nu[\mu_n]\}_{n\geq 0}$ is bounded above; hence (2.27) implies

$$\sup_n \int_D V(x)\, d\mu_n(x) < M \tag{2.28}$$

for some $M \in \mathbb{R}$. Fix $\epsilon > 0$ and let $L > 0$ be large enough that $M/L < \epsilon$. From (2.26), to $L$ there corresponds an $R$ such that

$$\inf_{x \in B_R^c(x_0)} V(x) > L.$$

For each $\mu_n$ we then have

$$L \int_{B_R^c(x_0)\cap D} d\mu_n(x) \leq \int_{B_R^c(x_0)\cap D} V(x)\, d\mu_n(x) \leq \int_D V(x)\, d\mu_n(x) < M,$$

hence for the compact set $K_\epsilon = B_R(x_0) \cap D$,

$$\mu_n(K_\epsilon) > 1 - \epsilon.$$

This shows that the minimizing sequence $\{\mu_n\}_{n\geq 0}$ is tight. By Prokhorov's theorem we may then extract a subsequence $\{\mu_{n_k}\}_{k\geq 0}$ which converges in the weak-* topology of measures to some $\overline{\rho} \in \mathcal{P}(D)$. It follows from the weak-* lower semicontinuity of $\mathcal{E}^\nu$ (Lemma 2.10) that

$$\mathcal{E}^\nu[\overline{\rho}] \leq \liminf_{n\to\infty} \mathcal{E}^\nu[\rho_n] = \lim_{n\to\infty} \mathcal{E}^\nu[\rho_n] = \inf_{\rho\in\mathcal{P}(D)} \mathcal{E}^\nu,$$

and so $\overline{\rho}$ realizes the infimum.

□

The previous theorem provides a way to guarantee existence of a minimizer in all domains $D$ satisfying Assumption 2, simply by using an external potential to contain the mass and enforce tightness. As the following theorem shows, in many domains a less restrictive external potential is sufficient to ensure a minimizer.

We will need some terminology for the next theorem. Define a *band* $S_a^i$ in $\mathbb{R}^d$ by

$$S_a^i = \left\{ x \in \mathbb{R}^d \,:\, |x_i| < a \right\}.$$

Also, we define a function $f : \mathbb{R}^d \to Y$, where $Y$ is some set, as *discrete-translation invariant in* $\vec{u}$ if there exists $\vec{u} \in \mathbb{R}^d$ such that for any $m \in \mathbb{Z}$,

$$f(x + m\vec{u}) = f(x) \quad \text{for all} \quad x \in \mathbb{R}^d.$$

**Theorem 2.19.** *Let $(x_1, \dots, x_d)$ be a fixed orthogonal coordinate system for $\mathbb{R}^d$. Suppose the hypotheses of Theorem 2.18 are satisfied, except that (2.26) is replaced with the following: for each coordinate $x_i$, at least one of the following holds:*

*(i) $D$ is bounded in $x_i$.*

*(ii) $V$ is unbounded in $x_i$ of the form*

$$\liminf_{a \to \infty} \left( \inf_{x \in (S_a^i)^c} V(x) \right) = +\infty.$$

*(iii) $D$ and $V$ are discrete-translation invariant in $s_i \hat{e}_i$ for some $s_i > 0$.*

*Then there exists a global minimizer $\overline{\rho} \in \mathcal{P}(D)$ of $\mathcal{E}^\nu$.*

*Proof.* As before, we consider a minimizing sequence $\{\mu_n\}_{n \geq 0} \subset \mathcal{P}(D)$ for $\mathcal{E}^\nu$ over $\mathcal{P}(D)$, where we assume that $\{\mathcal{E}^\nu[\mu_n]\}_{n \geq 0}$ is bounded above by some $\widetilde{M} > 0$. Again, (2.25) implies that $\{\mathcal{E}^\nu[\mu_n]\}_{n \geq 0}$ is bounded below, and so the upper bound (2.28) on $\{\mathcal{V}[\mu_n]\}_{n \geq 0}$ still holds.

We can no longer extract tightness just from $V$, however, so we will now exploit the fact that the interaction portion $\mathcal{K}$ of the energy is bounded in order to use Lemma 2.12, from which it follows that $\{\mu_n\}_{n \geq 0}$ is tight up to translations *in free space*. With each coordinate $x_i$ satisfying at least (i), (ii) or (iii), this is enough to guarantee the existence of a translated sequence $\{\widetilde{\mu}_n\}_{n \geq 0}$ that lies in $\mathcal{P}(D)$ and remains minimizing. With some abuse of notation, given the discussion in Theorem 2.18, we will use $\mu_n$ to refer interchangeably to a measure on $D$ and a measure on all of $\mathbb{R}^d$ such that $\mu_n(D^c) = 0$.

To see that the interaction portion of the energy is bounded, we reuse some arguments from [10]. Namely, the logarithmic HLS inequality together with (2.25) imply that for each $\mu \in \mathcal{P}^{ac}(D)$ with $d\mu(x) = \rho(x)\,dx$,

$$\begin{aligned}
\nu \mathcal{S}[\mu] &\geq -\nu d \int_{\mathbb{R}^d} \int_{\mathbb{R}^d} \log(|x - y|) \rho(x) \rho(y)\, dx\, dy - \nu d C_0 \\
&\geq -\frac{1 - \delta}{2} \int_{\mathbb{R}^d} \int_{\mathbb{R}^d} K(x - y)\, d\mu(x)\, d\mu(y) - \nu d C_0 + \frac{1 - \delta}{2} C \\
&= -(1 - \delta) \mathcal{K}[\mu] - \nu d C_0 + \frac{1 - \delta}{2} C,
\end{aligned}$$

hence for each $\mu_n$,

$$\delta\mathcal{K}[\mu_n] \leq \mathcal{K}[\mu_n] + \nu\mathcal{S}[\mu_n] + \mathcal{V}[\mu_n] + \nu d C_0 - \frac{1-\delta}{2}C \leq \mathcal{E}^\nu[\mu_n] + \widetilde{C}$$

which shows that $\{\mathcal{K}[\mu_n]\}_{n\geq 0}$ is bounded since $\sup_n \mathcal{E}^\nu[\mu_n] < \widetilde{M}$. By Lemma 2.12 we now have that $\{\mu_n\}_{n\geq 0}$ is tight up to translations in free space.

We now construct a tight, translated version of $\{\mu_n\}_{n\geq 0}$ that retains the property $\mu_n(D) = 1$ and remains energy-minimizing. To do so we address each coordinate $x_i$ and consider the three cases above. Let $\epsilon > 0$ be given.

(i) For each $x_i$ in which $D$ is bounded, let $L_i = \sup_{x\in D} |x_i|$ and note that for each $n$

$$\mu_n(S^i_{L_i}) = 1 > 1 - \epsilon.$$

(ii) Similarly, for each $x_i$ in which $V$ satisfies

$$\liminf_{a\to\infty} \left( \inf_{x\in(S^i_a)^c} V(x) \right) = +\infty,$$

there exists $L_i > 0$ such that

$$\mu_n(S^i_{L_i}) > 1 - \epsilon$$

uniformly in $n$ by a similar argument as in Theorem 2.18: since $\{\mathcal{V}[\mu_n]\}_{n\geq 0}$ is bounded above by some $M > 0$, let $L$ be large enough that $M/L < \epsilon$. Then there exists $L_i > 0$ such that

$$\inf_{x\in\left(S^i_{L_i}\right)^c} V(x) > L,$$

hence

$$\int_{\left(S^i_{L_i}\right)^c \cap D} d\mu_n(x) \leq \frac{1}{L}\int_{\left(S^i_{L_i}\right)^c \cap D} V(x)\, d\mu_n(x) \leq \frac{1}{L}\int_D V(x)\, d\mu_n(x) < \epsilon.$$

(iii) Now consider the index set $I$ of coordinates $x_i$ for which $D$ and $V$ are discrete-translation invariant in $s_i\hat{e}_i$ for some $s_i > 0$. First we note that if $D$ is discrete-translation invariant, then so are $\mathcal{K}$ and $\mathcal{S}$ by a change of variables. If $V$ is also discrete-translation invariant, then so is $\mathcal{V}$, hence for each $i \in I$, the energy $\mathcal{E}^\nu$ is discrete-translation invariant in $s_i\hat{e}_i$.

Let $\{\mu^1_n\}_{n\geq 0} = \{\mu_n(x - x^{n,1})\}_{n\geq 0}$ be a translated sequence which is tight but may no longer satisfy $\mu^1_n(D) = 1$. Without loss of generality we have $x^{n,1}_i = 0$ for $i \notin I$ using the arguments above for (i) and (ii), so translations have only occurred in coordinates $x_i$ for $i \in I$.

Now define another translated sequence $\{\mu_n^2\}_{n\geq 0}$ by

$$\mu_n^2 := \mu_n^1(x + \widetilde{x}^{n,1}) = \mu_n(x - x^{n,2})$$

where the translations are defined by

$$x^{n,2} := x^{n,1} - \sum_{\substack{i=1\\ i\in I}}^{d} \operatorname{mod}\left(x_i^{n,1}, s_i\right)\hat{e}_i := x^{n,1} - \widetilde{x}^{n,1}$$

where

$$\operatorname{mod}\left(x_i^{n,1}, s_i\right) := x_i^{n,1} - \Big\lfloor \frac{x_i^{n,1}}{s_i} \Big\rfloor s_i.$$

From this we get for each $i \in I$ that

$$x_i^{n,2} = \Big\lfloor \frac{x_i^{n,1}}{s_i} \Big\rfloor s_i = m_i^n s_i \quad \text{for some} \quad m_i^n \in \mathbb{Z},$$

hence by discrete translation invariance,

$$\mu_n^2(D) = \mu_n\left(D - x^{n,2}\right) = \mu_n\left(D - \sum_{\substack{i=1\\ i\in I}}^{d} m_i^n s_i \hat{e}_i\right) = \mu_n(D) = 1,$$

and so $\{\mu_n^2\}_{n\geq 0}$ lies in $\mathcal{P}(D)$. Similarly,

$$\mathcal{E}^\nu[\mu_n^2] = \mathcal{E}^\nu\left[\mu_n\left(x - \sum_{\substack{i=1\\ i\in I}}^{d} m_i s_i \hat{e}_i\right)\right] = \mathcal{E}^\nu[\mu_n],$$

thus $\{\mu_n^2\}_{n\geq 0}$ retains the minimizing property of the original sequence $\{\mu_n\}_{n\geq 0}$. To see that $\{\mu_n^2\}_{n\geq 0}$ is tight, we can use the fact that $\{\mu_n^1\}_{n\geq 0}$ is tight to find a compact set $K_\epsilon^1 \subset \mathbb{R}^d$ for which $\mu_n^1(K_\epsilon^1) > 1 - \epsilon$ for each $n$. Since

$$\left|x^{n,2} - x^{n,1}\right| \leq \sqrt{d}\max_{i\in I} s_i,$$

the compact set

$$K_\epsilon^2 = \left\{x \in D \,:\, \operatorname{dist}\left(x, K_\epsilon^1\right) \leq \sqrt{d}\max_{i\in I} s_i\right\}$$

satisfies $\mu_n^2(K_\epsilon^2) > 1 - \epsilon$ for each $n$. We may now apply Prokhorov's theorem and lower semicontinuity of the energy to extract a convergent subsequence $\left\{\mu_{n_k}^2\right\}_{k\geq 0}$ such that $\mu_{n_k}^2 \overset{*}{\rightharpoonup} \overline{\rho} \in \mathcal{P}(D)$ and $\mathcal{E}^\nu[\overline{\rho}] = \inf \mathcal{E}^\nu > -\infty$. This completes the proof. □

**Remark 2.20.** Theorem 2.19, although more technical, is designed to capture many practical cases. As it reads, one such case is that of the half-space domain $D = \mathbb{R}^{d-1} \times [0, \infty)$

together with a potential $V$ of the form

$$V(x) = V(x_d) \leq C x_d^p$$

which only depends on the final coordinate. This is the case commonly considered when modeling a swarm in a gravitational field. Another case is that of an infinite channel $D = B_R^{d-1}(0) \times \mathbb{R}$ where $B_R^{d-1}$ is a $(d-1)$-dimensional ball of radius $R$ centred at zero. Since the infinite channel is either bounded or translation invariant in each coordinate, a global minimizer exists for $V = 0$.

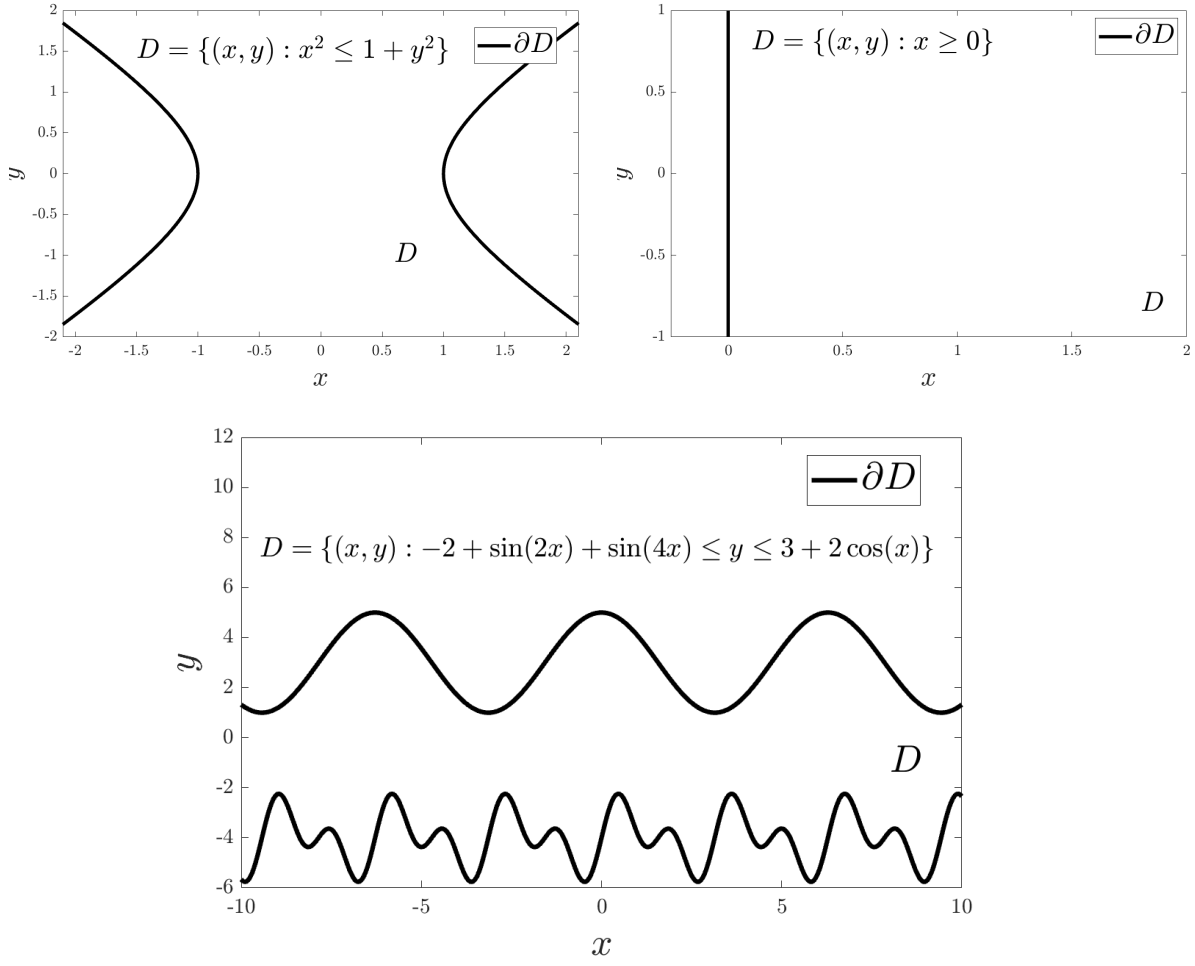


Figure 2.2: Example domains with different requirements on the external potentials for existence of a global minimizer. Top left: domain with hyperbolic boundaries which does not offer translation symmetry or boundedness in any coordinate, but for example $V = |x|^p$ satisfies the conditions of Theorem 2.18 for any $p > 0$ and so grants a minimizer. Top right: half plane—a minimizer exists under the potential $V = gx$ for any $g > 0$. Bottom: domain with periodic boundaries, discrete-translation invariant in $x$ and bounded in $y$, hence by Theorem 2.19 a minimizer exists under $V = 0$.

# Chapter 3

# Computation of Critical Points

In this section we introduce two iterative methods for computing critical points of $\mathcal{E}^\nu$ as well as an implicit-explicit scheme for solving the aggregation-diffusion equation (1.20) on a bounded domain using finite differences. Using these methods, we perform numerical experiments on a bounded interval. Motivated by Theorems 2.2 and 2.13, we examine purely attractive potentials and examine the limit of infinite attraction strength at finite distance. We then look at attractive-repulsive potentials and the formation of states with multiple separated aggregations. In the former case we believe that a unique critical point exists (the global minimizer), although we have not yet been able to prove this. In the latter case, we show directly an example of non-uniqueness of critical points (see Figure 3.6).

For each computed critical point we show that the Euler-Lagrange equation (2.3) is satisfied, and where applicable, we verify the boundary condition (2.23). We also note that each critical point computed using the iterative methods below has been verified to be stationary under the PDE solver; however, we omit this from the figures in below. Together these criteria verify that a critical point has been found, although we cannot determine whether a critical point is a local extremizer or saddle point using the methods in this chapter.

**Remark 3.1.** Due to the exponential decay of critical points it can be assumed that for sufficiently large $L$, critical points computed on the interval $D = [0, L]$ are good approximations of critical points computed on unbounded domains. In light of Theorem 2.15, which implies that for $V = 0$ no critical points exist on the half-line, computations made below with $V = 0$ should be interpreted as approximations to critical points in free space ($D = \mathbb{R}$), and computations made with $V \neq 0$ should be interpreted as approximations to critical points on the half line $D = [0, \infty)$.

## 3.1 Fixed-Point Iterator

The following scheme computes critical points of $\mathcal{E}^\nu$ by discretizing the map $T : \mathcal{P}(D) \to \mathcal{P}(D)$ given in (2.8). Recall that we define

$$T(\rho) := \frac{\exp\left(-\dfrac{K*\rho+V}{\nu}\right)}{\displaystyle\int_D \exp\left(-\frac{K*\rho+V}{\nu}\right)dx} = Z^{-1}(\rho)\exp\left(-\frac{K*\rho+V}{\nu}\right)$$

and that fixed points of $T$ are critical points of $\mathcal{E}^\nu$ (in particular, the set of fixed points of $T$ are exactly the critical points of $\mathcal{E}^\nu$ which are absolutely continuous and supported on the whole domain). We use the iterative scheme

$$\rho^{n+1} = (1-\tau_n)\rho^n + \tau_n T(\rho^n) \tag{3.1}$$

where

$$\tau_n = \begin{cases} 1, & \mathcal{E}^\nu\left[T(\rho^n)\right] < \mathcal{E}^\nu[\rho^n] \\ \tau_c, & \text{otherwise} \end{cases} \tag{3.2}$$

with inputs $\tau_c \in (0,1)$ and $\rho^0 \in \mathcal{P}^{ac}(D)$. In words, each iteration produces an absolutely continuous probability measure $\rho^{n+1}$ that is a convex combination of the previous iterate $\rho^n$ and its image under $T$, unless the energy of $T(\rho^n)$ is lower than that of $\rho^n$, in which case $\rho^{n+1} = T(\rho^n)$. Each step requires computation of the integral terms in $T(\rho^n)$ and $\mathcal{E}^\nu[\rho^n]$, which for $D = [0, L]$ is done by discretizing the interval into $N$ quadrature nodes and numerically integrating. For uniform grids, we use MATLAB's `conv` function to compute $K*\rho^n$, while for non-uniform grids we use trapezoidal integration. The scheme is terminated when

$$\|\rho^n - T(\rho^n)\|_{L^1(D)} < \text{tol} \quad \text{or} \quad n > N_{\max} \tag{3.3}$$

where tol and $N_{\max}$ are specified by the user.

### 3.1.1 Stability Constraints

The scheme (3.1) has many benefits. It is explicit, so only numerical integration is required at each step, which allows for flexibility of the spatial grid. It is also positivity preserving, something that the Newton continuation method and PDE solver below cannot guarantee. Due to the explicit nature, however, there are a few stability constraints.

#### Oscillations

The first stability constraint has to do with preventing spurious oscillations and can be explained by casting the scheme as a discretization of the following integro-differential

equation: assuming $\tau_n \ll 1$, (3.1) can be viewed as a forward-Euler discretization of

$$\begin{cases} \dfrac{\partial}{\partial t}\rho(x,t) = T(\rho(x,t)) - \rho(x,t), & (x,t) \in D \times (0,\infty) \\ \quad \rho(x,0) = \rho_0(x) \in \mathcal{P}^{ac}(D), & x \in D \end{cases} \tag{3.4}$$

whose steady states are exactly the fixed points of $T$. Details on the global well-posedness of (3.4) when $D$ is bounded, $K$ is bounded below, and $V$ is positive can be found in Appendix A, where it is shown that $T$ is $L^1$ Lipschitz continuous on $\mathcal{P}^{ac}(D)$ and that $\rho(x,t) \in \mathcal{P}^{ac}(D)$ for all $t \in [0,\infty)$.

For any point $x^* \in D$, the time evolution of $\rho(x^*,t)$ under the PDE (3.4) is such that $\rho(x^*,t)$ increases when $\rho(x^*,t) < T(\rho(x^*,t))$ and decreases when $\rho(x^*,t) > T(\rho(x^*,t))$. Analytically, if $\rho_0$ lies in the basin of attraction of some fixed point $\overline{\rho}$ of $T$, we have the convergence $\lim_{t\to\infty}\rho(x^*,t) = \overline{\rho}(x^*)$. If $\rho(x^*,t)$ oscillates around $\overline{\rho}(x^*)$ as it approaches $\overline{\rho}(x^*)$, however, numerically one needs to be concerned with the spurious growth of such oscillates. Indeed, oscillations do appear in the fixed-point method (3.1) for "timesteps" $\tau_c$ that are too large, in which case the iterates $\rho^n$ cycle indefinitely through a finite set of measures.

To arrive at a stable value of $\tau_c$ which prevents oscillations, we examine the bound on the $L^1$-Lipschitz constant $L_T$ of $T$ derived in Appendix A:

$$L_T \le \frac{2}{\nu}\left\|\widetilde{K}\right\|_{L^\infty(D-D)} \exp\left(\frac{1}{\nu}\left\|\widetilde{K}\right\|_{L^\infty(D-D)}\right),$$

where $D - D := \left\{x - y \in \mathbb{R}^d \,:\, x, y \in D\right\}$ and $\widetilde{K} := K - \min_{x\in(D-D)}$.

This may not be a very encouraging bound due to the exponential dependence on $\|K\|_\infty$, but it does suggest that $\tau_c$ should be proportional to $\nu$. In practice, we find that $\tau_c$ need not depend on $\|K\|_\infty$ and that the scheme converges to a fixed point for $\tau_c = \mathcal{O}(\nu)$. (In all computations below, $\tau_c = 5\nu$ was sufficient.) When $\nu$ is small, this increases the number of iterations, which necessitates the use of a faster method to arrive at a good initial guess, which is where the Newton continuation method below comes in.

**Normalization and Underflow**

Another numerical issue is round-off error. Assuming for the moment that $K$ and $V$ are both positive, when $\nu$ is small the argument of the exponent in $T$ is negative and large in magnitude. This results in underflow of digits when calculating $Z(\rho)$ and subsequent division by a small quantity. To avoid this, we exploit the fact that the set of critical points of $\mathcal{E}^\nu$ is unchanged by adding a constant to $K$ and at each step normalize the argument

of the exponent by adding to $K$ the factor $c_n := -\nu \log Z(\rho^{n-1})$. The potential used in simulations then changes at each iteration and is given by $K_n(x) = K_{n-1}(x) + c_n$ with $K_0 = K$. For $Z(\rho^n)$ we then have

$$Z(\rho^n) = Z(\rho^{n-1}) \int_D \exp\left(-\frac{K_{n-1} * \rho^n(x) + V}{\nu}\right) dx,$$

and so as $\rho^n \to \overline{\rho}$ we see that $Z(\rho^n) \to 1$. This normalization turns out to stabilize the problem, and results in the constant on the right-hand side of the Euler-Lagrange equation (2.3) conveniently converging to zero, since the true value $\lambda$ is equal to $-\nu \log Z(\overline{\rho})$.

## 3.2 Newton Continuation Method

The following method works very well for producing near-critical points of $\mathcal{E}^\nu$ when $V = 0$, and thus is used to arrive at a good initial guess for the fixed-point iterator. Consider the domain $D = [0, L]$ and a critical point $\overline{\rho}$ of $\mathcal{E}^\nu$ with $V = 0$. By differentiating the Euler-Lagrange equation in the form

$$K * \overline{\rho} + \nu \log(\overline{\rho}) = \lambda$$

we obtain

$$\overline{\rho} K' * \overline{\rho} + \nu \overline{\rho}' = 0.$$

If $\rho$ is an approximate minimizer with $\rho + \xi = \overline{\rho}$ for some perturbation $\xi \in L^1(D)$ with $\int_0^L \xi(x)dx = 0$ and $\xi \geq -\rho$, then we arrive at

$$\begin{aligned} 0 &= \overline{\rho} K' * \overline{\rho} + \nu \overline{\rho}' \\ &= (\rho K' * \rho + \nu \rho') + (\xi K' * \rho + \rho K' * \xi) + (\xi K' * \xi + \nu \xi') \\ &\approx (\rho K' * \rho + \nu \rho') + (\xi K' * \rho + \rho K' * \xi) + \nu \xi' \end{aligned}$$

or, neglecting the quadratic term $\xi K' * \xi$,

$$\rho K' * \xi + (K' * \rho)\xi + \nu \xi' = -\left(\rho K' * \rho + \nu \rho'\right).$$

From this we craft a Newton iteration of the form

$$\begin{cases} \mathcal{F}^n \xi^n = b^n, \\ \rho^{n+1} = \rho^n + \xi^n, \\ \rho^0 \in \mathcal{P}(D) \end{cases} \tag{3.5}$$

for right-hand side

$$b^n := -\left(\rho^n K' * \rho^n + \nu \rho^{n\prime}\right)$$

and integro-differential operator

$$\mathcal{F}^n\xi^n(x) := \rho^n \int_0^L K'(x-y)\xi^n(y)\,dy + \left(K' * \rho^n(x)\right)\xi^n(x) + \nu\frac{d}{dx}\xi^n(x).$$

Since $\mathcal{F}^n$ is linear in $\xi^n$, the iteration scheme (3.5) can be easily discretized. We use a mesh $0 = x_0 < \cdots < x_M = L$ where $\mathbf{p}^n$ is the iterate $\rho^n$ represented on the mesh. This gives the linear system

$$\mathbf{F}^n\mathbf{x}^n := \begin{bmatrix} \widetilde{\mathbf{F}}^n \\ a_n, \ldots, a_n \end{bmatrix} \mathbf{x}^n = \begin{bmatrix} \widetilde{\mathbf{b}}^n \\ 0 \end{bmatrix} =: \mathbf{b}^n.$$

$\widetilde{\mathbf{F}}^n$ takes the form

$$\widetilde{\mathbf{F}}^n = \operatorname{diag}\left(\mathbf{p}^{n-1}\right)\mathbf{K} + \operatorname{diag}\left(\mathbf{K}\mathbf{p}^{n-1}\right) + \nu\mathbf{D}_1$$

and

$$\widetilde{\mathbf{b}}^n = -\left(\operatorname{diag}\left(\mathbf{p}^{n-1}\right)\mathbf{K}\,\mathbf{p}^{n-1} + \nu\mathbf{D}_1\mathbf{p}^{n-1}\right).$$

The zero-mass condition is enforced by the bottom row of $\mathbf{F}^n$ and corresponding 0 on the right-hand side, where the factor $a_n$ is chosen at each stage to match the scaling of $\widetilde{\mathbf{F}}^n$. (Admittedly, the constraint $\xi \geq -\rho$ is not incorporated). In addition, $\mathbf{D}_1$ is the centred finite difference matrix used to discretize the first derivative and $\mathbf{K}$ is the matrix used to discretize the linear convolution with $K'$ to first-order accuracy in the mesh width. The iterates are updated using $\mathbf{p}^n = \mathbf{p}^{n-1} + \mathbf{x}^n$ and the scheme runs until either

$$\|\mathbf{x}\|_\infty < \text{tol} \quad \text{or} \quad n > N_{\max}. \tag{3.6}$$

To reach small values of $\nu$, we employ continuation on the diffusion coefficient. This entails solving (3.5) along the sequence $\nu_0 > \cdots > \nu_i > \cdots > \nu_Q = \nu$ and at the $i$th stage setting the initial guess $\mathbf{p}_i^0$ to the output of the $(i-1)$st stage, assuming the scheme has converged for $\nu_{i-1}$. For small $\nu$ a fine mesh is still unavoidable (with spacing on the order of $1/\nu$) to keep the condition number of $\mathbf{F}^n$ reasonably low. If $\mathbf{F}^n$ were to become rank-deficient, the least-squares solution can be constructed directly using the SVD and casting out singular values below a certain tolerance. This has been observed but not for any of the parameters used in the numerical experiments below.

## 3.3 PDE Solver

We now introduce an implicit-explicit finite difference discretization of the aggregation-diffusion PDE (1.20), which was communicated to us by Theodore Kolokolnikov. Although the following method is designed in one dimension for $D = [0, L]$, we note that it readily extends to tensor product domains in higher dimensions by taking Kronecker products of the operators introduced below. In particular, the extension to a square $[0, L] \times [0, L]$ is

straight forward.

In one dimension, the PDE we wish to solve is

$$\begin{cases} \dfrac{\partial}{\partial t}\rho(x,t) = -\dfrac{\partial}{\partial x}\left(\rho(x,t)v(x,t)\right) + \nu\dfrac{\partial^2}{\partial x^2}\rho(x,t) & (x,t) \in (0,L)\times(0,T) \\ v(x,t)\rho(x,t) = \nu\dfrac{\partial}{\partial x}\rho(x,t) & (x,t) \in \{0,L\}\times(0,T) \\ v(x,t) = -\displaystyle\int_0^L K'(x-y)\rho(y,t)dx - V'(x) & \\ \rho(x,0) = \rho_0(x) \in \mathcal{P}([0,L]). & \end{cases} \tag{3.7}$$

We will do so by treating the swarm velocity $v$ explicitly and the flux and diffusion terms implicitly. The main difficulties in discretizing the PDE are ensuring that the scheme obeys conservation of mass and satisfying the no-flux boundary conditions.

Let $x_0 = 0, \ldots, x_M = L$ and $t_0 = 0, \ldots, t_N = T$ be uniform grids in space and time defined by $x_j = j\Delta x = j\frac{L}{M}$ and $t_n = n\Delta t = n\frac{T}{N}$. As well, let $U^n = [U_0^n, \ldots, U_M^n]^T$ and $V^n = [V_0^n, \ldots, V_M^n]^T$ be approximations to the density $\rho(x, t_n)$ and swarm velocity $v(x, t_n)$ at time $t_n$ represented on the spatial grid. The scheme involves solving the following linear system, where second-order centred finite difference operators $\mathbf{D}_1$ and $\mathbf{D}_2$ have been used to approximate spatial derivatives, with their first and last rows modified to account for mass conservation:

$$\begin{cases} \dfrac{U_j^{n+1} - U_j^n}{\Delta t} = -\dfrac{1}{2\Delta x}\left(U_{j+1}^{n+1}V_{j+1}^n - U_{j-1}^{n+1}V_{j-1}^n\right) + \dfrac{\nu}{\Delta x^2}\left(U_{j+1}^{n+1} - 2U_j^{n+1} + U_{j-1}^{n+1}\right), \quad j = 1, \ldots, M-1 \\ \dfrac{U_0^{n+1} - U_0^n}{\Delta t} = -\dfrac{1}{2\Delta x}\left(U_0^{n+1}V_0^n + U_1^{n+1}V_1^n\right) + \dfrac{\nu}{\Delta x^2}\left(U_1^{n+1} - U_0^{n+1}\right) \\ \dfrac{U_M^{n+1} - U_M^n}{\Delta t} = \dfrac{1}{2\Delta x}\left(U_{M-1}^{n+1}V_{M-1}^n + U_M^{n+1}V_M^n\right) + \dfrac{\nu}{\Delta x^2}\left(U_M^{n+1} - U_{M-1}^{n+1}\right). \end{cases}$$

(As we will see below, modifying the first and last rows of $\mathbf{D}_1$ and $\mathbf{D}_2$ as above also implements the boundary conditions to leading order.) In matrix form, the update $U^{n+1}$ satisfies

$$\mathbf{A}^n U^{n+1} = U^n$$

where

$$\mathbf{A}^n = \mathbf{I}_{M+1} + \Delta t\, \mathbf{B}^n = \mathbf{I}_{M+1} + \Delta t\left[\mathbf{D}_1 \mathrm{diag}\left(V^n\right) - \nu\mathbf{D}_2\right],$$

$\mathbf{I}_{M+1}$ being the identity matrix. We compute the velocity $V^n$ from $U^n$ at each step with MATLAB's `conv`.

**Mass Conservation and Positivity**

At the PDE level, for all time $t > 0$ we have $\int_D \rho(x,t)dx = \int_D \rho(x,0)dx$, which is enforced at the discrete level if the columns of $\mathbf{B}^n$ sum to zero. To see this, in the discrete setting the mass constraint is $\sum_{j=0}^{M} U_j^n = \sum_{j=0}^{M} U_j^0$ for all times $t_n$, which for $e_{M+1}^T = [1, \ldots, 1]$ is equivalent to

$$e_{M+1}^T U^{n+1} = e_{M+1}^T U^n = e_{M+1}^T \mathbf{A}^n U^{n+1}$$

or

$$\left(e_{M+1}^T - e_{M+1}^T \mathbf{A}^n\right) U^{n+1} = 0$$

for all $n = 0, \ldots, N-1$. To ensure this, it is sufficient to enforce

$$e_{M+1}^T = e_{M+1}^T \mathbf{A}^n = e_{M+1}^T + \Delta t \left(e_{M+1}^T \mathbf{B}^n\right);$$

this is equivalent to $e_{M+1}^T \mathbf{B}^n = 0$, which states that the columns of $\mathbf{B}^n$ sum to zero. By the structure of $\mathbf{D}_1$ and $\mathbf{D}_2$, this is automatically satisfied for columns 1 through $M-1$, and with the 0-th and $M$-th rows modified as above, columns 0 and $M$ do indeed sum to zero as well, and so the scheme does conserve mass at the discrete level.

Positivity of solutions is not guaranteed *a priori* and negative mass may occur for spatial discretizations that are too coarse compared with the diffusivity $\nu$ or timesteps that are too large compared to the swarm velocity. As such, we heuristically enforce positivity by choosing $\Delta x \sim \sqrt{\nu}$ and picking a stable timestep, which, due to the implicit treatment of diffusion, concerns only the flux term. For $\Delta t$ too large, we find that the flux imparts dispersion, which can result in negative mass through small oscillations. To prevent this, at each step we enforce a CFL-type condition on the advective flux

$$\Delta t_n \leq C \frac{\Delta x}{\max |V_j^n|}.$$

Choosing $C = 10\sqrt{2}$ along with $\Delta x \leq \sqrt{\nu}$ seems to suffice for enforcing positivity.

**Boundary Conditions**

The modifications above to row 0 and row $M$ are not the only options for guaranteeing that the columns of $\mathbf{B}^n$ sum to zero, but they are the simplest modifications that also enforce the boundary conditions up to $\mathcal{O}(\Delta t, \Delta x)$, which we now demonstrate. The first row of the linear system $\mathbf{A}^n U^{n+1} = U^n$ is meant to enforce the $x = 0$ boundary condition and reads

$$U_0^{n+1} + \frac{\Delta t}{2\Delta x}\left(U_0^{n+1} V_0^n + U_1^{n+1} V_1^n\right) - \nu \frac{\Delta t}{\Delta x^2}\left(U_1^{n+1} - U_0^{n+1}\right) = U_0^n.$$

Multiplying by $\frac{\Delta x}{\Delta t}$ then gives

$$\frac{1}{2}\left(U_0^{n+1}V_0^n + U_1^{n+1}V_1^n\right) - \nu\left(\frac{U_1^{n+1} - U_0^{n+1}}{\Delta x}\right) + \Delta x\left(\frac{U_0^{n+1} - U_0^n}{\Delta t}\right) = 0.$$

Assuming for the moment that $U^n$ and $V^n$ are equal to the $\rho(x,t)$ and velocity $v(x,t)$ on the spatial grid, and in addition that $\rho(x,t)$ is smooth enough, we derive the deviation from the true boundary conditions using the Taylor approximations

$$\begin{aligned}
\frac{1}{2}\left(U_0^{n+1}V_0^n + U_1^{n+1}V_1^n\right) &= \rho(0,t_{n+1})v(0,t_{n+1}) + \frac{\Delta x}{2}\frac{\partial}{\partial x}\Big(\rho(0,t_{n+1})v(0,t_{n+1})\Big) + \mathcal{O}(\Delta t, \Delta x^2) \\
\frac{U_1^{n+1} - U_0^{n+1}}{\Delta x} &= \frac{\partial}{\partial x}\rho(0,t_{n+1}) + \frac{\Delta x}{2}\frac{\partial^2}{\partial x^2}\rho(0,t_{n+1}) + \mathcal{O}(\Delta x^2) \\
\frac{U_0^{n+1} - U_0^n}{\Delta t} &= \frac{\partial}{\partial t}\rho(0,t_{n+1}) - \frac{\Delta t}{2}\frac{\partial^2}{\partial t^2}\rho(0,t_{n+1}) + \mathcal{O}(\Delta t^2).
\end{aligned}$$

Inserting these into the first row, we get

$$\begin{aligned}
&\frac{1}{2}\left(U_0^{n+1}V_0^n + U_1^{n+1}V_1^n\right) - \nu\left(\frac{U_1^{n+1} - U_0^{n+1}}{\Delta x}\right) + \Delta x\left(\frac{U_0^{n+1} - U_0^n}{\Delta t}\right) \\
&\quad= \rho(0,t_{n+1})v(0,t_{n+1}) - \nu\frac{\partial}{\partial x}\rho(0,t_{n+1}) \\
&\qquad\quad + \frac{\Delta x}{2}\left(\frac{\partial}{\partial t}\rho(0,t_{n+1}) + \frac{\partial}{\partial x}\Big(\rho(0,t_{n+1})v(0,t_{n+1})\Big) - \nu\frac{\partial^2}{\partial x^2}\rho(0,t_{n+1})\right) \\
&\qquad\quad + \frac{\Delta x}{2}\frac{\partial}{\partial t}\rho(0,t_{n+1}) + \mathcal{O}(\Delta t, \Delta x^2) \\
&\quad= \mathcal{O}(\Delta t, \Delta x)
\end{aligned}$$

where we have used the boundary conditions, the fact that $\rho$ satisfies the PDE near $x = 0$, and the assumption $\frac{\partial}{\partial t}\rho(0,t) = \mathcal{O}(1)$. Hence, the boundary conditions are implemented to first order. Since $U$ and $V$ are first-order accurate in time and first-order accurate in space for points away from the boundary, this reduces the method to an overall first-order accuracy in space and time, which we have verified in standard convergence studies.

## 3.4 Numerical Experiments on an Interval

Using the methods above we numerically solve for critical points of $\mathcal{E}^\nu$ on $D = [0, L]$ and use the following two criteria for accuracy: we are primarily concerned with satisfying the Euler-Lagrange equation in its original form,

$$\Lambda(x) := K * \overline{\rho}(x) + \nu\log(\overline{\rho}(x)) + V(x) = \lambda \quad \text{for all} \quad x \in [0, L]$$

where $\lambda = \mathcal{E}^\nu[\overline{\rho}] + \mathcal{K}[\overline{\rho}]$, and so we check that the quantity

$$\Lambda_\infty = \|\Lambda - \mathcal{E}^\nu[\overline{\rho}] - \mathcal{K}[\overline{\rho}]\|_\infty \tag{3.8}$$

is below the chosen error tolerance for each numerical solution $\overline{\rho}$. We also check that the boundary condition (2.23) derived in Theorem 2.15 is satisfied, which reads

$$\overline{\rho}(0) - \overline{\rho}(L) = \frac{1}{\nu}\int_0^L V'(x)\overline{\rho}(x)\,dx.$$

However, in all numerical experiments we use $V(x) = gx$ and choose $L$ large enough that $\overline{\rho}(L)$ is negligible, so this reduces to

$$\overline{\rho}(0) = \frac{g}{\nu}, \tag{3.9}$$

which is exact for $D = [0, \infty)$. Thus, we check that the relative error

$$E_0 := \frac{|\overline{\rho}(0) - g/\nu|}{g/\nu} \tag{3.10}$$

is small for numerical solutions. In what follows, denote by $\rho_{FP}$, $\rho_{NM}$ and $\rho_{PDE}$ the numerical solutions produced by the fixed-point iterator, the Newton continuation method and the PDE solver, respectively.

### 3.4.1 Purely Attractive Interaction Potential

The first class of potentials we examine are purely attractive, power-law potentials

$$K_p(x) := \frac{1}{p}|x|^p$$

for $p > 0$, where repulsive forces are present in the swarm only in the form of diffusion. Without diffusion, for all $p > 0$ the global minimizer is a single $\delta$-aggregation with location determined by the external potential $V$, as this realizes the infimum of the interaction energy $\mathcal{K}$. The effect of switching on diffusion is to smooth out the $\delta$-aggregation. Indeed, Figures 3.2 and 3.3 show critical points which are continuous and unimodal, but are supported everywhere with fast-decaying tails. First we examine the case $p = 2$ in detail given the results in Theorem 2.13, and compare with other small values of $p$. Then we look into the limit of large $p$, which is motivated by the fact that minimizers of $\mathcal{E}^\nu$ are supported on the entire domain regardless of the attraction strength (see Theorem 2.2).

**Remark 3.2.** We believe that the computed critical points in this section represent minimizers, and moreover that the global minimizer is the unique critical point for all $K_p$ (as is the case for $p = 2$); however, we leave the proof of these assertions to future work.

**Moderate Attraction Strength and Connection to Theorem 2.13**

We first examine the case $p = 2$ to benchmark the fixed-point iterator. Recall from Theorem 2.13 that a unique critical point exists for $p = 2$, which by Theorem 2.18 must be the global minimizer. Moreover, we have an explicit formula for the global minimizer (up to solving equation (2.22), which is done using MATLAB's `fzero` command). Figure 3.1 contains computed solutions for $p = 2$ and $V = gx$ for several values of $g$ along with convergence data. Agreement with the exact solution $\rho_{ex}$, the Euler-Lagrange equation as measured by $\Lambda_\infty$, and the boundary condition measured by $E_0$ are all on the order of the chosen error tolerance of 1e−6. We see especially good agreement with the Euler-Lagrange equation, gaining two orders of accuracy relative to the error tolerance.

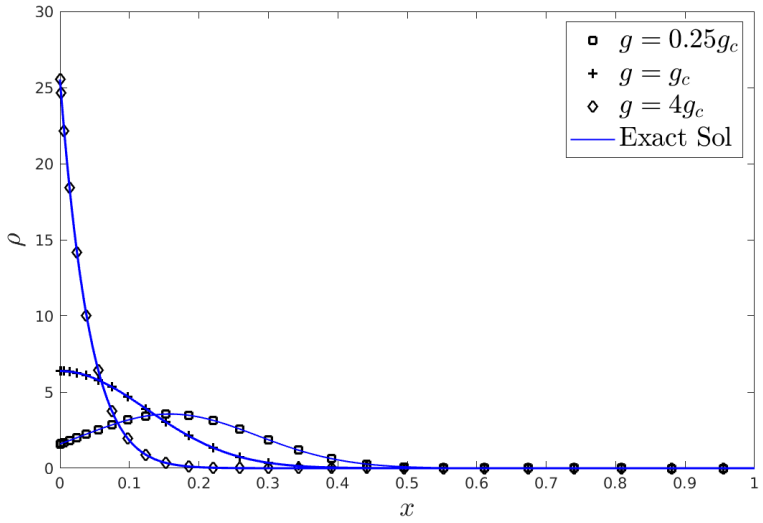


| $g$ | $\|\rho_{FP} - \rho_{ex}\|_1$ | $\Lambda_\infty$ | $E_0$ | Total Iterations |
|---|---|---|---|---|
| $0.25g_c$ | 3.92e−6 | 9.54e−8 | 7.91e−6 | 44 |
| $g_c$ | 2.16e−6 | 6.63e−8 | 7.38e−7 | 16 |
| $4g_c$ | 8.13e−6 | 3.88e−9 | 7.40e−6 | 10 |

Figure 3.1: Global minimizers under $K_p$ with $p = 2$, $V(x) = gx$ and $\nu = 2^{-6} \approx 0.0156$ computed using the fixed-point iterator. The method is initialized at $\rho_0 = 4\mathbb{1}_{[0,0.25]}$ with error tolerance set to 1e−6 and maximum iterations set to $N_{\max} = 2000$. A spatial grid of $N = 2^{10}$ points is used with points spaced quadratically to resolve the boundary at $x = 0$ (not all points are plotted). The value $g_c := \sqrt{2\nu/\pi}$ is emphasized because solutions achieve their maximum at $x = 0$ if and only if $g \geq g_c$. For all three solutions the scheme converged in well under $N_{\max}$ iterations.

---

Figure 3.2 shows computed critical points for $p \in (1, 8]$ to compare with the case $p = 2$, and demonstrates that increasing $p$ decreases the maximum height of the solution. A grid of $2^{10}$ uniformly spaced points was used (instead of quadratically spaced as in Figure 3.1),

which clearly affects the accuracy at the boundary: $E_0$ remains on the order of $10^{-2}$ despite the error tolerance of 1e−6. Still, we see excellent agreement with the Euler-Lagrange equation, as $\Lambda_\infty$ remains well below the error tolerance for each computed critical point. Notice also that the number of iterations required for convergence when $g = \nu$ increases dramatically as $p$ decreases. This is most likely due to the fixed-point method inefficiently resolving the tail of solutions, but we leave this for future investigation (see Remark 3.3).

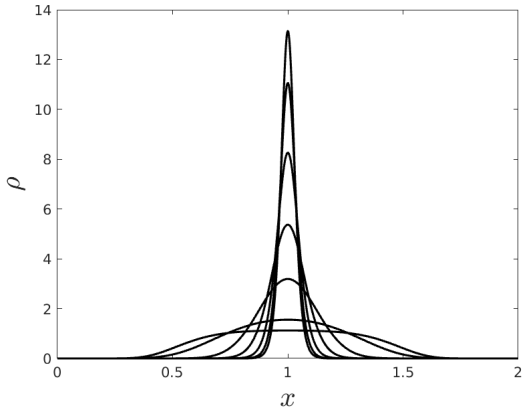


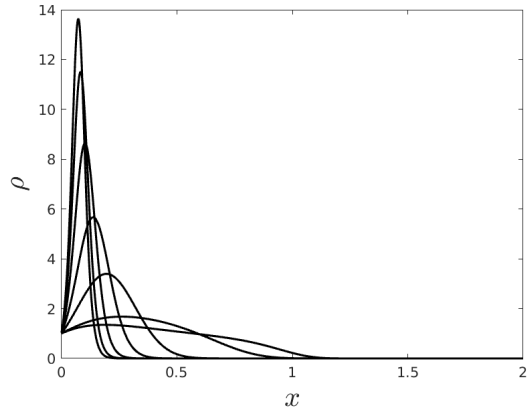


| $p$ | $\Lambda_\infty$ | Iterations |
|---|---|---|
| 1.0625 | 1.14e−8 | 18 |
| 1.125 | 4.45e−9 | 13 |
| 1.25 | 5.15e−9 | 12 |
| 1.5 | 5.30e−9 | 9 |
| 2 | 1.57e−15 | 2 |
| 4 | 8.41e−8 | 19 |
| 8 | 7.99e−7 | 45 |

| $p$ | $\Lambda_\infty$ | $E_0$ | Iterations |
|---|---|---|---|
| 1.0625 | 9.26e−8 | 5.47e−2 | 2000 |
| 1.125 | 4.22e−8 | 4.68e−2 | 178 |
| 1.25 | 5.29e−8 | 3.56e−2 | 141 |
| 1.5 | 7.43e−8 | 2.33e−2 | 97 |
| 2 | 1.54e−7 | 1.33e−2 | 60 |
| 4 | 5.41e−7 | 5.79e−3 | 30 |
| 8 | 5.24e−7 | 5.04e−3 | 22 |

Figure 3.2: Critical points of $\mathcal{E}^\nu$ computed using the fixed-point iterator with $K_p$ for $p \in [1, 8]$, $V(x) = gx$ and $\nu = 2^{-6}$. Left: profiles for $g = 0$. Right: profiles for $g = \nu$. As $p$ increases, the maximum height of solutions decreases. The method is initialized at $\rho^0 = 0.5\mathbb{1}_{[0,2]}$ for $g = 0$ and closer to the wall at $\rho^0 = \mathbb{1}_{[0,1]}$ for $g = \nu$. The error tolerance is set to 1e−6 and the maximum iterations set to $N_{\max} = 2000$. A spatial grid of $N = 2^{10}$ uniformly spaced points is used.

---

**Limit of Large Attraction**

We now examine numerically the limit of large $p$, which is motivated by the fact that minimizers $\overline{\rho}$ of $\mathcal{E}^\nu$ satisfy $\text{supp}\,(\overline{\rho}) = D$ regardless of how strong the (power-law) attraction is (see Theorem 2.2). This is a striking feature because intuitively one might expect that for very large attraction the swarm would be confined to a compact set. Only as $p \to +\infty$, however, do we reach a state with compact support, and we derive this family of compactly supported states below in one dimension. We compute critical points for powers up to

$p = 256$ to suggest convergence to the compactly supported states included in Figure 3.3, as well as to exhibit the versatility of the fixed-point iterator.

The limit as $p \to \infty$ is clearly singular, as the limiting interaction potential $K_\infty$ defined by

$$\lim_{p\to\infty} K_p(x) = K_\infty(x) := \begin{cases} 0, & x \in [-1,1] \\ +\infty, & x \notin [-1,1] \end{cases}$$

is no longer locally integrable. As such, the space of probability measures on which the resulting energy is finite is very limited. Despite this, we can still determine minimizers for $\mathcal{E}^\nu$ under $K_\infty$.

Recall that the interaction energy $\mathcal{K}$ is infinite for measures that do not satisfy a moment bound determined by the growth of $K$ at infinity (in other words, swarms that are too spread out can have infinite interaction energy). This is why in Assumption 1 of Chapter 2 we assume that $K(x) \lesssim |x|^{p_K}$ as $|x| \to \infty$, so that we can limit our attention to the Wasserstein space $(\mathcal{P}_{p_K}(D), \mathcal{W}_{p_K})$ upon which the interaction energy is finite. For $K_\infty$ it is not hard to show that the corresponding interaction energy $\mathcal{K}_\infty$ satisfies

$$\mathcal{K}_\infty[\mu] = \begin{cases} 0, & \text{if } \mu \text{ is supported on a unit interval} \\ +\infty, & \text{otherwise,} \end{cases}$$

and so the space we should be looking for minimizers in is

$$\{\mu \in \mathcal{P}_\infty(D) \,:\, \operatorname{supp}(\mu) \subset [a, 1+a] \text{ for some } a \in \mathbb{R}\}.$$

To arrive at this, for the interaction energy we have

$$\mathcal{K}_\infty[\mu] = \frac{1}{2}\int_D \int_D K_\infty(x-y)\, d\mu(y)\, d\mu(x) = \frac{1}{2}\int_{\operatorname{supp}(\mu)} (K_\infty * \mu(x))\, d\mu(x),$$

which is finite if and only if $K_\infty * \mu$ is finite $\mu$-a.e. By computing

$$\begin{aligned} K_\infty * \mu(x) &= \int_{\operatorname{supp}(\mu)} K_\infty(x-y)\, d\mu(y) \\ &= \int_{\operatorname{supp}(\mu)\cap[x-1,x+1]^c} K_\infty(x-y)\, d\mu(y) \\ &= \begin{cases} 0, & \mu([x-1,x+1]^c) = 0 \\ +\infty, & \text{otherwise,} \end{cases} \end{aligned}$$

we see that $\mathcal{K}_\infty[\mu] = +\infty$ unless $\mu([x-1,x+1]^c) = 0$ for $\mu$-a.e. $x \in D$, which can be shown to be equivalent to $\mu$ having support on a unit interval. From this we deduce that

a minimizer $\overline{\rho}_\infty$ has support on a unit interval and satisfies $K_\infty * \overline{\rho}_\infty(x) = 0$ for $\overline{\rho}_\infty$-a.e. $x$, hence the Euler-Lagrange equation reads

$$\nu \log(\overline{\rho}_\infty(x)) + V(x) = \lambda, \qquad \overline{\rho}_\infty\text{-a.e. } x \in D$$

or, using $\operatorname{supp}(\overline{\rho}_\infty) = [0,1]$,

$$\overline{\rho}_\infty = \begin{cases} \mathbb{1}_{[0,1]} & \text{for } V = 0 \\ Z^{-1} e^{-V/\nu} \mathbb{1}_{[0,1]} & \text{for } V \neq 0. \end{cases} \tag{3.11}$$

Figure 3.3 shows critical points for $K_p$ and $V = gx$ for larger values of $p$ together with the corresponding limiting measure $\overline{\rho}_\infty$ derived above. For $g = 0$, as $p$ increases we see solutions increasing to $\overline{\rho}_\infty$ inside $[0.5, 1.5]$ and decreasing to zero elsewhere. For $g = \nu$ the boundary condition (3.9) reduces to $\overline{\rho}(0) = 1$, which is satisfied through increasingly sharp transitions as $p$ increases, and is not satisfied in the limit by $\overline{\rho}_\infty$. We still see $\Lambda_\infty$ values near the error tolerance, except for $p = 256$, where the method clearly breaks down, as the scheme converges in fewer than $N_{\max}$ iterations yet $\Lambda_\infty$ is $\mathcal{O}(1)$.

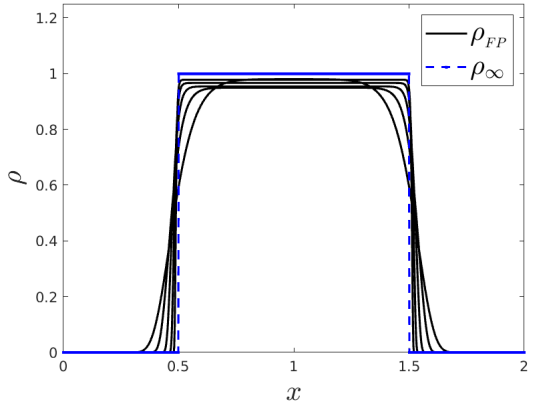


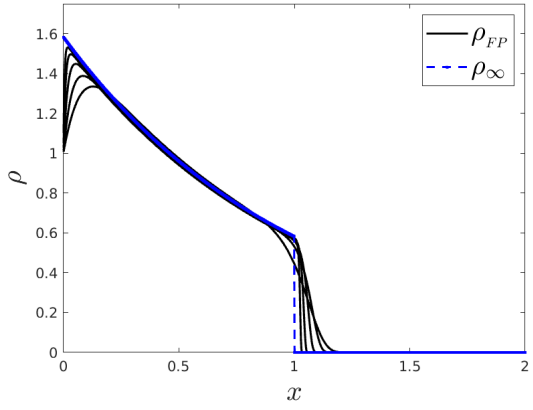


| $p$ | $\Lambda_\infty$ | Iterations |
|---|---|---|
| 16 | 1.92e−6 | 64 |
| 32 | 3.84e−6 | 131 |
| 64 | 8.50e−6 | 168 |
| 128 | 1.57e−5 | 186 |
| 256 | 2.33e−1 | 180 |

| $p$ | $\Lambda_\infty$ | $E_0$ | Iterations |
|---|---|---|---|
| 16 | 5.11e−6 | 7.16e−3 | 16 |
| 32 | 6.86e−6 | 1.29e−2 | 116 |
| 64 | 1.30e−5 | 2.55e−2 | 115 |
| 128 | 2.70e−5 | 5.10e−2 | 136 |
| 256 | 2.48e−1 | 9.97e−2 | 140 |

Figure 3.3: Critical points of $\mathcal{E}^\nu$ computed using the fixed-point iterator with $K_p$ for $p = 2^k$, $k = 4, \ldots, 8$, $V(x) = gx$ and $\nu = 2^{-6}$. Left: profiles for $g = 0$. Right: profiles for $g = \nu$. As $p$ increases, $\overline{\rho}$ drops off sharply outside an interval of length 1, approaching the compactly supported state $\overline{\rho}_\infty$ defined in (3.11). Parameters for the fixed-point iterator are the same as in Figure 3.2.

**Remark 3.3.** We do not examine the limit of small $p$ in this thesis, but note that it is not too hard to show that critical points for $K_p$ approach a $\delta$-aggregation as $p \to 0$. To see this numerically, one must reduce the number of iterations for convergence seen in Figure 3.2 for small $p$, which can be done by computing solutions on smaller and smaller domains. For instance, we find that the fixed-point iterator converges in 277 iterations on $D = [0, 0.5]$ for $p = 1$ and $g = \nu$, and expect similar results for smaller $p$ on smaller domains.

### 3.4.2 Attractive-Repulsive Interaction Potential

The second class of interaction potentials we consider involve attraction at large distances and repulsion at short distances. So-called attractive-repulsive potentials have been the subject of a substantial amount of research in recent years (see [2, 4, 15, 16, 18, 19, 26]) for their potential to model biological swarms, which predominantly seem to obey the following basic rules: if two individuals are too close, increase their distance, if too far away, decrease their distance.

We will restrict our attention to $C^1$ regularizations of the potential

$$K_{QANR}(x) = \frac{1}{2}|x|^2 + 2\phi(x)$$

which features quadratic attraction and Newtonian repulsion given by the free-space Green's function $\phi(x)$ for the negative Laplacian $-\Delta$:

$$\phi(x) := \begin{cases} -\dfrac{1}{2}|x| & \text{in } \mathbb{R}, \\ -\dfrac{1}{2\pi}\log|x| & \text{in } \mathbb{R}^2. \end{cases} \tag{3.12}$$

In one dimension, the $C^1$ regularized versions of $K_{QANR}$ form the one-parameter family

$$K_\epsilon(x) := \frac{1}{2}x^2 + 2\phi_\epsilon(x) := \frac{1}{2}x^2 + \begin{cases} -|x|, & |x| > \epsilon \\ -\dfrac{\epsilon}{2} - \dfrac{1}{2\epsilon}x^2, & |x| \le \epsilon \end{cases} \tag{3.13}$$

for $\epsilon \in (0, 1]$, such that $\lim_{\epsilon \to 0} K_\epsilon = K_{QANR}$. See Figure 3.4 for a schematic of these potentials along with the pairwise forces they impart between particles.

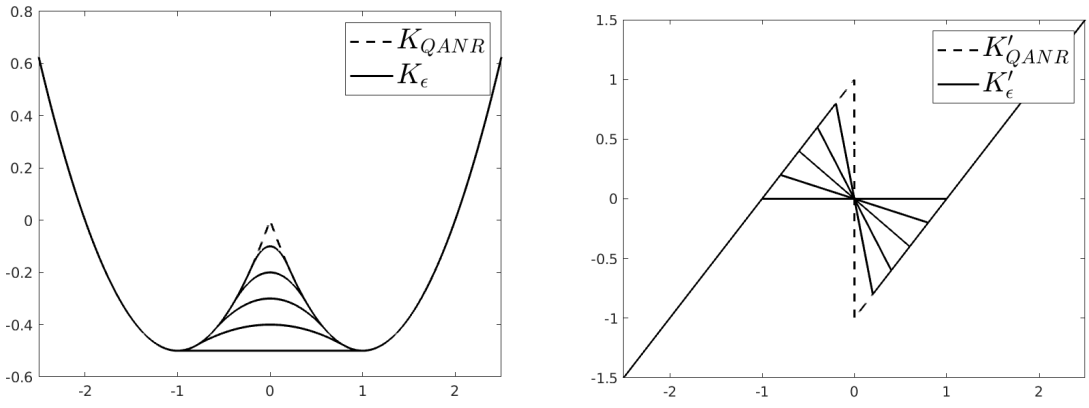


Figure 3.4: $K_{QANR}$ and $K_\epsilon$ for $\epsilon = 0.2, 0.4, 0.6, 0.8, 1$. Potentials are plotted on the left, forces on the right (recall that $-K'(x)$ gives the force felt between two particles separated by a distance $x$). As $\epsilon$ decreases we go from infinitesimal repulsion at infinitesimal distances to finite repulsion at infinitesimal distances.

---

We examine the potentials $K_\epsilon$ for two reasons. Firstly, as the parameter $\epsilon$ is decreased from 1 to 0, the number of aggregates in a given steady state appears to increase; however, a complete theory for determining the number of aggregates as a function of $\epsilon$ is currently lacking for the aggregation-diffusion model. (A partial theory exists for the plain aggregation model in free space without external forces, which we review below). One might expect that with linear diffusion there would exist a unique number of aggregates for any fixed $\epsilon$; however, we give numerical evidence to the contrary in Figure 3.6. In light of this, we suggest a numerical procedure involving continuation on the diffusion coefficient $\nu$ for extracting states with globally minimizing configurations of aggregates, which we believe are unique for each fixed $\epsilon$.

We also choose to examine $K_\epsilon$ because $K_{QANR}$ and $K_\epsilon$ have been shown to produce disconnected, unstable states in the plain aggregation model when $D$ is the half-line or half-plane [18, 19], which initially motivated our study of the model with linear diffusion. Below we construct similar states numerically on the half-line, where instead of a $\delta$-aggregation at the boundary we have a boundary layer, and we find that as the external potential $V$ is increased, the boundary layer steepens and aggregations away from the boundary merge. This adds another layer to the discussion on uniqueness of the number of aggregates and provokes questions about biological applications.

**Remark 3.4.** The findings in this section are preliminary and are presented mostly to motivate further study, as well as to demonstrate that our numerical methods are also suitable for attractive-repulsive potentials.

**Non-Uniqueness in the Number of Aggregates**

To get a sense of the problem, Figure 3.5 displays solutions under $K_\epsilon$ for various $\epsilon$ and $V = 0$, showing that decreasing $\epsilon$ increases the number of aggregates. (Numerical information can be found in Remarks 3.5 and 3.6 as well as Figure 3.7). As mentioned above, it is not fully understood how the distribution of aggregates (i.e. the number of aggregates and their relative positions and masses) changes as a function of $\epsilon$. For $\nu = 0$ and $D = \mathbb{R}$, it is proven by Fellner and Raoul in [16] that as $\epsilon \to 0$ minimizers of the related potential $\widetilde{K_\epsilon}(x) = \frac{1}{2}x^2 + \phi_\epsilon(x)$ converge weakly-* to the global minimizer for $\widetilde{K}(x) = \frac{1}{2}x^2 + \phi(x)$, which is the characteristic function of the unit ball. The authors of [16] also derive an upper bound on the number of aggregates under $\widetilde{K_\epsilon}$ for any given $\epsilon > 0$, showing that for any $n < \frac{1}{\epsilon}$ there exists a stable configuration of $n$ $\delta$-aggregations, possibly with unequal mass. In our case, with $K_\epsilon$ it appears that this bound is $n < \frac{2}{\epsilon}$.

One might expect that for each $\epsilon$, switching on diffusion selects a unique number of aggregates in all minimizing states. Similar results have been documented: Evers and Kolokolnikov establish in [15] that adding any level of diffusion to an equilibrium consisting of two aggregates of unequal mass for the plain aggregation model under the double-well potential $K(x) = -\frac{1}{2}x^2 + \frac{1}{4}x^4$ causes the state to become metastable, where mass is transfered between the two aggregates until their masses equilibrate, which only happens after infinite time. As evidenced by the numerical example in Figure 3.6, where a four-aggregate and a five-aggregate state both exist as critical points for the same $\epsilon$ and $\nu$ values, it seems that diffusion does not guarantee a unique number of aggregates. It is clear that the four-aggregate state is preferred, as it has lower energy and requires fewer iterations of the fixed-point iterator. We believe that the numerical method used to compute each solution, in particular using continuation on the diffusion coefficient, suggests a method for computing the globally-minimizing configuration for each $\epsilon$. Both the four-aggregate and five-aggregate state are computed with diffusion coefficient $\nu = 2^{-13}$, but the four-aggregate state is reached by starting the Newton continuation method at $\nu_0 = 10\nu$, whereas the five-aggregate state is started out at $\nu_0 = 2\nu$. The more energy-favourable state is reached from a larger starting $\nu_0$, which suggests that using continuation from larger diffusion might be a mechanism for extracting the global minimizer. We can use ice crystallization as a physical analogy: more imperfections form in ice crystals when water is frozen abruptly, indicating a non-energy-minimizing configuration, than when water is frozen slowly (see for instance [30]).

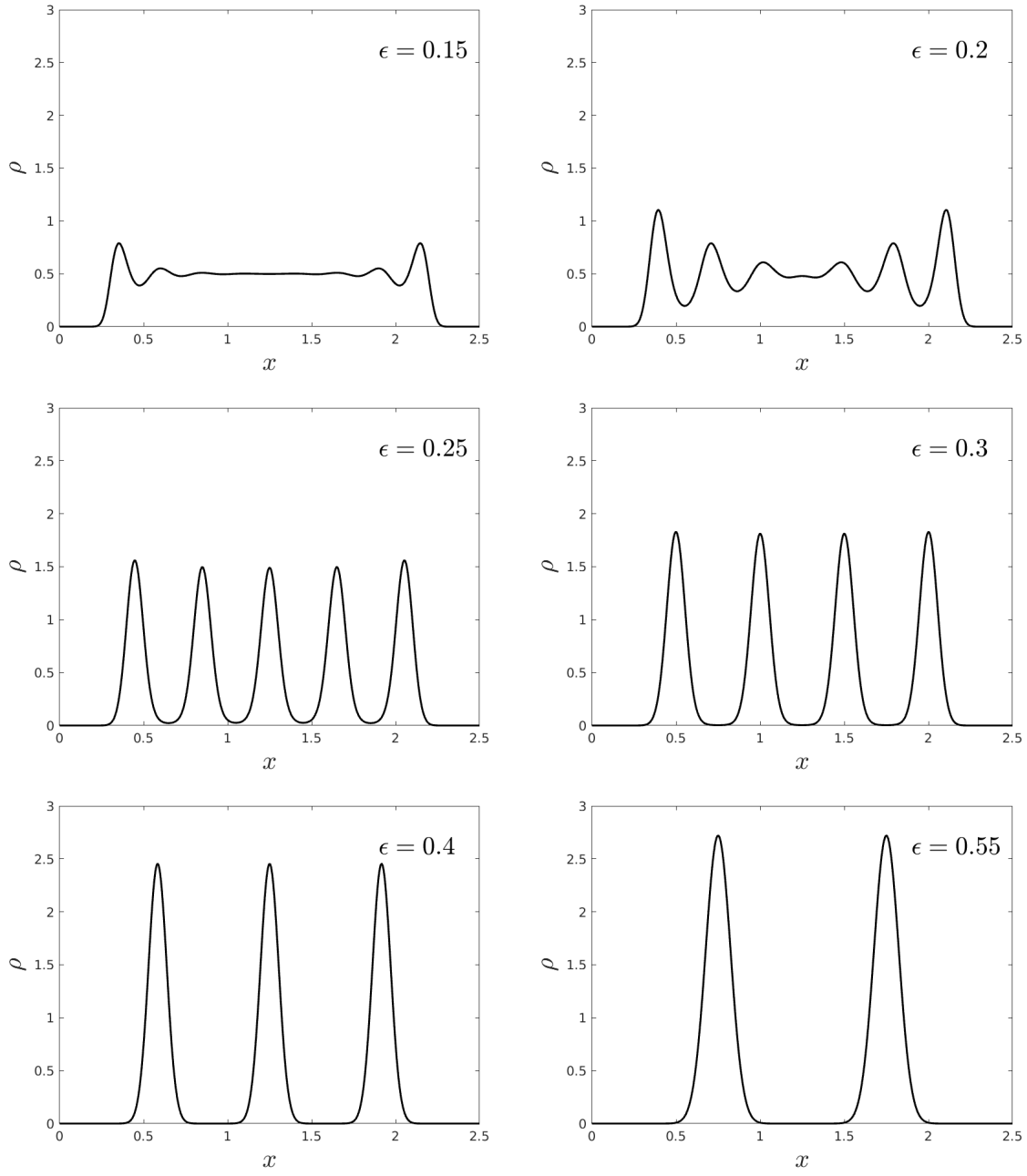


Figure 3.5: Critical points of $\mathcal{E}^\nu$ computed using fixed-point iteration combined with the Newton continuation method for $K_\epsilon$, $V = 0$ and $\nu = 2^{-11} \approx 0.0005$.

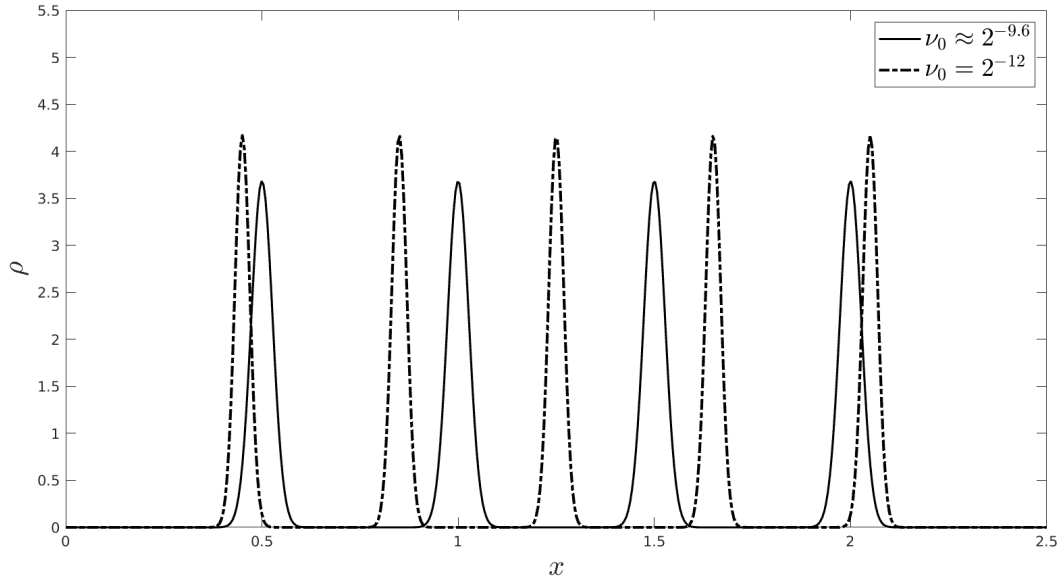


| $\nu_0$ | $\mathcal{E}^\nu$ | $\Lambda_\infty$ | Iterations |
|---|---|---|---|
| $10\nu$ | $-0.74841$ | 5.73e$-$7 | 26 |
| $2\nu$ | $-0.74826$ | 1.19e$-$6 | 1149 |

Figure 3.6: Multiple critical points for $K_\epsilon$ with $\epsilon = 0.3$ and $\nu = 2^{-13}$. In each case, the fixed-point iterator was initiated at the output $\rho_{NM}$ of the Newton continuation method started from $\nu_0$. With $\nu_0 = 10\nu$, we arrive at the four-aggregate state which has slightly lower energy and lower $\Lambda_\infty$, and needs far fewer iterations for convergence of the fixed-point method. For $\nu_0 = 2\nu$, a five-aggregate critical point emerges. Due to the high number of iterations required, this state is at best a $\mathcal{W}_p$-$r$ local minimum for a small radius $r$, but very well could be a saddle point or local maximum.

---

**Remark 3.5.** Multiple aggregates under $K_\epsilon$ only appear distinct to the eye for small diffusion (we use $\nu = 2^{-11}$ in Figure 3.5 and $\nu = 2^{-13}$ in Figure 3.6). Their computation is a delicate matter. We use a uniform grid of 400 points with tolerance 1e$-$6 for the fixed-point iterator, which is initiated at the output $\rho_{NM}$ of the Newton iteration. To calculate $\rho_{NM}$ for solutions in Figure 3.5, continuation was employed using 40 diffusion values between $\nu_0 = 2^{-8}$ and $\nu = 2^{-11}$. A tolerance of 1e$-$10 was used for the Newton iterator, with convergence in under 50 iterations for each diffusion coefficient.

**Remark 3.6.** We note that $\rho_{NM}$, as well as the output $\rho_{PDE}$ from the PDE solver initiated at $\rho_{NM}$, are indistiguishable from $\rho_{FP}$ to the eye and so have been omitted from Figure 3.5. More importantly, we find that $\rho_{NM}$ and $\rho_{PDE}$ don't satisfy the Euler-Lagrange equation as well as $\rho_{FP}$, with $\Lambda_\infty$ values on the order of $10^{-2}$. This can be explained by the PDE method and Newton iterator failing to resolve the tails of solutions, as depicted in Figure 3.7.

| $\epsilon$ | $\Lambda_\infty$ | Iterations |
|---|---|---|
| 0.15 | 4.47e−8 | 506 |
| 0.2 | 9.66e−8 | 1073 |
| 0.25 | 1.27e−7 | 582 |
| 0.3 | 2.49e−7 | 76 |
| 0.4 | 2.96e−6 | 22 |
| 0.55 | 1.52e−7 | 93 |

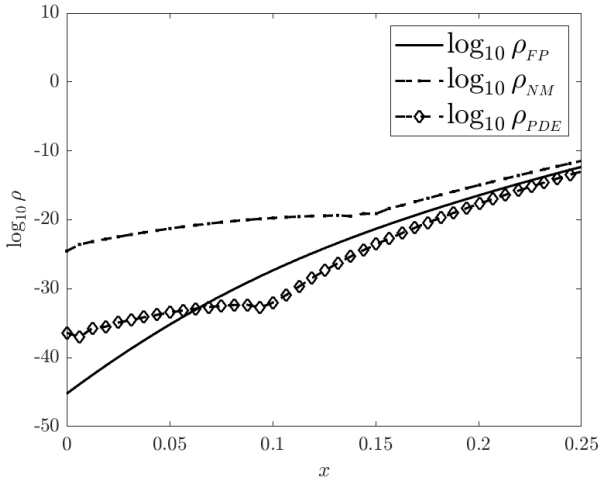


Figure 3.7: Left: Convergence data for solutions $\rho_{FP}$ in Figure 3.5. Right: logarithmic plots of the tails of computed solutions for $\epsilon = 0.4$, where clearly $\rho_{FP}$ has the best resolution.

---

**Boundary Layers and Merging Aggregates**

This last numerical experiment involves the external potential $V(x) = gx$ and focuses on the phenomenon of aggregates merging together as the "gravity" strength $g$ is increased. Figure 3.8 shows states $\rho_{FP}$ and $\rho_{PDE}$ reached by the fixed-point iterator and PDE solver, respectively, under $K_\epsilon$ for fixed $\epsilon = 0.5$. Both $\rho_{FP}$ and $\rho_{PDE}$ are initiated at the output of the Newton continuation method for $g = 0$, which consists of three aggregates. Here we are not as interested in small diffusion and so we use the moderate diffusion level $\nu = 2^{-9}$.

By plotting $\rho_{FP}$ and $\rho_{PDE}$ together we see that the effect of "turning on" gravity dynamically produces the same state as the critical point computed directly using the fixed-point iterator, suggesting uniqueness of the critical point. These states are qualitatively similar to the equilibria of the plain aggregation model on the half-line which were found to be unstable in [18] and [19] and consist of a boundary aggregation and "free-swarm" component of disjoint supports. When $g$ is increased, we see in Figure 3.8 that the two aggregates away from the boundary merge together, instead of also getting pinned to the boundary. This is somewhat unexpected, but can be explained by the fact that the boundary aggregation imparts a repulsive force from the left, while gravity imparts a force from the right, and so the effect is compression. A possible biological interpretation could be that fewer, larger aggregates are more favourable for withstanding external stresses. In any case, from Figure 3.8 it appears that states consisting of a boundary aggregation and "free-swarm" component naturally appear in aggregation-diffusion models with external gravity.

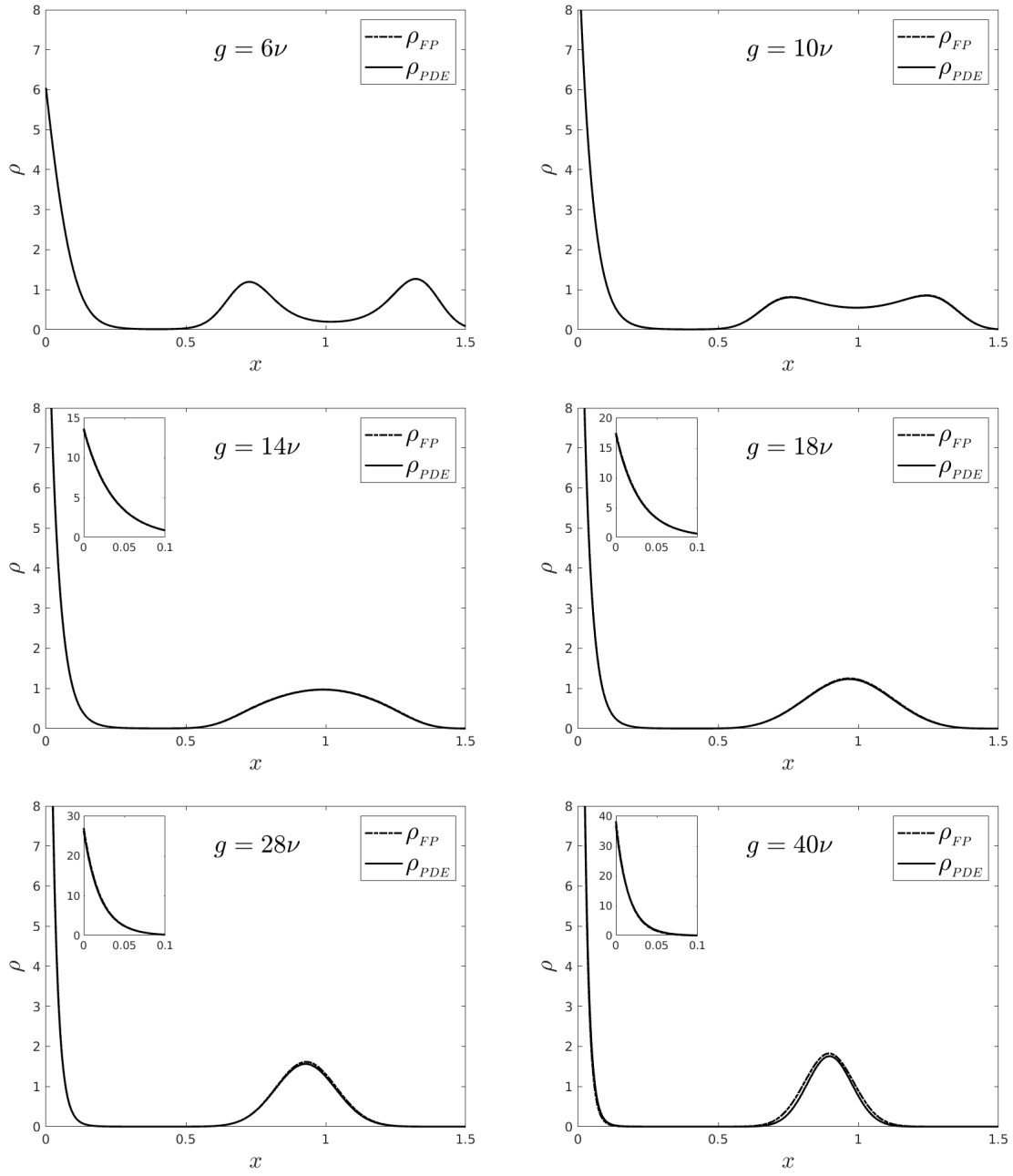


Figure 3.8: Merging of aggregates under increasing gravity. Solutions using the fixed-point iterator and PDE solver are overlaid. The numerical scheme and parameters are as in Remark 3.5, with $\rho_{FP}$ and $\rho_{PDE}$ both initiated at $\rho_{NM}$. Gravity values $g$ are set to multiples of $\nu$ to visually check the boundary condition $\overline{\rho}(0) = \frac{g}{\nu}$ (see inset plots). In each case the fixed-point iterator converged in under 2000 iterations to within the desired error tolerance and produces $\Lambda_\infty$ values on the order of the error tolerance. The PDE solver does not produce $\Lambda_\infty$ values within tolerance for reasons discussed in Remark 3.6.

# Chapter 4

# Zero-Diffusion Limit Numerics

This chapter is devoted to numerically verifying the analytical rate with which solutions of the aggregation-diffusion model (1.20) converge to solutions of the plain aggregation model (1.14) as $\nu \to 0$, which is my main contribution to the recently submitted article [17]. Specifically, we show that the asymptotic rate

$$\mathbb{E}\left[\mathcal{W}_\infty^2\left(\mu_t^{\nu,X}, \mu_t^X\right)\right] = \mathcal{O}(\nu)$$

presented in [17] (and reproduced below in Theorem 4.3) is realized in numerical simulations of the particle systems $X_t^\nu$ and $X_t$ for typical domains $D \subset \mathbb{R}^2$ and attractive-repulsive potentials $K$. To show this, we evolve the particle systems explicitly in time with suitable boundary conditions, and compute the distance $\mathcal{W}_\infty$ at times of interest using a matching algorithm. A Monte Carlo algorithm is then employed to estimate the expectation. The procedure is highly dependent on the accuracy of particle simulations; however, we find that suitably scaling the timestep $\Delta t$ with the diffusion coefficient $\nu$ successfully reveals the $\mathcal{O}(\nu)$ convergence rate with great gains in computation time.

We recall the particle systems from Chapter 1 here. The particle system $X_t$ underlying the plain aggregation (non-diffusive) model in domains with boundaries satisfies

$$\begin{cases} \dfrac{d}{dt}X_t^i = P_x\left(-\dfrac{1}{N}\displaystyle\sum_{j\neq i}^{N}\nabla_{X_t^i}K\left(X_t^i - X_t^j\right) - \nabla V\left(X_t^i\right)\right) \\ X_0^i = x_0^i \in \mathbb{R}^d, \end{cases} \tag{4.1}$$

while the particle system $X_t^\nu$ underlying the aggregation-diffusion model satisfies

$$\begin{cases} dX_t^{\nu,i} = \left(-\dfrac{1}{N}\displaystyle\sum_{j\neq i}^{N}\nabla_{X_t^{\nu,i}}K\left(X_t^{\nu,i} - X_t^{\nu,j}\right) - V\left(X_t^{\nu,i}\right)\right)dt + \sqrt{2\nu}\,dB_t^i + dR_t^i \\ \text{Law}\left(X_0^{i,\nu}\right) = \mu_0^\nu \in \mathcal{P}_2(D). \end{cases} \tag{4.2}$$

## 4.1 Motivation

Analytically, the rate with which solutions of the aggregation model with linear diffusion converge to solutions of the plain aggregation model, presented in [17], verifies that linear diffusion is a robust mechanism for regularizing the plain aggregation model: it ensures that solutions of the two models can be made arbitrarily close to each other (in the Wasserstein sense) by choosing $\nu$ small enough. In the context of domains with boundaries, regularization of the plain aggregation model by linear diffusion is motivated by the desire to investigate how the swarm escapes from unstable equilibria. (Recall from Chapter 1 that in domains with boundaries, the plain aggregation model (1.14) readily develops into unstable states $\overline{\mu}_{ds}$ which consist of a boundary swarm and a free swarm with disjoint supports.)

In [19], Fetecau et al. prove convergence in the zero-diffusion limit for *nonlinear* diffusion and show how the swarm escapes from an unstable equilibrium on the half-line using PDE simulations. Nonlinear diffusion leads to repeated mass transfers from the boundary at $x = 0$ into the free swarm, a process which successively lowers the energy. In higher dimensions, it is much harder to numerically investigate such phase transitions in domains with boundaries using PDE methods, as complex geometries and small diffusion lead to a large computational overhead. This provided the initial motivation for pursuing analysis of the model with linear diffusion (and to this thesis): linear diffusion has the advantage of a stochastic particle interpretation, the numerics for which are well suited for both higher dimensions *and* small diffusion. As such, the zero-diffusion limit *numerics* in [17] (my main contribution) are presented to show that stochastic particle simulations are a practical computational framework in which to explore instabilities of the plain aggregation model *in higher dimensions*.

In addition, the convergence rate in [17] improves on a similar convergence rate proved by Zhang in [34] and for more general potentials $K$ and $V$ (details below). These improvements were found by Hui Huang (together with Fetecau, Sun and myself) to be a direct result of utilizing the underlying stochastic particle systems of the models. This provides further motivation for using stochastic particle simulations to numerically verify the convergence rate: we wish to show that in practice (i.e. numerically), one can expect $\mathcal{O}(\nu)$ convergence in the zero-diffusion limit, and for more general potentials.

## 4.2 Analytical Results

Here we reproduce the analytical results from [17] which establish the zero-diffusion limit in bounded, convex domains under the following assumptions on $D$, $K$ and $V$, where Theorem 4.3 will be verified numerically.

**Definition 4.1.** *A function $f \in C^1(D)$ is $\lambda$-convex on a convex set $D$ if*

$$f(y) \geq f(x) + \langle \nabla f(x), y - x \rangle + \frac{\lambda}{2}|y - x|^2 \qquad \text{for any } x, y \in D. \tag{4.3}$$

In other words, a function $f$ is $\lambda$-convex if the function $f(x) - \frac{\lambda}{2}|x|^2$ is convex.

**Assumption 3.**

1. *$D \subset \mathbb{R}^d$ is convex and bounded, and $\partial D \in C^1$.*
2. *$K(x) = K(-x)$ for all $x \in \mathbb{R}^d$.*
3. *$K \in C^1(D - D)$ is $\lambda_K$-convex on $D - D$ for some $\lambda_K \in \mathbb{R}$.*
4. *$V \in C^1(D)$ is $\lambda_V$-convex on $D$ for some $\lambda_V \in \mathbb{R}$*

We then have the following convergence results at the PDE and particle levels, where for any $a \in \mathbb{R}$ we let $a^- := \min\{0, a\}$.

**Theorem 4.2** (Theorem 3.5, [17])**.** *Assume that $K$, $V$ and $D$ satisfy Assumption 3. For any $T > 0$, let $\mu_t^\nu$ and $\mu_t$ be weak solutions to (1.20) and (1.14) on $[0, T]$, respectively, with both systems sharing the same initial data $\mu_0 \in \mathcal{P}(D)$. Then it holds that*

$$\mathcal{W}_2^2(\mu_t^\nu, \mu_t) \leq 2d\nu t \left(1 - 2(\lambda_K^- + \lambda_V^-)te^{-2(\lambda_K^- + \lambda_V^-)t}\right) \quad \text{for all} \quad t \in [0, T].$$

**Theorem 4.3** (Theorem 4.3, [17])**.** *Assume that $\{X_0^i\}_{i=1}^N$ are $N$ i.i.d. random variables with the common law $\mu_0$. Let $\{X_t^{\nu,i}\}_{i=1}^N$ and $\{X_t^i\}_{i=1}^N$ satisfy particle systems (4.2) and (4.1) with associated empirical measures $\mu_t^{\nu,X}$ and $\mu_t^X$, respectively, and suppose that $\{X_t^{\nu,i}\}_{i=1}^N$ and $\{X_t^i\}_{i=1}^N$ share the same initial data $\{X_0^i\}_{i=1}^N$. Then it holds that*

$$\mathbb{E}\left[\mathcal{W}_\infty^2(\mu_t^{\nu,X}, \mu_t^X)\right] \leq 2d\nu t \left(1 - 2(\lambda_K^- + \lambda_V^-)te^{-2(\lambda_K^- + \lambda_V^-)t}\right) \quad \text{for all} \quad t \in [0, T]. \tag{4.4}$$

## 4.3 Numerical Method

In this section we introduce the numerical method behind taking the zero-diffusion limit for aggregation models satisfying Assumption 3 above. In what follows, denote the numerical solutions to the diffusive (4.2) and non-diffusive (4.1) particle systems along the partition $0 = \tau_0 < \tau_1 < \cdots < \tau_L = T$ by

$$\widetilde{X}^{\nu}_{\tau_n} := \left\{\widetilde{X}^{\nu,i}_{\tau_n}\right\}_{i=1}^{N} \quad \text{and} \quad \widetilde{X}_{\tau_n} := \left\{\widetilde{X}^{i}_{\tau_n}\right\}_{i=1}^{N},$$

respectively, with empirical measures $\mu^{\nu,\widetilde{X}}_{\tau_n}$ and $\mu^{\widetilde{X}}_{\tau_n}$.

### 4.3.1 Particle Simulation

#### Plain Aggregation

To compute numerical solutions of the non-diffusive particle system (4.1) we use explicit Euler timestepping with projection. To approximate the continuous projection operator $P_x$ given by (1.13), particles landing outside the domain at the end of a given timestep are placed onto the closest point in $\partial D$ using the projection operator

$$\pi_{\partial D}(x) = \begin{cases} \text{argmin}_{z\in\partial D}|x-z|, & x \notin D \\ x, & x \in D. \end{cases} \tag{4.5}$$

A schematic for the projection operator is given in Figure 4.1. Note that $\pi_{\partial D}(x)$ is uniquely determined for all $x \in \mathbb{R}^d$ due to the convexity of $D$. The update at time $\tau_{n+1}$ for system (4.1) is then computed using

$$\widetilde{X}^{i}_{\tau_{n+1}} = \pi_{\partial D}\left(\widetilde{X}^{i}_{\tau_n} - \Delta t_n\Big(\frac{1}{N}\sum_{j\neq i}\nabla K(\widetilde{X}^{i}_{\tau_n} - \widetilde{X}^{j}_{\tau_n}) + \nabla V(\widetilde{X}^{i}_{\tau_n})\Big)\right) \tag{4.6}$$

where $\Delta t_n := \tau_{n+1} - \tau_n$. We note that by comparing to a fine-grid solution this method can been shown to converge with $\mathcal{O}(\Delta t)$. Such a low-order method suffices because the accuracy bottleneck for showing the zero-diffusion limit appears in the stochastic simulations (see Section 4.3.3 below).

#### Aggregation-Diffusion

For numerical solutions of the stochastic particle system (4.2) we use the symmetrized reflection scheme introduced by Bossy, Gobet and Talay in [6], which is simply the stochastic Euler-Maruyama method with symmetric reflection through the boundary. For this we

define the reflection operator $\mathbf{R}$:

$$\mathbf{R}(x) = \begin{cases} x\,, & \text{if } x \in D, \\ x - 2\left(x - \pi_{\partial D}(x)\right), & \text{otherwise,} \end{cases} \tag{4.7}$$

where $n$ is the unit outward normal to $\partial D$ at $\pi_{\partial D}(x)$. In words, the operator $\mathbf{R}$ takes the mirror reflection across $\partial D$ of points outside $D$ (see Figure 4.1). For points in a small enough neighbourhood of $D$, such reflections lie in $D$.

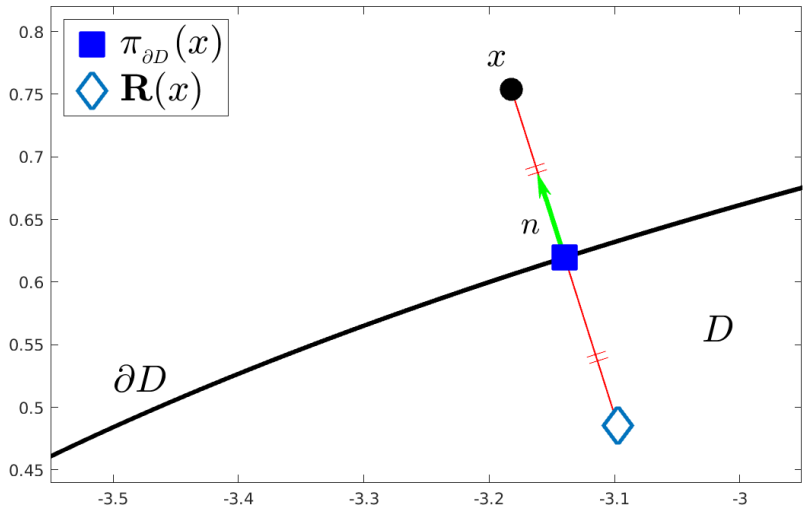


Figure 4.1: Illustration of the projection $\pi_{\partial D}$ (see (4.5)) and the reflection operator $\mathbf{R}$ (see (4.7)) for a point $x \notin D$.

---

For the particle system (4.2), the update is then

$$\widetilde{X}^{\nu,i}_{\tau_{n+1}} = \mathbf{R}\Big(\widetilde{X}^{\nu,i}_{\tau_n} - \Delta t_n\Big(\frac{1}{N}\sum_{j\neq i}\nabla K(\widetilde{X}^{\nu,i}_{\tau_n} - \widetilde{X}^{\nu,j}_{\tau_n}) + \nabla V(\widetilde{X}^{\nu,i}_{\tau_n})\Big) + \sqrt{2\nu\Delta t_n}\mathcal{N}^d(0,1)\Big) \tag{4.8}$$

where $\mathcal{N}^d(0,1)$ denotes the standard $d$-dimensional Gaussian random variable with mean zero and variance one.

One reason for using the symmetrized Euler scheme is that its weak convergence rate is shown in [6] to be $\mathcal{O}(\Delta t)$ when applied to an isolated reflecting diffusion process, which to our knowledge is the highest weak order of convergence found in the literature for reflected SDEs. Recall that a numerical approximation $\widetilde{X}_T$ to a stochastic process $X_T$ at time $T$ is

said to have a weak convergence rate of $\mathcal{O}(\Delta t^p)$ when

$$e_f^{weak}(\Delta t) := \left| \mathbb{E}\Big[f(\widetilde{X}_T)\Big] - \mathbb{E}\Big[f(X_T)\Big] \right| = \mathcal{O}(\Delta t^p)$$

for all $f$ in some class of test functions [20]. For instance, the authors of [6] establish the weak convergence rate of the symmetrized Euler scheme for $f \in C_b^5(D)$. Analysis of the method applied to interacting diffusions, as in our scenario, is still open, however Figure 4.2 shows that the method appears to converge with $\mathcal{O}(\Delta t)$ for a system of $N = 5$ particles.

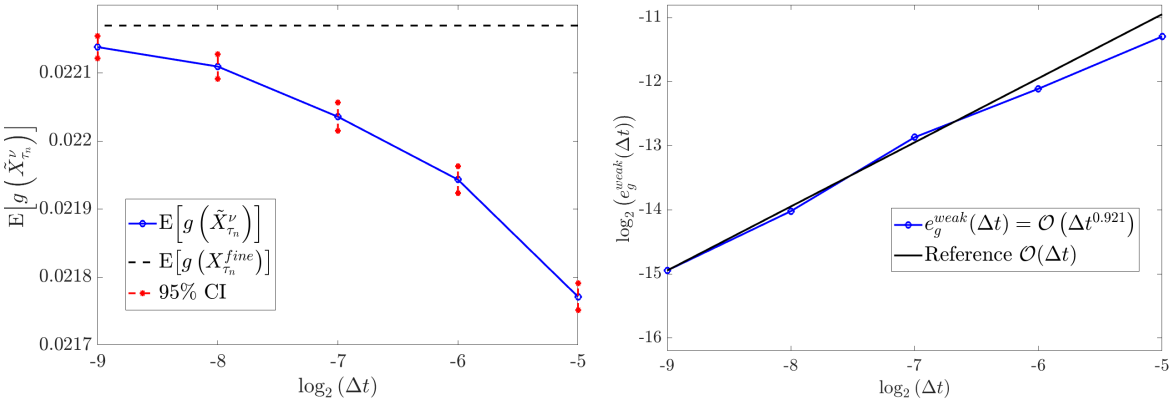


Figure 4.2: Weak convergence of the Euler-Maruyama scheme with symmetric reflection (4.8) applied to the particle system (4.2) for $\nu = 0.01$ and $N = 5$ particles in the disk $D_C$ using the interaction potential $K_{3/2}$ (Section 4.4.1). We use the test function $g : \mathbb{R}^{Nd} \to \mathbb{R}$ given by $g(x) = \frac{1}{N}|x|^2$, which is relevant to computations of the Wasserstein distance (4.9) as it contains the squared Euclidean distance. We compare at time $\tau_n = 0.25$ to a fine-grid solution $X^{fine}_{\tau_n}$ computed with timestep $\Delta t = 2^{-15}$, and use $2 \times 10^5$ sample trajectories all sharing the same initial data to approximate expectations. Left: semi-log plot showing convergence of $\mathbb{E}\left[g\left(\widetilde{X}^{\nu}_{\tau_n}\right)\right]$ to $\mathbb{E}\left[g\left(X^{fine}_{\tau_n}\right)\right]$ as well as 95% confidence intervals. Right: log-log plot showing a convergence rate of approximately $\mathcal{O}(\Delta t)$.

---

### 4.3.2 Wasserstein Distance Between Empirical Measures

From the numerical particle systems $\widetilde{X}^{\nu}_{\tau_n}$ and $\widetilde{X}_{\tau_n}$ we compute the distance $\mathcal{W}_\infty^2\left(\mu^{\nu,\widetilde{X}}_{\tau_n}, \mu^{\widetilde{X}}_{\tau_n}\right)$ by utilizing a convenient reduction of the Monge-Kantorovich transport problem in the case of empirical measures [32]:

$$\mathcal{W}_\infty^2\left(\mu^{\nu,\widetilde{X}}_{\tau_n}, \mu^{\widetilde{X}}_{\tau_n}\right) = \min_{\sigma \in S_N} \left\{ \max_i \left| \widetilde{X}^{\nu,i}_{\tau_n} - \widetilde{X}^{\sigma(i)}_{\tau_n} \right|^2 \right\}, \tag{4.9}$$

where $S_N$ is the set of permutations on $N$ elements. A minimizer $\sigma$ thus defines a bijection between the two particle systems, or a "perfect matching", which minimizes the farthest

distance between any two matched particles $\widetilde{X}^{\nu,i}_{\tau_n}$ and $\widetilde{X}^{\sigma(i)}_{\tau_n}$. In this way, we verify Theorem 4.3 by using a matching algorithm and the theory of bipartite graphs to compute (4.9) at times $\tau_n$.

**Remark 4.4.** We recently discovered that the following method, although developed independently, appears in Chapter 6 of [7], a textbook on linear assignment problems. The problem of computing (4.9) above is referred to in the linear programming community as the *bottleneck assignment problem.*

**Method Overview**

Let $\widetilde{X}^{\nu}_{\tau_n}$ and $\widetilde{X}_{\tau_n}$ represent the $2N$ vertices of a complete, weighted bipartite graph $G$ with bipartite adjacency matrix $A$ having edge weights

$$A_{ij} = \left|\widetilde{X}^{\nu,i}_{\tau_n} - \widetilde{X}^{j}_{\tau_n}\right|^2.$$

The edge weight $A_{ij}$ represents the cost of transporting particle $\widetilde{X}^{\nu,i}_{\tau_n}$ into particle $\widetilde{X}^{j}_{\tau_n}$. Finding an optimal transport plan between the empirical measures $\mu^{\nu,\widetilde{X}}_{\tau_n}$ and $\mu^{\widetilde{X}}_{\tau_n}$ is equivalent to finding a perfect matching in $G$ with least maximum-matching cost, where a perfect matching, as alluded to above, is a bijection between the two partitions $\widetilde{X}^{\nu}_{\tau_n}$ and $\widetilde{X}_{\tau_n}$ of $G$.

We find a perfect matching in $G$ with least maximum-matching cost as follows: let $C = \{c_k\}_{k=1}^{k_{\max}}$ be the sequence of unique edge weights $A_{ij}$ in increasing order, where clearly $1 \leq k_{\max} \leq N^2$. For each $k \leq k_{\max}$, let $B^k$ be the bipartite adjacency matrix for the subgraph of $G$ obtained by removing all edges of cost greater than $c_k$:

$$B^k_{ij} := \begin{cases} 1, & A_{ij} \leq c_k \\ 0, & A_{ij} > c_k. \end{cases}$$

We then have

$$\mathcal{W}^2_\infty\left(\mu^{\nu,\widetilde{X}}_{\tau_n}, \mu^{\widetilde{X}}_{\tau_n}\right) = \min\left\{c_k \,\middle|\, B^k \text{ contains a perfect matching}\right\} =: c_{\overline{k}}$$

which identifies the transport distance uniquely with the integer $\overline{k}$. We find $\overline{k}$ by increasing $k$ until the maximum-cardinality matchings of $B^k$ have length $N$, indicating that any maximum-cardinality matching is also a perfect matching. For this we use the Dulmage-Mendelsohn decomposition developed in [13], which decomposes a bipartite adjacency matrix into a block-diagonal matrix with one of the blocks revealing the length $N_k$ of the maximum-cardinality matchings. The decomposition can be computed in MATLAB using

the command `dmperm`.

A necessary condition for $B^k$ to contain a perfect matching is that $B^k$ represents a subgraph with the same vertex set as $G$ (also known as a spanning subgraph), which is identified by $B^k$ having no rows or columns of all zeros. Hence, we must have $\overline{k} \geq k_0$ where

$$k_0 = \min \left\{ k \,:\, B^k \text{ has no rows or columns of all zeros } \right\}.$$

(Without this condition we necessarily exclude at least one pair of particles from any maximum matching and so do not end up with a valid transport plan.) The algorithm is as follows:

**Algorithm**

Let $k = k_0$.
While $k \leq k_{\max}$:

1. Compute the Dulmage-Mendelsohn decomposition of $B^k$.
2. Let $N_k$ be the length of a maximum-cardinality matching of $B^k$.
3. If $N_k = N$, return $\overline{k} = k$, else set $k = k + 1$.

We then have $\mathcal{W}_\infty^2 \left( \mu_{\tau_n}^{\nu,\widetilde{X}}, \mu_{\tau_n}^{\widetilde{X}} \right) = c_{\overline{k}}$. Computation of a maximum matching using `dmperm` can be shown to take $\mathcal{O}(N^2)$ flops and so the algorithm must terminate with a worst-case running time of $\mathcal{O}(N^2(N^2 - k_0))$. For the purposes of the zero-diffusion limit, however, this appears closer to $\mathcal{O}(N^2)$, as for small $\nu$ we see that $\overline{k}$ is reasonably close to $k_0$.

### 4.3.3 Error Analysis

The above algorithm is used to compute the distance between *numerical* empirical measures. To reveal the asymptotic $\mathcal{O}(\nu)$ rate, the particle simulations must be sufficiently accurate, which is dictated by the timestep $\Delta t$. Rather than pick a very small, uniform timestep for all simulations (i.e. for every value of $\nu$), which would result in exceedingly long computation times, we give here a heuristic argument for using the scaling

$$\Delta t \sim \sqrt{\nu}.$$

Fix $\nu$ and consider copies of the numerical particle systems $\widetilde{X}_{\tau_n}^{\nu}$ and $\widetilde{X}_{\tau_n}$, both with uniform timestep $\Delta t$, and copies of the exact particle systems $X_t^\nu$ and $X_t$, with all four systems initialized at the same $X_0$. For a fixed time $\tau_n$, let $\sigma_n$ be a minimizing permutation for $\mathcal{W}_\infty^2 \left( \mu_{\tau_n}^{\nu,X}, \mu_{\tau_n}^{X} \right)$ as in equation (4.9). We can then relate the numerical and exact $\mathcal{W}_\infty$

distances as follows:

$$\begin{aligned}
\mathcal{W}_\infty^2\left(\mu_{\tau_n}^{\nu,\widetilde{X}},\mu_{\tau_n}^{\widetilde{X}}\right) &\le \max_i\left|\widetilde{X}_{\tau_n}^{\nu,i}-\widetilde{X}_{\tau_n}^{\sigma_n(i)}\right|^2\\
&= \max_i\left|\widetilde{X}_{\tau_n}^{\nu,i}-\widetilde{X}_{\tau_n}^{\sigma_n(i)}\right|^2-\left(\max_i\left|X_{\tau_n}^{\nu,i}-\widetilde{X}_{\tau_n}^{\sigma_n(i)}\right|^2-\max_i\left|X_{\tau_n}^{\nu,i}-\widetilde{X}_{\tau_n}^{\sigma_n(i)}\right|^2\right)\\
&\le \left(\max_i\left|\widetilde{X}_{\tau_n}^{\nu,i}-\widetilde{X}_{\tau_n}^{\sigma_n(i)}\right|^2-\max_i\left|X_{\tau_n}^{\nu,i}-\widetilde{X}_{\tau_n}^{\sigma_n(i)}\right|^2\right)\\
&\quad+\max_i\left|X_{\tau_n}^{\nu,i}-X_{\tau_n}^{\sigma_n(i)}\right|^2+2C\Delta t\left(\max_i\left|X_{\tau_n}^{\nu,i}-X_{\tau_n}^{\sigma_n(i)}\right|\right)+(C\Delta t)^2\\
&= \left(\max_i\left|\widetilde{X}_{\tau_n}^{\nu,i}-\widetilde{X}_{\tau_n}^{\sigma_n(i)}\right|^2-\max_i\left|X_{\tau_n}^{\nu,i}-\widetilde{X}_{\tau_n}^{\sigma_n(i)}\right|^2\right)\\
&\quad+\mathcal{W}_\infty^2\left(\mu_{\tau_n}^{\nu,X},\mu_{\tau_n}^{X}\right)+2C\Delta t\,\mathcal{W}_\infty\left(\mu_{\tau_n}^{\nu,X},\mu_{\tau_n}^{X}\right)+(C\Delta t)^2
\end{aligned}$$

where we have used the triangle inequality

$$\left|X_{\tau_n}^{\nu,i}-\widetilde{X}_{\tau_n}^{\sigma_n(i)}\right|\le\left|X_{\tau_n}^{\nu,i}-X_{\tau_n}^{\sigma_n(i)}\right|+\left|\widetilde{X}_{\tau_n}^{\sigma_n(i)}-X_{\tau_n}^{\sigma_n(i)}\right|\le\left|X_{\tau_n}^{\nu,i}-X_{\tau_n}^{\sigma_n(i)}\right|+C\Delta t$$

and $C\Delta t$, $C>0$, is the error in the approximation $\widetilde{X}_{\tau_n}$ due to the explicit Euler rule.

Taking expectations on both sides (see Remark 4.5) and using the $\mathcal{O}(\nu)$ convergence of Theorem 4.3, we get

$$\begin{aligned}
\mathbb{E}\left[\mathcal{W}_\infty^2\left(\mu_{\tau_n}^{\nu,\widetilde{X}},\mu_{\tau_n}^{\widetilde{X}}\right)\right] &\le C_1(\Delta t\,;\,\nu)+\mathbb{E}\left[\mathcal{W}_\infty^2\left(\mu_{\tau_n}^{\nu,X},\mu_{\tau_n}^{X}\right)\right]\\
&\quad+2C\Delta t\,\mathbb{E}\left[\mathcal{W}_\infty\left(\mu_{\tau_n}^{\nu,X},\mu_{\tau_n}^{X}\right)\right]+(C\Delta t)^2\\
&\le C_1(\Delta t\,;\,\nu)+\widetilde{C}\left(\nu+\sqrt{\nu}\Delta t+\Delta t^2\right)
\end{aligned}$$

for constant $\widetilde{C}$ independent of $\Delta t$ and $\nu$, and weak error in the approximation $\widetilde{X}_{\tau_n}^{\nu,}$ given by

$$C_1(\Delta t\,;\,\nu)=\left|\mathbb{E}\left(\max_i\left|\widetilde{X}_{\tau_n}^{\nu,i}-\widetilde{X}_{\tau_n}^{\sigma_n(i)}\right|^2\right)-\mathbb{E}\left(\max_i\left|X_{\tau_n}^{\nu,i}-\widetilde{X}_{\tau_n}^{\sigma_n(i)}\right|^2\right)\right|.$$

Here the test function used in the weak error is of the form

$$f_{\sigma,y}\left(x\right):=\max_i\left|\pi_i(x)-\pi_{\sigma(i)}(y)\right|^2$$

where $\pi_i(x)$ is the projection onto the $i$th coordinate of $x\in D^N$ and $y\in D^N$ is fixed.

Now, if we let $\Delta t=\mathcal{O}(\sqrt{\nu})$, we see that

$$\mathbb{E}\left[\mathcal{W}_\infty^2\left(\mu_{\tau_n}^{\nu,\widetilde{X}},\mu_{\tau_n}^{\widetilde{X}}\right)\right]=\mathcal{O}(\nu)$$

as desired provided that

$$C_1(\Delta t\,;\,\nu) = \mathcal{O}(\Delta t\sqrt{\nu}). \tag{4.10}$$

At the moment we are unable to provide a proof of the asymptotic behaviour (4.10). As mentioned above, the convergence plot in Figure 4.2 suggests that $C_1(\Delta t\,;\,\nu) = \mathcal{O}(\Delta t)$ for fixed $\nu$, consistent with the weak convergence of the symmetrized Euler scheme. As well, using $\Delta t = \sqrt{\nu}$ is seen in the results below to produce the desired $\mathcal{O}(\nu)$ convergence rate, so we adopt the scaling $\Delta t \sim \sqrt{\nu}$ as a heuristic and leave further justification to future work.

**Remark 4.5.** Strictly speaking, we cannot guarantee that the weak numerical copy $\widetilde{X}^{\nu}_{\tau_n}$ is defined on the same probability space as the copy $X^{\nu}_{\tau_n}$ of the exact solution, so we take expectation with respect to their product measures under the assumption that the underlying Brownian motions are independent in the product space.

### 4.3.4 Monte Carlo Algorithm

To calculate the expectation in Theorem 4.3, we average over sample trajectories using the following Monte Carlo algorithm. For convenience, denote the expectation of the squared distance between *exact* empirical measures by

$$W^{\nu}(\tau_n) := \mathbb{E}\left[\mathcal{W}_{\infty}^2\left(\mu^{\nu,X}_{\tau_n}, \mu^{X}_{\tau_n}\right)\right]$$

and the expectation of the squared distance between *numerical* empirical measures by

$$\widetilde{W}^{\nu}(\tau_n) := \mathbb{E}\left[\mathcal{W}_{\infty}^2\left(\mu^{\nu,\widetilde{X}}_{\tau_n}, \mu^{\widetilde{X}}_{\tau_n}\right)\right].$$

The following algorithm is used to approximate $\widetilde{W}^{\nu}(\tau_n)$ from numerically simulated sample trajectories. We then discuss how this in turn provides a good approximation of $W^{\nu}(\tau_n)$.

#### Sample Trajectories, Sample Average and Confidence Intervals

For $\nu$ fixed, the $m$th sample trajectory $\widetilde{Y}_m\left(\tau_n\,;\,\nu\right)$ is computed as follows:

1. Generate initial particle positions $\widetilde{X}_{\tau_0} = \widetilde{X}^{\nu}_{\tau_0} = \{X_0^i\}_{i=1}^N$ randomly from the common law $\mu_0$.

2. Advance particle systems $\widetilde{X}_{\tau_n}$ and $\widetilde{X}^{\nu}_{\tau_n}$ independently in time according to (4.6) and (4.8).

3. Use (4.9) to compute $\widetilde{Y}_m\left(\tau_n\,;\,\nu\right) := \mathcal{W}_{\infty}^2\left(\mu^{\nu,\widetilde{X}}_{\tau_n}, \mu^{\widetilde{X}}_{\tau_n}\right)$ at each time $\tau_n$.

We then estimate $\widetilde{W}^{\nu}(\tau_n)$ by averaging over the sample trajectories $\widetilde{Y}_m\left(\tau_n\,;\,\nu\right)$ and compute approximate confidence intervals using methods from [27] and [23], which we recall here.

First, we divide the $M$ samples into an $N_1 \times N_2$ array $\left\{\widetilde{Y}_{ij}\left(\tau_n\,;\,\nu\right)\right\}$ and define the batch averages and sample average, respectively, by

$$\widetilde{E}_i\left(\tau_n\,;\,\nu\right) := \frac{1}{N_2}\sum_{j=1}^{N_2}\widetilde{Y}_{ij}\left(\tau_n\,;\,\nu\right) \quad \text{and} \quad \widetilde{E}_M\left(\tau_n\,;\,\nu\right) := \frac{1}{M}\sum_{m=1}^{M}\widetilde{Y}_m\left(\tau_n\,;\,\nu\right).$$

Then we define the sample variance by

$$\widetilde{\sigma}^2_{N_1} := \frac{1}{N_1-1}\sum_{i=1}^{N_1}\left(\widetilde{E}_i\left(\tau_n\,;\,\nu\right) - \widetilde{E}_M\left(\tau_n\,;\,\nu\right)\right)^2.$$

By the Central Limit Theorem we have that the batch averages $\widetilde{E}_i\left(\tau_n\,;\,\nu\right)$ are approximately Gaussian, which implies that the random variable

$$T_{N_1} := \frac{\widetilde{E}_M\left(\tau_n\,;\,\nu\right) - \widetilde{W}^{\nu}(\tau_n)}{\sqrt{\widetilde{\sigma}^2_{N_1}/M}}$$

has approximately the standard Student's $t$-distribution with $N_1 - 1$ degrees of freedom, noting that $\widetilde{W}^{\nu}(\tau_n)$ is the true mean of the trajectories $\widetilde{Y}_m\left(\tau_n\,;\,\nu\right)$. Letting $\Psi$ be the cumulative distribution for $T_{N_1}$, the $100(1-\alpha)$ confidence intervals are then

$$CI_\alpha(\tau\,;\,\nu) := \left[\widetilde{E}_M\left(\tau_n\,;\,\nu\right) - \delta\,,\,\widetilde{E}_M\left(\tau_n\,;\,\nu\right) + \delta\right]$$

where

$$\delta = \left(\sqrt{\frac{\widetilde{\sigma}^2_{N_1}}{M}}\right)\Psi^{-1}\left(\frac{1-\alpha}{2}\right).$$

This arises from the approximation

$$\mathbb{P}\left(\left|\widetilde{E}_M\left(\tau_n\,;\,\nu\right) - \widetilde{W}^{\nu}(\tau_n)\right| < \delta\right) \approx \mathbb{P}\left(|T_{N_1}| < \delta\sqrt{\frac{M}{\widetilde{\sigma}^2_{N_1}}}\right) = 2\Psi\left(\delta\sqrt{\frac{M}{\widetilde{\sigma}^2_{N_1}}}\right) =: 1-\alpha.$$

As such, $CI_\alpha(\tau\,;\,\nu)$ constructed in this way can be assumed to contain the true (numerical) mean $\widetilde{W}^{\nu}(\tau_n)$ with probability $1-\alpha$ so long as $N_2$ is large enough that the batch averages $\widetilde{E}_i\left(\tau_n\,;\,\nu\right)$ are well approximated by Gaussian random variables. According to [23], this is a reasonable assumption in practice for $N_2 > 15$.

### Convergence in the Zero-Diffusion Limit

Finally, for any fixed $\tau_n$ we calculate the convergence rate $p$ of the sample average, such that $\widetilde{E}_M\left(\tau_n\,;\,\nu\right) = \mathcal{O}(\nu^p)$ with probability $1-\alpha$, by repeating the steps above along a decreasing sequence of diffusion coefficients $\{\nu_k\}$. A rate of $p = 1$ agrees with the analytical

rate in Theorem 4.3. To reiterate the levels of approximation taking place, the sample average $\widetilde{E}_M(\tau_n\,;\,\nu)$ is an approximation of the numerical mean $\widetilde{W}^\nu(\tau_n)$, which in turn is an approximation of the true mean $W^\nu(\tau_n)$, at time $\tau_n$. If the error in the particle simulations is controlled such that $\widetilde{W}^\nu(\tau_n) = \mathcal{O}(\nu)$ (possible in practice from the the scaling $\Delta t \sim \sqrt{\nu}$ as in Section 4.3.3), and the number of samples $M$ is taken large enough that $CI_\alpha(\tau\,;\,\nu)$ also scales as $\mathcal{O}(\nu)$, then we can expect to see $\widetilde{E}_M(\tau_n\,;\,\nu) = \mathcal{O}(\nu)$ in agreement with theory.

## 4.4 Numerical Results

As mentioned above, Theorems 4.2 and 4.3 improve on a previous result found in [34] in two ways: the rate of convergence is improved from $\mathcal{O}\left(\nu^{\frac{1}{d+2}}\right)$ to $\mathcal{O}(\nu)$, which no longer depends on the dimension $d$, and the regularity requirement on the potentials $K$ and $V$ is weakened from $C^2$ to $C^1$. This allows for interaction potentials $K$ with jump discontinuities in the second derivative, or worse, points $x$ where $\nabla K(x)$ is not Lipschitz continuous. We use potentials below that reflect this weakened regularity constraint, showing that the improved $\mathcal{O}(\nu)$ asymptotic convergence shows up in the numerics on two canonical domains $D \subset \mathbb{R}^2$.

### 4.4.1 Simulation Parameters

For all simulations, we fix the number of particles at $N = 1000$, the number of sample trajectories at $M = 250$ and the external potential at $V = 0$. Convergence as $\nu \to 0$ is shown on the time interval $t \in [0, 1]$, which is seen in Figures 4.3 and 4.4 to be long enough to capture interesting dynamics. The timestep is set to $\Delta t = \sqrt{\nu}$ given the arguments above, where the convergence rate as $\nu \to 0$ is calculated from the sample averages $\widetilde{E}_M(\tau_n\,;\,\nu)$ for $\nu = 2^{-16}, 2^{-18}, \ldots, 2^{-30}$. All pseudo-random number generation is done in MATLAB with initial seed chosen randomly for each sample trajectory from the system time on the computer.

In connection with previous results in [18] and [19] on the formation of disconnected states under $K_{QANR}$, we examine attractive-repulsive potentials similar to those in Chapter 3, with $C^1$-regularized Newtonian repulsion and power-law attraction:

$$K(x) = \phi_\epsilon(x) + \frac{1}{p}|x|^p. \tag{4.11}$$

Recall that in two dimensions the Newtonian potential is $\phi(x) = -\frac{1}{2\pi}\log|x|$. We regularize $\phi$ using

$$\phi_\epsilon(x) = \begin{cases} \dfrac{1}{4\pi}\left(1 - 2\log(\epsilon)\right) - \dfrac{1}{4\pi\epsilon^2}|x|^2, & |x| \le \epsilon\ , \\ -\dfrac{1}{2\pi}\log|x|, & |x| > \epsilon, \end{cases} \tag{4.12}$$

where $\epsilon$ is fixed at 0.05 throughout in order to stay reasonably close to the Newtonian repulsion given by $\phi$.

We examine the two cases

$$K_2(x) := \phi_\epsilon(x) + \frac{1}{2}|x|^2 \quad \text{and} \quad K_{3/2}(x) := \phi_\epsilon(x) + \frac{2}{3}|x|^{3/2},$$

because $K_2$ has a jump in the second derivative and $\nabla K_{3/2}$ is not Lipschitz continuous at $x = 0$. Both $K_2$ and $K_{3/2}$ are $C^1(\mathbb{R}^2)$, have a jump in the second derivative at $x = \epsilon$, and are $\lambda$-convex with $\lambda = -\frac{1}{\pi\epsilon^2}$, but $K_2$ is of class $W^{2,\infty}_{loc}(\mathbb{R}^2)$ while $K_{3/2}$ falls into $C^1(\mathbb{R}^2) \setminus W^{2,\infty}_{loc}(\mathbb{R}^2)$ due to the Lipschitz singularity at $x = 0$.

The domains we consider are the half-plane $D_H = [0, \infty) \times \mathbb{R}$ and the disk $D_C = \{x \in \mathbb{R}^2 : |x| \leq 0.2\}$. Given the potentials above, $D_H$ provides an example of self-organization near the boundary of a domain where there is abundant free space to move away from the boundary, while $D_C$ presents a situation where the natural support of the swarm is confined by $\partial D$. The two cases lead to starkly different boundary interactions at large times, as seen by the snapshots at $T = 100$ in Figures 4.3 and 4.4. Initial positions $X_0$ (shared by both particle systems) are drawn randomly for each trajectory from a uniform square distribution with $\text{Law}(X_0) = \chi_{[0,1/4]\times[-1/8,1/8]}$ for $D_H$ and $\text{Law}(X_0) = \chi_{[-1/20,1/20]\times[0,1/10]}$ for $D_C$.

**Remark 4.6.** Since $D_H$ is unbounded, it violates the boundedness assumption of Theorem 4.3; however, particle simulations in $D_H$ can be interpreted as occurring in a large domain $D \subset \mathbb{R}^2$ such that $\partial D$ is flat near $X_0$ and $D$ far exceeds the natural support of the particle systems for $t \in [0, 1]$ with high probability.

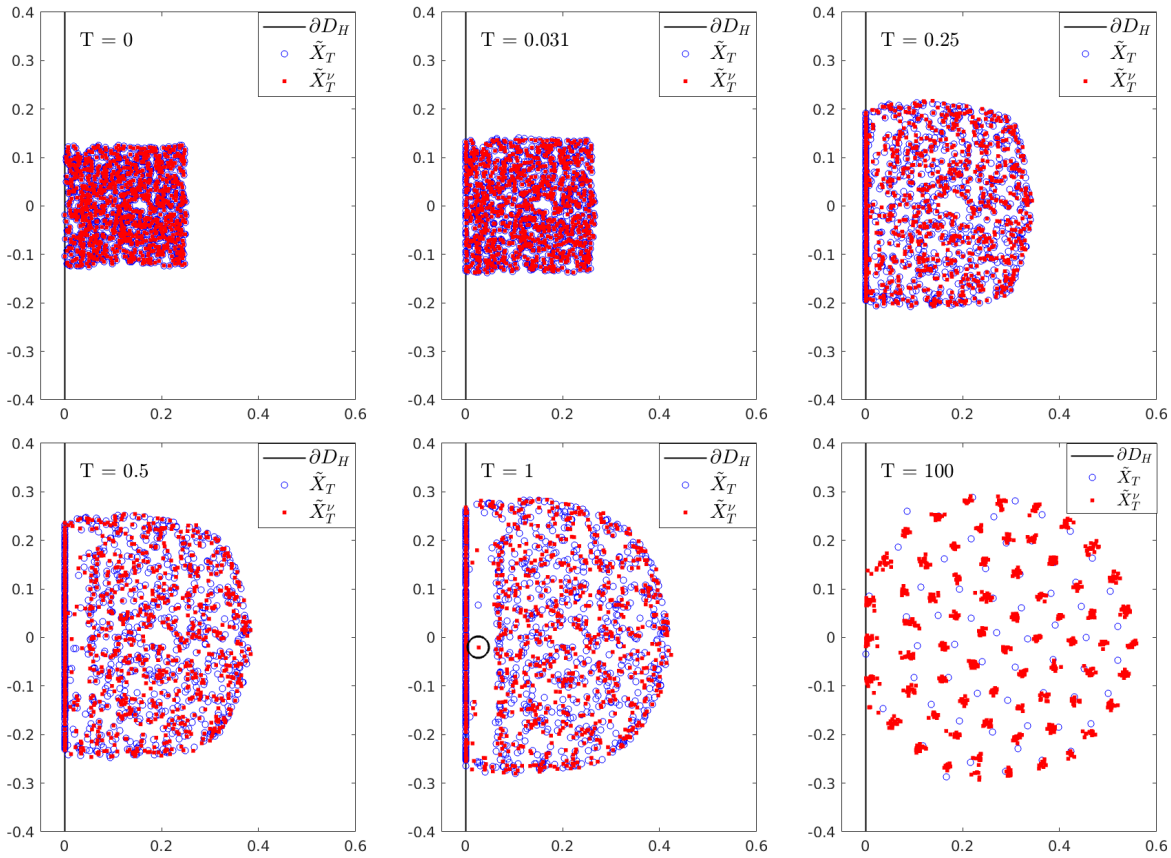


Figure 4.3: Swarming in the half-plane $D_H$ with the interaction potential $K_{3/2}$, $\Delta t = 2^{-8}$ and $\nu = 2^{-16}$. Blue circles and red squares represent non-diffusive and diffusive particles, respectively. The particle systems rapidly expand until $T \approx 1$, after which attractive forces confine the swarm. At $T = 1$ a representative particle is circled in the space between the boundary aggregation and the free swarm, illustrating the pair-separation effect mentioned in the text below. By time $T = 100$ the swarm has nearly escaped the boundary and is contained in a disk in free space, with diffusive particles forming concentrated clumps and non-diffusive particles forming $\delta$-aggregations.

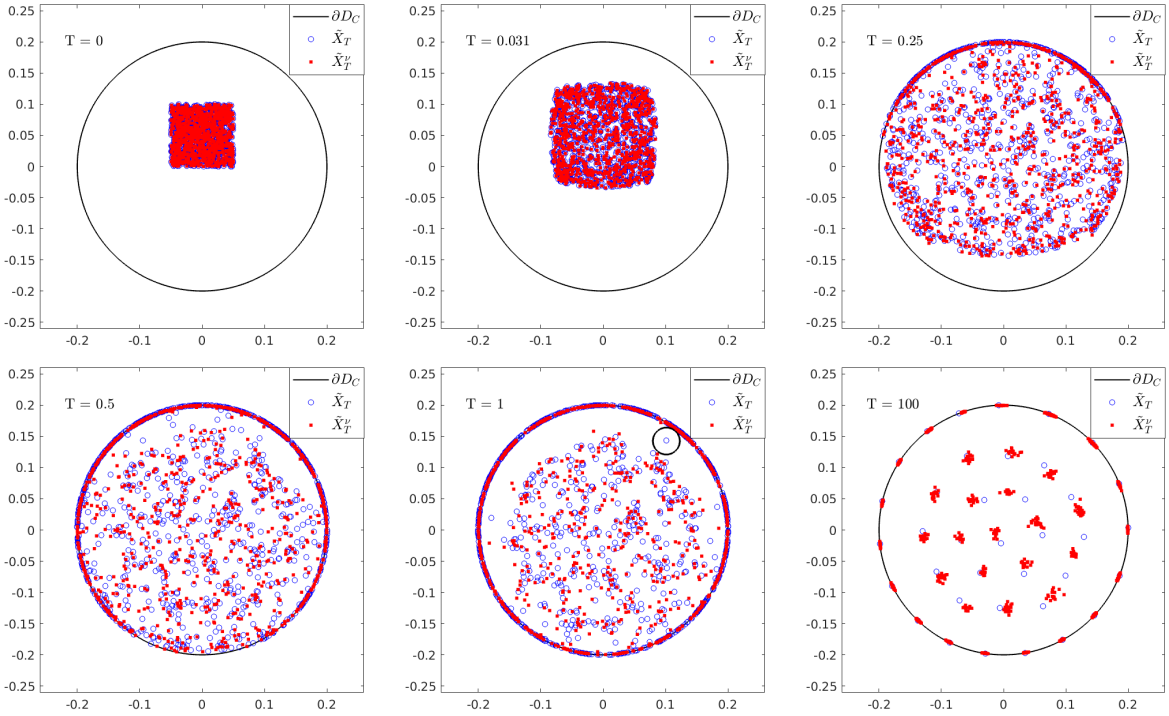


Figure 4.4: Swarming in the disk $D_C$, with $K, \nu$ and $\Delta t$ as in Figure 4.3. By time $T \approx 1$, particles have formed a boundary aggregation and a free swarm, as in the domain $D_H$, with another representative particle (circled) caught between the boundary and free swarm. By time $T = 100$ the swarm has formed a disk of particle aggregates centred in the domain along with periodic aggregations along the boundary.

---

### 4.4.2 Results

The convergence rate for each of the four {domain, potential} combinations $\{D_H, K_2\}$, $\{D_H, K_{3/2}\}$, $\{D_C, K_2\}$ and $\{D_C, K_{3/2}\}$ is conveyed in Figure 4.5. At times $T = 0.031$, $T = 0.25$ and $T = 0.5$ we capture the desired $\mathcal{O}(\nu)$ convergence, while by time $T = 1$ the convergence behaviour is not as well resolved, particularly for $K_{3/2}$ on $D_C$, where the desired rate is only seen asymptotically for $\nu \lesssim 10^{-6.7}$. This can be attributed to a number of factors. Statistical errors can be expected to grow over time, as even the coarsest trajectories have at least $n = 256$ timesteps by $T = 1$ (see in particular the growth of confidence intervals in Figure 4.6). Since $K_{3/2}$ results in a non-Lipschitz interaction force between particles, we are also outside of the usual theory for numerical SDE, which could be a factor. Furthermore, for $\epsilon = 0.05$ the $\lambda$-convexity constant is rather high, at $\lambda \approx -133$. According to Theorem 4.3, which states for $V = 0$ and $D \subset \mathbb{R}^2$ that

$$\mathbb{E}\left[\mathcal{W}_\infty^2\left(\mu_t^{\nu,X}, \mu_t^X\right)\right] \leq 4\nu t\left(1 - 2\lambda^- t e^{-2\lambda^- t}\right),$$

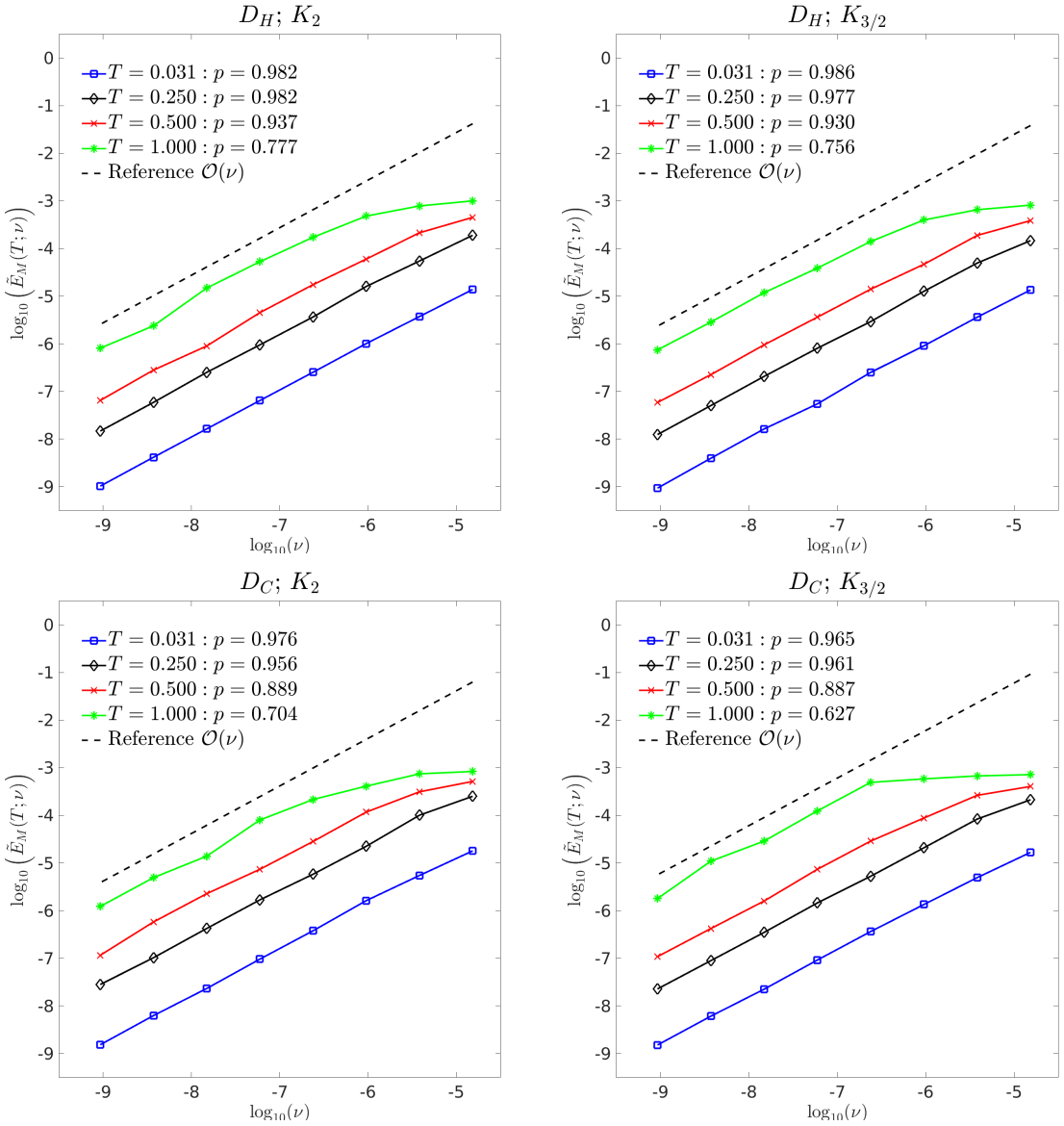


Figure 4.5: (Top) Convergence results. Clockwise from top left: $\{D_H, K_2\}$, $\{D_H, K_{3/2}\}$, $\{D_C, K_{3/2}\}$ and $\{D_C, K_2\}$. Agreement with the theoretical rate of $\mathcal{O}(\nu)$ is very good for $T \lesssim 0.5$, while for $T = 1$ we see $\mathcal{O}(\nu)$ convergence only for sufficiently small $\nu$, below approximately $\nu = 10^{-6.7}$.

it is possible to see rapid exponential divergence in time of the solutions for any fixed $\nu$, although the estimate above arrives from a Grönwall-type argument and should not be assumed to be a tight bound.

Examining the divergence in time a little more closely, we do observe an exponential curve which matches the form above, although with growth constant far below $2\lambda$. As shown in Figure 4.6 for $\nu = 2^{-28}$ and $K_{3/2}$, the data $\{\tau_n, E^\nu(\tau_n)\}_{n=0}^L$ obtains a nonlinear least-squares fit to $y(t) = at(1 + bte^{bt})$ with residual less than $10^{-12}$, where $b \approx 2.37$ on $D_H$ and $b \approx 4.14$ on $D_C$.

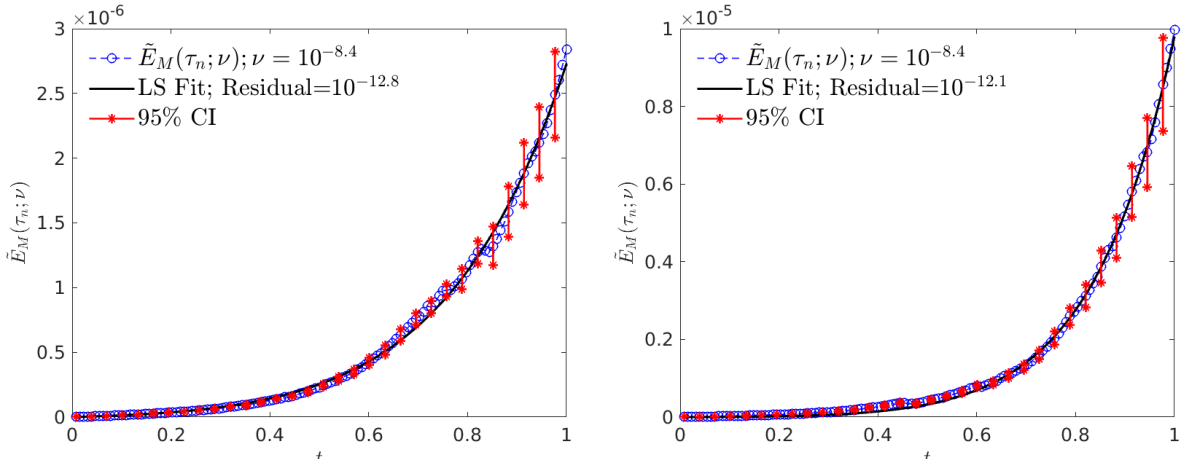


Figure 4.6: Evolution of $\widetilde{E}_M(\tau_n;\nu)$ over time with $\nu = 2^{-28} \approx 10^{-8.4}$ and interaction potential $K_{3/2}$ for the half-plane $D_H$ (left) and disk $D_C$ (right). As expected, the variance of $\widetilde{E}_M(\tau_n;\nu)$ grows significantly over time (as seen by the 95% confidence intervals), yet we see excellent agreement using a nonlinear least-squares fit to a curve of the form $y(t) = at(1 + bte^{bt})$, matching that of the bounding curve in Theorem 4.3.

---

The reasons above for the lack of perfect agreement at $T = 1$ are plausible, although we believe the real reason is more physical. By time $T = 1$ the swarm has mostly separated into a boundary aggregation and a free swarm component. Particles occupying the space *in between* the boundary aggregation and the free swarm are eventually separated as one flies with high velocity into the boundary and the other is pulled gradually into the free swarm. For a pair of particles $\widetilde{X}^{\nu,i}_{\tau_n}$ and $\widetilde{X}^{i}_{\tau_n}$ sharing the same initial position and which end up in the space between the boundary and free aggregations, it is highly likely that one particle will be pulled onto the boundary and the other particle will be left drifting towards the free swarm (examples of this are circled in Figures 4.3 and 4.4 at time $T = 1$). This pair-separation effect puts a lower bound on $\mathcal{W}^2_\infty\left(\mu^{\nu,\widetilde{X}}_{\tau_n}, \mu^{\widetilde{X}}_{\tau_n}\right)$ which we believe only disappears for $\nu$ below a certain threshold. This could provide an answer for why the $\mathcal{O}(\nu)$ convergence is not visible in the numerics at later times for $\nu > 10^{-6}$.

# Chapter 5

# Conclusion

## 5.1 Summary of Results

We have explored a model for self-organization of autonomous particles in spatial domains with boundaries, where the motion of particles is determined by competing particle-particle interactions, external forces and Brownian motion. The addition of Brownian motion at the particle level, or linear diffusion at the continuum, is motivated by the dynamic evolution into unstable equilibria seen in the model without diffusion [18, 19]. We have analyzed equilibria of the model at the continuum level (Ch. 2), extending and adding to similar results in free space found in [10]. The analysis is complemented by a series of numerical methods and experiments (Ch. 3) designed to motivate researchers to investigate challenging parameter regimes, such as small diffusion, large attraction, and/or low regularity of the potentials $K$ and $V$. In correspondence with the plain aggregation model, we have also established the zero-diffusion limit numerically (Ch. 4) in order to motivate further numerical exploration of aggregation-diffusion phenomena using stochastic particle methods, the analysis of which is still in its infancy, especially for interacting reflected SDEs.

### 5.1.1 Existence of Global Minimizers

By exploiting the underlying gradient flow structure of model (1.20), in Chapter 2 we analyze equilibria of the model as critical points of the associated energy functional $\mathcal{E}^\nu$ defined in (1.24). Compared to the model in free space (1.18), we find that the linearly-diffusive aggregation system in domains with boundaries (1.20) retains the condition for non-existence of global minimizers found in [10] (Theorem 2.6), up to a factor of $d$, but that more is needed to guarantee existence of a global minimizer due to the escaping mass phenomenon (Theorems 2.13 and 2.15). As such, we find that in addition to bounding the energy below, existence of global minimizers in general domains $D$ requires that mass be suitably contained by an external potential $V$, unless $D$ is sufficiently symmetric, as detailed in Theorems 2.18 and 2.19. To the best of our knowledge, such metastable escaping mass

phenomena have not previously been documented.

### 5.1.2 Computation of Critical Points

Due to the multiple instances of metastability in the aggregation-diffusion model (as well as escaping mass, see metastable mass transfer in [15]), it is desirable to compute equilibria directly in a time-independent manner. As such, in Chapter 3 we introduce a fixed-point method and a Newton continuation method for computing critical points of $\mathcal{E}^\nu$ directly from the Euler-Lagrange equation. For comparison with dynamics, we also detail an implicit-explicit finite-difference scheme for solving the PDE (1.20). Examples are given for $D = [0, L]$, although extension to general bounded tensor grids is possible.

These methods allow one to examine several limiting cases for the parameters at play in the model. If one wishes to compute critical points for $\nu \ll 1$, the Newton iterator should be employed with continuation on $\nu$, followed by the fixed-point iterator to resolve decay properties of the solution. Due to its stability with respect to time-step, the PDE solver may also be used to efficiently translate the solution to its final centre of mass under the external potential $V$ before employing the fixed-point iterator. Overall, the fixed-point iterator is seen to be the most robust in producing solutions to the Euler-Lagrange equation. The regularizing effect of the $e^{-x}$ term allows for treatment of interaction potentials $K$ with large attraction, and since the method does not require computation of derivatives, it is well suited for experimentation with $K$ and $V$ at low regularities. To the best of our knowledge, (i) numerical implementation of the Euler-Lagrange equation in the form (2.8) and (ii) analysis of the integro-differential equation (3.4), are both new developments with potential for further analysis and use in simulations.

### 5.1.3 Zero-Diffusion Limit

Here we numerically verify that the distance between the diffusive and non-diffusive particle systems $X_t$ and $X_t^\nu$, respectively, behaves as predicted from Theorem 4.3. That is, we find that numerically the stochastic particle system $X_t^\nu$ converges to the deterministic particle system $X_t$ in expectation as $\nu \to 0$ with the predicted $\mathcal{O}(\nu)$ convergence rate, when the domain is bounded and convex. This means that we can expect numerical simulations of the linearly-diffusive aggregation model at the stochastic particle level to be controllably close to the dynamics of the plain aggregation model. Such verification is meant to convince readers that (i) linear diffusion (Brownian motion at the particle level) is a robust regularization of the plain aggregation model, both analytically and in practice, and (ii) stochastic particle numerics are a valid and efficient way to explore perturbations of the plain aggregation model induced by small noise.

## 5.2 Future Directions

### 5.2.1 Identifying Minimizers

It is well known (see [4, 18, 10]) that the energy $\mathcal{E}$ associated with the plain aggregation model enjoys a convenient test for minimizers: $\overline{\rho}$ is a minimizer of $\mathcal{E}$ if and only if

(i) $K * \overline{\rho}(x) + V(x) = \lambda$ on $\text{supp}\,(\overline{\rho})$, and

(ii) $K * \overline{\rho}(x) + V(x) \geq \lambda$ on $D \cap (\text{supp}\,(\overline{\rho}))^c$,

where $\lambda$ is a contant. The first condition is the Euler-Lagrange equation, while the second condition identifies a critical point as a minimizer. Since $\text{supp}\,(\overline{\rho}) = D$ for minimizers of $\mathcal{E}^\nu$, condition (ii) no longer applies in the case of aggregation with linear diffusion, thus we have no simple way to check that a given critical point is a minimizer. An immediate future direction would be to analyze the second variation of the energy to assess the stability of critical points. A $\mathcal{W}_p$-$r$ local minimizer $\overline{\rho}$ satisfies

$$\left.\frac{d^2}{dt^2}\right|_{t=0} \mathcal{E}^\nu[\overline{\rho} + t(\eta - \overline{\rho})] \geq 0 \quad \text{for all} \quad \eta \in B_p\left(\overline{\rho}, r\right),$$

which implies

$$\int_D \left(K * (\overline{\rho} - \eta)\right)(\overline{\rho} - \eta)dx + \nu \int_D \frac{(\overline{\rho} - \eta)^2}{\overline{\rho}} dx \geq 0. \tag{5.1}$$

To ensure that (5.1) holds for all $\eta \in B_p\left(\overline{\rho}, r\right)$, one might look at the spectrum of the convolution operator $G(f) := K * f$ over the space $S = \left\{f \in L^1(D) : \int_D f(x)dx = 0\right\}$, since $\overline{\rho} - \eta \in S$. If the spectrum of $G$ is bounded below by some $\gamma$, then it appears that a threshold diffusion coefficient $\nu_\gamma$ might exist such that for $\nu > \nu_\gamma$, every critical point is a minimizer. Indeed, let $\overline{\rho} - \eta$ be an eigenfunction of $G$ for such $\gamma$. Then

$$\begin{aligned}\int_D \left(K * (\overline{\rho} - \eta)\right)(\overline{\rho} - \eta)dx + \nu \int_D \frac{(\overline{\rho} - \eta)^2}{\overline{\rho}}\, dx &= \gamma \int_D (\overline{\rho} - \eta)^2\, dx + \nu \int_D \frac{(\overline{\rho} - \eta)^2}{\overline{\rho}}\, dx \\ &= \int_D \frac{(\overline{\rho} - \eta)^2}{\overline{\rho}} \left(\gamma\overline{\rho} + \nu\right)\, dx.\end{aligned}$$

For $\nu > |\gamma| \left\|\overline{\rho}\right\|_\infty$ it appears that the second variation is positive and $\overline{\rho}$ is a minimizer, which suggests finding an upper bound on $\left\|\overline{\rho}\right\|_\infty$ over all critical points. This might be possible with help from the fixed-point characterization of critical points (2.8). It would be very beneficial to devise a stability criterion for equilibria that is practical, in analogy to condition (ii) above, for equilibria of the plain aggregation model.

### 5.2.2 Uniqueness of Minimizers

The fixed-point characterization of critical points (2.8) might also play an even more important role, that of determining cases for uniqueness of minimizers. In [3] the authors

do just this on $D = \mathbb{R}$ and purely attractive $K$ and $V = 0$, providing hope that similar techniques can be extended to more general settings. At the time of writing this, we are actively pursuing such an extension to $D = [0, \infty)$, where we hope to show that large enough $V$ enforces uniqueness of fixed points. Figure 3.6 displaying non-uniqueness in the absence of $V$ suggests that small diffusion might degrade the uniqueness of minimizers, which agrees with the conjectured critical diffusion $\nu_\gamma$ above. In general, it seems possible to arrive at regions of parameter space in which minimizers are unique simply by characterizing fixed points, which would put the numerical fixed-point iteration method on stronger footing.

### 5.2.3 Connection to the Plain Aggregation Model

Finally, we return to the plain aggregation model. As mentioned above, investigation of the aggregation model with linear diffusion was motivated by the formation of unstable states $\overline{\mu}_{ds}$ in the plain aggregation model, which consist of a boundary aggregation and free-swarm component with disjoint supports ([18], [19]). To this end, the driving question is this: does the aggregation model with linear diffusion also evolve into unstable equilibria in domains with boundaries?

On $D = [0, \infty)$ with $V = 0$ we can now provide an answer: for an equilibrium $\overline{\mu}_{ds}$ of the plain aggregation model which contains a boundary aggregation, the fate of $\overline{\mu}_{ds}$ when linear diffusion is "switched on" is entirely explained by the escaping mass phenomenon: mass will begin to translate to the right, with timescale proportional to the mass density at $x = 0$. Specifically, using the calculation in Remark 2.17, we see that

$$\frac{d}{dt} M_1(\mu_t^\nu) = \nu \, \rho_t^\nu(0),$$

which must be positive for all time since $\operatorname{supp}(\mu_t^\nu) = D$. In this way, "regularization" by linear diffusion has replaced an unstable state with a metastable state.

We have much less conclusive evidence on what happens in higher dimensions when linear diffusion is added, only that such unstable disconnected equilibria can only form when some external potential $V$ is applied to push the swarm into the boundary [19]. We see in Figure 3.8 the formation of "separated equilibria", with a boundary aggregation and free swarm connected by a thin layer of mass, which we expect to be minimizers. Perhaps such separated states are a generic, and stable, effect of domains with boundaries. If so, this might warrant investigation of specific biological swarms which frequently interact with boundaries, such as red blood cells traveling down a blood vessel, or locust swarms sweeping across the Sahara desert, to identify when, if ever, it is more favorable to remain in separate aggregates, one being along the boundary.

### 5.2.4 Numerical Methods for Aggregation-Diffusion Equations

For computation of steady states, the methods in Chapter 3 are sufficient for one dimension, but require at least one linear convolution per iteration and should be made more efficient before scaling to higher dimensions. We do not offer any suggestions in this direction; we remark only that the FFT was attempted to increase resolution and decrease computation time, yet this attempt was unsuccessful due to lack of symmetry of the domain together with non-decaying potentials $K$ and $V$.

For dynamic simulations, stochastic particle methods do have their shortcomings and other options are out there. In [9] the authors develop a deterministic "blob" particle method for the aggregation equation with general diffusion, which avoids the need to average over many simulations as is required with stochastic methods. A robust suite of finite volume methods exists for simulation at the PDE level, although these only capture moderate diffusion levels, for which the dynamics are not necessarily related to the plain aggregation model. In general, all particle methods fail to resolve the decay of solutions, which for linear diffusion is exponential, under small noise. Continuum PDE methods, while allowing for positive mass over the entire (bounded) domain, in general fail to alleviate this problem, as they impose stringent time-step restrictions (for instance, on the advective flux), even when diffusion is handled implicitly.

In this way, for complicated geometries in dimensions 2 and greater, it appears that robust and accurate numerical experimentation of small-noise aggregation-diffusion phenomena is best carried out through stochastic particle methods; however, the analysis of such methods is far from complete. A useful avenue for the aggregation-diffusion community would be to devise higher-order-in-time numerical methods for simulating systems of interacting reflected diffusions which interact through potentials that are more singular than globally Lipschitz, as is often required in numerical methods for SDEs.

## 5.3 Closing Remarks

The suggestions above for further research on the aggregation-diffusion model (1.20) in domains with boundaries have not included making any changes to the model. There is a multitude of ways in which the model can be improved. For biological applications, non-radial and/or time-dependent interaction and external potentials could be used. Semi-permeable boundaries and other non-conservative effects could be included to allow swarms which grow or decay in time. Instead of an external potential, one might even consider placing the swarm in a surrounding fluid. These suggestions all only involve one aggregating species, which of course could be increased to include interactions between multiple species (work has been done in this direction, but not in domains with boundaries). All in all,

there is still a significant gap between the current aggregation-diffusion models and real-world applications. We hope, by presenting results and methods within the framework of random, nonlocally interacting systems in general spatial domains, that we have convinced readers that it is possible to bridge this gap, and that we are on our way to understanding the paradigm of self-organization using modern applied mathematics.

# Bibliography


[1] L. Ambrosio, N. Gigli, and G. Savaré. *Gradient Flows: in Metric Spaces and in the Space of Probability Measures*. Birkhäuser, Basel, 2008.

[2] D. Balagué, J.A. Carrillo, T. Laurent, and G. Raoul. Dimensionality of local minimizers of the interaction energy. *Archive for Rational Mechanics and Analysis*, 209(3):1055–1088, 2013.

[3] S. Benachour, B. Roynette, D. Talay, and P. Vallois. Nonlinear self-stabilizing processes–I existence, invariant probability, propagation of chaos. *Stochastic Processes and their Applications*, 75(2):173–201, 1998.

[4] A.J. Bernoff and C.M. Topaz. A primer of swarm equilibria. *SIAM Journal on Applied Dynamical Systems*, 10(1):212–250, 2011.

[5] P. Billingsley. *Convergence of Probability Measures*. John Wiley & Sons, Chicago, 2013.

[6] M. Bossy, E. Gobet, and D. Talay. A symmetrized Euler scheme for an efficient approximation of reflected diffusions. *Journal of Applied Probability*, 41(3):877–889, 2004.

[7] R.E. Burkard, M. Dell'Amico, and S. Martello. *Assignment Problems*. SIAM, Philadelphia, 2009.

[8] J.A. Carrillo, Y.-P. Choi, and S.P. Perez. A review on attractive–repulsive hydrodynamics for consensus in collective behavior. In N. Bellomo, P. Degond, and E. Tadmor, editors, *Active Particles, Volume 1*, pages 259–298. Birkhäuser, Cham, 2017.

[9] J.A. Carrillo, K. Craig, and F.S. Patacchini. A blob method for diffusion. *Calculus of Variations and Partial Differential Equations*, 58(2):53, 2019.

[10] J.A. Carrillo, M.G. Delgadino, and F.S. Patacchini. Existence of ground states for aggregation-diffusion equations. *Analysis and Applications*, 17(3):393–423, 2019.

[11] J.A. Carrillo, M. DiFrancesco, A. Figalli, T. Laurent, and D. Slepčev. Global-in-time weak measure solutions and finite-time aggregation for nonlocal interaction equations. *Duke Mathematical Journal*, 156(2):229–271, 2011.

[12] J.A. Carrillo, D. Slepčev, and L. Wu. Nonlocal-interaction equations on uniformly prox-regular sets. *Discrete and Continuous Dynamical Systems Series A*, 36(3):1209–1247, 2014.

[13] A.L. Dulmage and N.S. Mendelsohn. Coverings of bipartite graphs. *Canadian Journal of Mathematics*, 10:517–534, 1958.

[14] L.C. Evans. *Partial Differential Equations*. American Mathematical Society, Providence, R.I., 2010.

[15] J. Evers and T. Kolokolnikov. Metastable states for an aggregation model with noise. *SIAM Journal on Applied Dynamical Systems*, 15(4):2213–2226, 2016.

[16] K. Fellner and G. Raoul. Stable stationary states of non-local interaction equations. *Mathematical Models and Methods in Applied Sciences*, 20(12):2267–2291, 2010.

[17] R.C. Fetecau, H. Huang, D. Messenger, and W. Sun. Zero-diffusion limit for aggregation equations over bounded domains. *Submitted, preprint arXiv:1809.01763 [math.AP]*, 2018.

[18] R.C. Fetecau and M. Kovacic. Swarm equilibria in domains with boundaries. *SIAM Journal on Applied Dynamical Systems*, 16(3):1260–1308, 2017.

[19] R.C. Fetecau, M. Kovacic, and I. Topaloglu. Swarming in domains with boundaries: approximation and regularization by nonlinear diffusion. *Discrete and Continuous Dynamical Systems Series B*, 24(4):1815–1842, 2019.

[20] D.J. Higham. An algorithmic introduction to numerical simulation of stochastic differential equations. *SIAM Review*, 43(3):525–546, 2001.

[21] P.-E. Jabin and Z. Wang. Mean field limit for stochastic particle systems. In N. Bellomo, P. Degond, and E. Tadmor, editors, *Active Particles, Volume 1*, pages 379–402. Birkhäuser, Cham, 2017.

[22] R. Jordan, D. Kinderlehrer, and F. Otto. The variational formulation of the Fokker–Planck equation. *SIAM Journal on Mathematical Analysis*, 29(1):1–17, 1998.

[23] P. Kloeden and E. Platen. *Numerical Solution of Stochastic Differential Equations*. Springer, Verlag, 1995.

[24] M. Kovacic. *Swarm Equilibria in Domains with Boundaries*. PhD thesis, Simon Fraser University, 2018.

[25] P.-L. Lions. The concentration-compactness principle in the calculus of variations. The locally compact case, part 1. *Annales de l'I.H.P Analyse Non Linéaire*, 1(2):109–145, 1984.

[26] A. Mogilner, L. Edelstein-Keshet, L. Bent, and A. Spiros. Mutual interactions, potentials, and individual distance in a social aggregation. *Journal of Mathematical Biology*, 47(4):353–389, 2003.

[27] J.S. Rosenthal. *A First Look at Rigorous Probability Theory*. World Scientific, Singapore, 2006.

[28] A.V. Skorokhod. Stochastic equations for diffusion processes in a bounded region I. *Theory of Probability & its Applications*, 6(3):264–274, 1961.

[29] A.V. Skorokhod. Stochastic equations for diffusion processes in a bounded region II. *Theory of Probability & its Applications*, 7(1):3–23, 1962.

[30] R. Sman. Refrigeration: A deep dive into the deep freeze. https://www.newfoodmagazine.com/article/23904/refrigeration-impact-of-ice-crystal-size-and-freezing-rate/, 2016. Accessed: 2019-06-30.

[31] A.-S. Sznitman. Nonlinear reflecting diffusion process, and the propagation of chaos and fluctuations associated. *Journal of Functional Analysis*, 56(3):311–336, 1984.

[32] C. Villani. *Optimal Transport: Old and New*. Springer Science & Business Media, Berlin, 2008.

[33] L. Wu and D. Slepčev. Nonlocal interaction equations in environments with heterogeneities and boundaries. *Communications in Partial Differential Equations*, 40(7):1241–1281, 2015.

[34] Y. Zhang. On continuity equations in space-time domains. *Discrete and Continuous Dynamical Systems Series A*, 38(10):4837–4873, 2018.

# Appendix A

# Well-Posedness of the Fixed-Point Map

In what follows, we will write $\rho \in \mathcal{P}^{ac}(D)$ to mean $d\rho(x) = \rho(x)\,dx$, using $\rho$ interchangeably to refer to the measure and its density.

**Theorem A.1.** *Let $D \subset \mathbb{R}^d$ be the closure of a bounded open set and $\nu > 0$. In addition, let $V \in L^\infty(D) \cap L^1(D)$, and $K \in L^\infty(D-D) \cap L^1(D-D)$. Define the map $T : \mathcal{P}(D) \to \mathcal{P}^{ac}(D)$ by*

$$T(\rho) := \frac{1}{Z(\rho)} \exp\left(-\frac{1}{\nu} K * \rho - \frac{1}{\nu} V\right)$$

*where*

$$Z(\rho) := \int_D \exp\left(-\frac{1}{\nu} K * \rho(x) - \frac{1}{\nu} V(x)\right) dx.$$

*Then the integro-differential equation*

$$\begin{cases} \dfrac{\partial}{\partial t}\rho(x,t) = T(\rho(x,t)) - \rho(x,t), & (x,t) \in D \times (0,\infty) \\ \rho(x,0) = \rho_0(x) \in \mathcal{P}^{ac}(D), & x \in D, \end{cases} \tag{A.1}$$

*has a unique solution $\rho(x,t) \in L^\infty\left((0,\infty), \mathcal{P}^{ac}(D)\right)$ for every $\rho_0 \in \mathcal{P}^{ac}(D)$.*

*Proof.* We will show that $T$ satisfies an $L^1$-Lipschitz bound, which then allows us to use a standard contraction mapping argument to deduce existence and uniqueness.

First note that since $|K|$ is bounded on $D - D$, we can write $K = \widetilde{K} + M$ for

$$M = \min_{z \in (D-D)} K(z)$$

such that $\widetilde{K}$ is non-negative. We now deduce some basic estimates. Note that for any $\rho \in \mathcal{P}^{ac}(D)$ we have

$$K * \rho(x) = \int_D K(x-y)\rho(y)\,dy = \int_D \widetilde{K}(x-y)\rho(y)\,dy + M$$

which implies, together with the positivity of $\widetilde{K}$, that

$$M \leq K * \rho \leq \left\|\widetilde{K}\right\|_{L^\infty(D-D)} + M. \tag{A.2}$$

From this we have

$$\left\|\exp\left(-\frac{1}{\nu}K * \rho\right)\right\|_{L^\infty(D)} \leq \exp\left(-\frac{M}{\nu}\right) \tag{A.3}$$

and

$$\left\|\exp\left(-\frac{1}{\nu}K * \rho\right)\right\|_{L^\infty(D)} \geq \exp\left(-\frac{M}{\nu} - \frac{1}{\nu}\left\|\widetilde{K}\right\|_{L^\infty(D-D)}\right), \tag{A.4}$$

where (A.4) provides a lower bound for $Z$:

$$\begin{aligned} Z(\rho) &= \int_D \exp\left(-\frac{1}{\nu}K * \rho - \frac{1}{\nu}V\right)\,dx \\ &= \int_D \exp\left(-\frac{M}{\nu} - \frac{1}{\nu}\widetilde{K} * \rho - \frac{1}{\nu}V\right)\,dx \\ &\geq \exp\left(-\frac{M}{\nu} - \frac{1}{\nu}\left\|\widetilde{K} * \rho\right\|_{L^\infty(D)}\right)\left(\int_D \exp\left(-\frac{1}{\nu}V\right)\,dx\right) \end{aligned}$$

and so

$$Z(\rho) \geq \exp\left(-\frac{M}{\nu} - \frac{1}{\nu}\left\|\widetilde{K}\right\|_{L^\infty(D-D)}\right)\left\|\exp\left(-\frac{1}{\nu}V\right)\right\|_{L^1(D)}. \tag{A.5}$$

For $\rho_1, \rho_2 \in \mathcal{P}^{ac}(D)$ we also have:

$$\begin{aligned} &\left\|\exp\left(-\frac{1}{\nu}K * \rho_1 - \frac{1}{\nu}V\right) - \exp\left(-\frac{1}{\nu}K * \rho_2 - \frac{1}{\nu}V\right)\right\|_{L^1(D)} \\ &\qquad \leq \left\|\exp\left(-\frac{1}{\nu}V\right)\right\|_{L^1(D)}\left\|\exp\left(-\frac{1}{\nu}K * \rho_1\right) - \exp\left(-\frac{1}{\nu}K * \rho_2\right)\right\|_{L^\infty(D)}, \end{aligned}$$

which allows us to bound the difference in the normalization factors:

$$|Z(\rho_1) - Z(\rho_2)| = \left| \int_D \exp\left(-\frac{1}{\nu}K * \rho_1 - \frac{1}{\nu}V\right) dx - \int_D \exp\left(-\frac{1}{\nu}K * \rho_2 - \frac{1}{\nu}V\right) dx \right| \quad \text{(A.6)}$$

$$\leq \left\| \exp\left(-\frac{1}{\nu}K * \rho_1 - \frac{1}{\nu}V\right) - \exp\left(-\frac{1}{\nu}K * \rho_2 - \frac{1}{\nu}V\right) \right\|_{L^1(D)} \quad \text{(A.7)}$$

$$\leq \left\| \exp\left(-\frac{1}{\nu}V\right) \right\|_{L^1(D)} \left\| \exp\left(-\frac{1}{\nu}K * \rho_1\right) - \exp\left(-\frac{1}{\nu}K * \rho_2\right) \right\|_{L^\infty(D)}. \quad \text{(A.8)}$$

Together this gives, for $Z_1 = Z(\rho_1)$ and $Z_2 = Z(\rho_2)$,

$$\begin{aligned}
\|T(\rho_1) - T(\rho_2)\|_1 &= \left\| Z_1^{-1} \exp\left(-\frac{1}{\nu}K * \rho_1 - \frac{1}{\nu}V\right) - Z_2^{-1} \exp\left(-\frac{1}{\nu}K * \rho_1 - \frac{1}{\nu}V\right) \right\|_1 \\
&\leq Z_2^{-1} \left\| \exp\left(-\frac{1}{\nu}K * \rho_1 - \frac{1}{\nu}V\right) - \exp\left(-\frac{1}{\nu}K * \rho_1 - \frac{1}{\nu}V\right) \right\|_1 \\
&\qquad + \frac{|Z_1 - Z_2|}{Z_1 Z_2} \left\| \exp\left(-\frac{1}{\nu}K * \rho_1 - \frac{1}{\nu}V\right) \right\|_1 \\
&= Z_2^{-1} \left\| \exp\left(-\frac{1}{\nu}K * \rho_1 - \frac{1}{\nu}V\right) - \exp\left(-\frac{1}{\nu}K * \rho_2 - \frac{1}{\nu}V\right) \right\|_1 \\
&\qquad + Z_2^{-1} |Z_1 - Z_2|,
\end{aligned}$$

where we have used $Z_1^{-1} = \left(Z_1^{-1} - Z_2^{-1}\right) + Z_2^{-1}$ together with the triangle inequality and the definition of $Z_1$. Now, employing the estimates (A.5) and (A.8), we arrive at

$$\begin{aligned}
&\|T(\rho_1) - T(\rho_2)\|_1 \\
&\quad \leq 2 \exp\left(\frac{M}{\nu} + \frac{1}{\nu}\left\|\widetilde{K}\right\|_{L^\infty(D-D)}\right) \left\| \exp\left(-\frac{1}{\nu}K * \rho_1\right) - \exp\left(-\frac{1}{\nu}K * \rho_2\right) \right\|_{L^\infty(D)}, \quad \text{(A.9)}
\end{aligned}$$

and using $K = \widetilde{K} + M$ along with the Lipschitz property of $e^{-x}$, we deduce that

$$\begin{aligned}
\|T(\rho_1) - T(\rho_2)\|_1 &\leq 2 \exp\left(\frac{1}{\nu}\left\|\widetilde{K}\right\|_{L^\infty(D-D)}\right) \left\| \exp\left(-\frac{1}{\nu}\widetilde{K} * \rho_1\right) - \exp\left(-\frac{1}{\nu}\widetilde{K} * \rho_2\right) \right\|_{L^\infty(D)} \\
&\leq \frac{2}{\nu} \exp\left(\frac{1}{\nu}\left\|\widetilde{K}\right\|_{L^\infty(D-D)}\right) \left\| \widetilde{K} * |\rho_1 - \rho_2| \right\|_{L^\infty(D)} \\
&\leq \frac{2}{\nu}\left\|\widetilde{K}\right\|_{L^\infty(D-D)} \exp\left(\frac{1}{\nu}\left\|\widetilde{K}\right\|_{L^\infty(D-D)}\right) \|\rho_1 - \rho_2\|_{L^1(D)}.
\end{aligned}$$

This shows that $T$ has $L^1$-Lipschitz constant $L_T$ satisfying

$$L_T \leq \frac{2}{\nu}\left\|\widetilde{K}\right\|_{L^\infty(D-D)} \exp\left(\frac{1}{\nu}\left\|\widetilde{K}\right\|_{L^\infty(D-D)}\right), \quad \text{(A.10)}$$

which does not depend on the external potential $V$ (or $M$, the infimum of $K$).

Now, we will show that a unique solution exists for the integro-differential equation (A.1) using a contraction argument. Integrating in $t$ gives us the integral equation

$$\rho(x,t) = \rho(x,0) + \int_0^t \left(T(\rho(x,s)) - \rho(x,s)\right)\, ds := G(\rho(x,t)).$$

We will show that $G$ is a contraction mapping on the space

$$X := L^\infty\left((0,\infty), \mathcal{P}^{ac}(D)\right)$$

under the norm

$$\|\rho_1 - \rho_2\|_X := \sup_{t\in(0,\infty)} e^{-(L_T+1)t} \|\rho_1(\cdot,t) - \rho_2(\cdot,t)\|_{L^1(D)}\,.$$

First, note that $X$ is complete as it is a closed, convex subset of the space $L^\infty\left((0,\infty), L^1(D)\right)$, which is already complete under the given norm. Next, we show that $G$ maps $X$ back into $X$: for every $s \in (0,\infty)$, we know that $\rho(x,s)$ and $T(\rho(x,s))$ lie in $\mathcal{P}^{ac}(D)$, and so

$$\int_D G(\rho(x,t))\, dx = \int_D \rho(x,0)\, dx + \int_0^t \left(\int_D T(\rho(x,s))\, dx - \int_D \rho(x,s)\, dx\right) ds = 1$$

for every $t \in (0,\infty)$. One can also show, by a bootstrapping argument, that $G(\rho(x,t))$ is non-negative for every $t$. From here we note that

$$\|G(\rho_1(\cdot,t)) - G(\rho_2(\cdot,t))\|_{L^1(D)} \le (L_T+1)\int_0^t \|\rho_1(x,s) - \rho_2(x,s)\|_{L^1(D)}\, ds,$$

and so

$$\|G(\rho_1) - G(\rho_2)\|_X \le (L_T+1) \sup_{t\in(0,\infty)} \left\{ e^{-(L_T+1)t} \int_0^t \|\rho_1(x,s) - \rho_2(x,s)\|_{L^1(D)}\, ds \right\}.$$

Choosing $t^* \in (0,\infty)$ which realizes the supremum, we arrive at

$$\begin{aligned}
\|G(\rho_1) - G(\rho_2)\|_X &\le \left((L_T+1)e^{-(L_T+1)t^*} \int_0^{t^*} e^{(L_T+1)s}\, ds\right) \|\rho_1 - \rho_2\|_X \\
&\le \left(1 - e^{-(L_T+1)t^*}\right) \|\rho_1 - \rho_2\|_X \\
&< \|\rho_1 - \rho_2\|_X\,.
\end{aligned}$$

This shows that $G$ is a contraction map on $X$. Existence and uniqueness of a solution follow from the contraction mapping theorem. □